INVESTIGATION OF MECHANICAL PROPERTIES OF CONCRETE DEVELOPED FROM A BINDER COMPOSITE OF SUGAR CANE BAGASSE ASH AND PORTLAND CEMENT

MICHAEL EVANS NZUGUA
21/X/GMSP/14328/PE

A DISSERTATION SUBMITTED TO THE DIRECTORATE OF RESEARCH AND GRADUATE TRAINING IN PARTIAL FULFILLMENT FOR THE REQUIREMENTS FOR THE AWARD OF THE DEGREE OF MASTER OF SCIENCE IN PHYSICS OF KYAMBOGO UNIVERSITY

OCTOBER, 2024

DECLARATION

I hereby declare that this dissertation is my original work. To the best of my knowledge, the work presented here has not been presented at any institution of higher learning.

Michael Evans Nzugua

Signature…….Date……....

APPROVAL

This research dissertation titled **Investigation of Mechanical Properties of Concrete Developed from a Binder Composite of Sugar Cane Bagasse Ash and Portland Cement** is ready for submission to the Board of Directorate of Research and Graduate Training and the Senate of Kyambogo University with our approval as the supervisors.

Dr. Panzi Emma Mukhokosi

Signature…… Date……

Prof. Sam Obwoya Kinyera

Signature…….Date.....

DEDICATION

This research is a tribute to the incredible network of love, encouragement, and strength that surrounds me. To my dad, Mr. Nzugua Maurice and mom Ms Karen Akoth, whose sacrifices and boundless love have been the foundation of my aspirations. Your sacrifices have allowed me the privilege of pursuing knowledge and striving for excellence.

To my siblings, your encouragement and understanding have been a constant source of motivation. This research is dedicated to the shared experiences, laughter, and the unbreakable bond we've forged through the years. To my friends, Ivan Ssikubwabo and Balabye Stephen, who have been a constant source of joy, laughter, and intellectual exchange, your camaraderie has illuminated my path. The discussions and, collaborative efforts have immeasurably steered me academically. This research is dedicated to the camaraderie we've built, which fuelled my passion for learning and discovery.

Together, you form the backbone of my aspirations and the foundation upon which my dreams stand. With heartfelt appreciation and affection, I dedicate this work to each of you.

ACKNOWLEDGEMENT

I would like to express my sincere appreciation to my supervisors led by Dr. Emma Panzi Mukhokosi, and Prof. Obwoya Sam Kinyera for their unwavering guidance, insightful feedback, and continuous encouragement throughout the research process and the entire Kyambogo Physics department. Your expertise and mentorship have been crucial in shaping the direction and quality of this work.

I extend my heartfelt thanks to the East Africa Community Scholarship sponsored by KFW and administered through IUCEA for their generous support throughout the entire period. This scholarship did not only alleviate financial burdens but also allowed me to fully concentrate on the research. I would also wish to acknowledge the government of Kenya through the Ministry of Public Service and Ministry for Roads and Transport (State Department of Roads, Materials Testing and Research Division) for granting me the academic leave which I needed to make this a realization.

I am indebted to the Kyambogo Physics Laboratory and Makerere University Materials Laboratory of Uganda and the Materials Testing and Research Division Laboratory from Kenya for providing a conducive research environment and access to your facilities.

Special recognition goes to the dedicated individuals from these laboratories, more so, Mr. Kawuki Joseph and Mr. Wabwire Bernard from Uganda laboratories and Mr. Kibet Lokwang of Kenya Laboratory. Your enthusiasm, technical skills, and willingness to share knowledge have enriched this project immeasurably.

Finally, I want to acknowledge my family and friends for your belief in my abilities has been a constant source of motivation.

This research is a collective achievement. I am fortunate to have had the privilege of working with such a remarkable group of individuals and institutions. “Ahsanteni sana”.

TABLE OF CONTENTS

DECLARATION ..... **i**

APPROVAL ..... **ii**

DEDICATION ..... **iii**

ACKNOWLEDGEMENT ..... **iv**

TABLE OF CONTENTS ..... **v**

ABSTRACT ..... **x**

LIST OF TABLES ..... **xi**

LIST OF FIGURES ..... **xii**

LIST OF ABBREVIATIONS ..... **xiii**

CHAPTER ONE: INTRODUCTION **1**

1.1 BACKGROUND 1

1.2 PROBLEM STATEMENT 3

1.3 RESEARCH OBJECTIVES 4

1.3.1 General Objectives 4

1.3.2 Specific Objectives 5

1.4 JUSTIFICATION FOR THE STUDY 5

1.5 SCOPE OF WORK 5

CHAPTER TWO: LITERATURE REVIEW **7**

2.1 INTRODUCTION 7

2.2 CEMENT PRODUCTION AND CHALLENGES 7

2.3 CHEMICAL CONSTITUENTS OF SUGARCANE BAGASSE ASH 10

2.3.1 Mineral composition 10

2.3.2 Pozzolanicity 12

2.4 SURFACE MORPHOLOGY OF SUGARCANE BAGASSE ASH 14

2.4.1 Microstructure morphology 14
2.5 STRENGTH OF DEVELOPED CONCRETE FROM VARYING SUGARCANE BAGASSE ASH DOSE 15
2.5.1 Compressive strength 15
2.5.2 Flexural strength 16
2.6 SUMMARY OF LITERATURE REVIEWED 19
CHAPTER THREE: METHODOLOGY 21
3.1 INTRODUCTION 21
3.2 RESEARCH DESIGN 21
3.3 MATERIALS SAMPLING 21
3.3.1 Fine aggregates 21
3.3.2 Coarse aggregate 21
3.3.3 Mixture water and Portland cement 23
3.3.4 Sugarcane bagasse ash 23
3.4 MIX DESIGN 26
3.5 TEST SETUP AND PROCEDURE 27
3.5.1 Mixing, vibrating, casting and curing 27
3.5.2 Compressive strength 29
3.5.3 Flexural strength 30
3.6 CHARACTERIZATION METHODS 31
3.6.1 X-Ray Diffraction 31
3.6.2 Scanning Electron Microscope 32
3.6.3 Energy Dispersive X-ray 33
3.6.4 X-Ray Fluorescence 33
CHAPTER 4: RESULTS AND DISCUSSION 35

4.0 INTRODUCTION 35
4.1 MATERIALS CHARACTERIZATION 35
4.1.1 Portland cement phase identification 35
4.1.2 Portland cement elemental composition 39
4.1.3 Portland cement microstructure morphology 41
4.1.4 Chemical composition for Portland cement 43
4.2 SUGARCANE BAGASSE ASH MATERIAL CHARACTERIZATION 44
4.2.1 Raw sugarcane bagasse ash mineral composition analysis 44
4.2.1.2 Elemental composition for raw sugarcane bagasse ash 47
4.2.1.3 Microstructure morphology for raw sugarcane bagasse ash 49
4.2.2 Processed sugarcane bagasse ash 50
4.2.2.1 Processed Sugarcane bagasse ash mineral phases identification 51
4.2.2.2 Elemental composition for processed sugarcane bagasse ash 53
4.2.2.3 Microstructure morphology for processed sugarcane bagasse ash 55
4.2.2.4 Chemical composition for processed sugarcane bagasse ash 56
4.3 POZZOLANICITY 57
4.3.1 Introduction 57
4.3.2 Hydration products analysis for SCBA-600 concrete 58
4.3.3 Elemental composition analysis for powdered SCBA-600 concrete 60
4.3.4 Microstructure morphology for SCBA -600 concrete 63
4.3.5 Improvement of sugarcane bagasse ash pozzolanic properties on calcination 64
4.4 HARDENED CONCRETE PROPERTIES 66
4.4.1 Introduction 66
4.4.2 Compressive strength 67
4.4.3 Flexural strength 72

CHAPTER 5: CONCLUSION AND RECOMMENDATIONS 75

5.1 INTRODUCTION 75

5.2 SPECIFIC CONCLUSION 75

5.2.1 Evaluation of the surface morphology and chemical constituents of sugarcane bagasse ash and Portland cement 75

5.2.1.1 Surface morphology of sugarcane bagasse ash and Portland cement 75

5.2.1.2 Chemical constituents of sugarcane bagasse ash and Portland cement 77

5.2.2 Determining the structural properties of sugarcane bagasse ash and Portland cement 78

5.2.2.1 Sugarcane bagasse ash and Portland cement mineral composition 78

5.2.2.3 Pore structure and refinement 78

5.2.3 Examining structural, flexural and compressive strength properties of the developed concrete from varying sugarcane bagasse ash dose 79

5.2.3.1 Structural properties 79

5.2.3.2 Compressive strength 79

5.2.3.3 Flexural strength 80

5.3 CONCLUSION SUMMARY 80

5.4 RECOMMENDATIONS 82

6.0 REFERENCES 84

APPENDIX A- EDX Analysis 93

A1: Bamburi Powerplus CEM I/42.5N Portland cement elemental composition- EDX analysis 93

A2: Raw SCBA elemental composition - EDX analysis 94

A3: Processed SCBA (SCBA-600) - EDX analysis 95

A4: Hardened concrete block surface from SCBA-20 Mix -EDX analysis 96

APPENDIX B- XRF Analysis 97

B1: Bamburi Powerplus CEM I/42.5N Portland cement XRF analysis 97

B2: Processed SCBA (SCBA-600) XRF analysis 99

APPENDIX C- Scanning Electron Micrographs (SEM)..... 100

C1: Bamburi Powerplus CEM I/42.5N Portland cement SEM images at different magnifications 100

C2: Raw SCBA SEM images at different magnifications 101

C3: Processed SCBA (SCBA-600) SEM images at different magnifications 102

C4: Hardened concrete surface from SCBA-20 Mix SEM images..... 103

APPENDIX D- Hardened Concrete Mechanical Properties Statistical Analysis 104

D1: Flexural strength statistical analysis..... 104

D2: Compressive strength statistical analysis 106

APPENDIX E- Copy Rights Permissions 108

APPENDIX F- Research Introductory Letter 109

ABSTRACT

Cement production has been growing over time. Statistics indicate more growth as the human population increases. However, cement production relies on natural resources such as limestone rocks. The mining of these minerals poses grave environmental hazards. Increased limestone mining and its use in cement production have led to, deforestation, soil and water contamination and greenhouse gas (GHG) emissions mostly carbon dioxide (CO_2). This has led to global warming and the rising of sea levels. The East Africa Community (EAC) countries have immense sugarcane cane bagasse ash (SCBA) which remains unexploited as a supplementary-cementitious material (SCM). This study delved into using EAC SCBA as a pozzolan. SCBA investigated was collected from Kenya's coastal area. Raw SCBA, processed SCBA, Portland cement (PC) and the developed concrete were characterised by various techniques to determine the surface morphology, chemical composition, structural properties and mineralogical composition. The raw SCBA was calcinated at 600 ^{o}C to get processed SCBA (SCBA-600). SCBA-600 was then used to design the concrete mix. PC was replaced from 0 to 30 % in steps of 10 %. The flexural and compressive strengths were determined in the hardened state after twenty-eight days of concrete curing. The compressive and flexural strength of the mix containing 20 % SCBA was higher than the control mix by 9.65 and 6.51 %, respectively. The microstructural properties of the developed concrete revealed dense particle distribution, indicating good micro/nanofiller effects of the interfacial transition zone. The processed SCBA was found to meet class N and F of natural pozzolan as per ASTM –C 618. The samples were analysed using XRD, SEM, EDX, and XRF techniques. The concrete design was done following IS 10262-2009 and IS 456. The casting and curing were done as per ASTM C-192 and lastly, the mechanical strengths were done as per ASTM C-39 and ASTM C78-00 standards specifications. These positive results from the experimental investigation, technically portray the Kenya coastal SCBA as a potential SCM.

LIST OF TABLES

Table 1. 1: Estimated CO_2 emission equivalent by selected cement-producing countries. 2
Table 1. 2: Chemical Constituents of SCBA from different geographical locations. 4
Table 2. 1: Typical mineral composition for Portland cement. 8
Table 2. 2: Cement production reactions and heat evolution. 9
Table 2. 3: Percentile range of SCBA minerals constituents' variations from different nations. 10
Table 2. 4: Chemical composition requirement for natural pozzolan. 11
Table 2. 5: SCBA dosage for optimum strength and the maximum allowable dosage. 18
Table 3. 1: Physical properties of fine and coarse aggregates. 22
Table 3. 2: The physical properties of SCBA-600 and Bamburi Powerplus CEM I/42.5N cement. 26
Table 3. 3: Mix proportion for control mix (SCBA-0). 27
Table 3. 4: Mix Proportion with SCBA doses (kg/m^3). 27
Table 3. 5: Mix proportion with SCBA dose kg/ 0.016878 m^3 27
Table 4. 1: Bamburi Powerplus CEM I/42.5N Portland cement XRD identified mineral phases. 38
Table 4. 2: Bamburi Powerplus CEM I/42.5N Portland cement Chemical oxides composition. 43
Table 4. 3: The raw SCBA mineral composition at different peak angles. 47
Table 4. 4: The SCBA-600 mineral composition at different peak angles. 53
Table 4. 5: Mineral oxides composition of the SCBA-600 57
Table 4. 6: Powdered SCBA-600 concrete hydration products at different peak angles. 60
Table 4. 7: EDX SAIC elemental analysis. 61
Table 4. 8: Enhancement of SCBA elemental properties upon heating- EDX analysis. 66
Table 4. 9: Compressive strength after twenty-eight days of concrete curing. 68
Table 4. 10: Composition of major PC phases by mass. 68
Table 4. 11: Flexural strength after twenty-eight days of concrete curing. 72

LIST OF FIGURES

Figure 1. 1: Kwale International Sugar Company Limited (KISCOL) location. 6
Figure 2. 1: Microstructure morphology of raw and processed SCBA. 14
Figure 3. 1: Simplified flow chart of methodology. 22
Figure 3. 2: The photo camera image of the as-received Bamburi Powerplus CEM I/42.5N. 23
Figure 3. 3: The photo camera images show different SCBA processing stages. 25
Figure 3. 4: SCBA sample preparation. 26
Figure 3. 5: The photo camera images showing the test set-up and procedure. 29
Figure 3. 6: The photo camera image of UTM assembly for compressive strength test. 30
Figure 3. 7: The photo camera image of UTM assembly for flexural strength test. 31
Figure 3. 8: Sample coating and loading into the SEM, camera images. 33
Figure 3. 9: Energy dispersive X-ray fluorescence spectrometer. 34
Figure 4. 1: Bamburi Powerplus CEM I/42.5N, XRD phase identification using ICSD standards. 36
Figure 4. 2: Enlarged graph of XRD-identified phases of Bamburi Powerplus CEM I/42.5N. 37
Figure 4. 3: Bamburi Powerplus CEM I/42.5N Portland cement EDX elemental analysis. 40
Figure 4. 4: Bamburi Powerplus CEM I/42.5N Portland cement SEM microstructure morphology... 41
Figure 4. 5: Raw SCBA XRD phases identification using ICSD standards. 45
Figure 4. 6: Enlarged graph showing crystallization phases of raw SCBA, mineral composition. 45
Figure 4. 7: Elemental composition of raw SCBA. 48
Figure 4. 8: SEM microstructure morphology and elemental composition for raw SCBA. 49
Figure 4. 9: XRD spectra of the processed SCBA (SCBA-600) using ICSD standards. 51
Figure 4. 10: XRD spectra of the SCBA-600 using ICSD standards. 52
Figure 4. 11: The EDX spectra for SCBA-600. 54
Figure 4. 12: SEM microstructure morphology for processed SCBA (SCBA-600). 55
Figure 4. 13: XRD spectra of the powdered SCBA-600 concrete using ICSD standards. 58
Figure 4. 14: XRD spectra for crystallization phases of hydrated powdered SCBA-600 concrete. 59
Figure 4. 15: Elemental composition of powdered SCBA-600 concrete. 61
Figure 4. 16: SCBA-600 concrete, SEM, surface morphology and hydration products. 63
Figure 4. 17: The comparison of the pozzolanic mineral phases in Raw SCBA and SCBA-600. 65
Figure 4. 18: Average compressive strength at twenty-eight days of concrete curing. 71
Figure 4. 19: Average flexural strength after twenty-eight days of concrete curing. 72

LIST OF ABBREVIATIONS

CA	-	Coarse aggregate
EAC	-	East Africa Community
FA	-	Fly Ash
FAg	-	Fine Aggregate
GGCS	-	Ground granulated corex slag
GHGs	-	Green House Gases
ITZ	-	Interfacial Transition Zone
IUCEA	-	Inter-University Council for East Africa
KISCOL	-	Kwale International Sugar Company Limited.
LOI	-	Loss on Ignition
MC	-	Mass of cement
MSCBA	-	Mass of sugarcane bagasse ash
MTRD	-	Materials Testing and Research Division
MW	-	Mass of water
PC	-	Portland cement
SAI	-	$SiO_2+Al_2O_3+Fe_2O_3$
SCBA	-	Sugarcane Bagasse Ash

SCM	-	Semi cementitious materials
SEM	-	Scanning electron microscope
SG	-	Specific gravity
XRD	-	X-Ray Diffraction
XRF	-	X-Ray Fluorescence

CHAPTER ONE: INTRODUCTION

1.1 BACKGROUND

Concrete, a combination of Portland cement (PC), water and aggregates is a widely used construction material due to its available raw materials, hardened properties, adaptability to various moulds and low repair cost [1], [2], [3]. PC is manufactured in a controlled chemical combination of silica, lime, alumina, sulphur trioxide, magnesia, soda and iron oxide [4]. It has great applications in the construction industry ranging from the construction of great iconic buildings, Burj Khalifa and KICC in Dubai and Kenya respectively to great iconic infrastructures such as the source of Nile Bridge in Uganda. However, the PC production chain leads to environmental decadence due to increased mining of raw materials and clinker production. Mining these materials changes geomorphology, land-use pattern, water quality, habitat loss, sedimentation, subsidence and clinker production, leading to increased carbon footprint [5].

The exponential growth in the construction industry has increased demand for PC [6]. PC production has risen by a factor of 25 globally in comparison to the 1950's. This has led to an increase in capacity by 73 % from 2005 to 2013 alone [7]. Cement products are anticipated to increase from 3.27 metric tons realised in 2010 to 4.83 billion metric tons in 2030 [8]. By 2050, PC production is expected to reach 3.7 Gt to 4.4 Gt [6]. PC production is third-ranked after aluminium and steel in energy consumption. Producing 1 ton of PC requires 110 kWh of electrical energy and 1.6 tons of raw minerals [6], [9]. PC raw minerals processing affects the environment negatively, that is soil, air and water contamination, and depletion of natural resources [10]. In addition, producing 1 ton of PC produces 1 ton of carbon dioxide (CO_2), [2] which increases the greenhouse gas (GHG) effect and accelerates global warming [6], [11], [12]. The average CO_2 equivalent produced in Mt per annum (Mt/a) of cement by selected

cement-producing countries globally is shown in Table 1.1. This is indicative of how harmful PC production can be.

Considering the GHG emissions and their associated effects, extensive research has been carried out on possible supplementary cementitious material (SCM). SCM are high siliceous materials that react with water and portlandite ($Ca(OH)_2$) to realise a product of cement nature [9]. Recently, research on SCMs to reduce CO_2 emissions, raw materials mining and at the same time increase concrete properties is on the rise. The commonly investigated SCMs are fly ash (FA), and ground granulated corex slag (GGCS) [8], [13]. However, FA production involves coal burning which may increase environmental carbon footprints leading to increased global warming [14]. Furthermore, GGCS being a by-product of steel industries, its availability is not guaranteed since there could be a decline in steel products leading to its paucity [14]. Therefore, there is a need to look for alternative SCMs such as agricultural by-products, and sugar cane bagasse ash (SCBA) is of interest to this study. Producing one tone of sugar produces 24.017 kg of CO_2 [15]. Hence, little GHG emission especially CO_2.

SCBA is obtained from sugar cane mills. The fibrous product after cane crushing, is called sugarcane bagasse (SB). SB acts as fuel in boilers to produce steam that drives turbines generating electricity.

Table 1. 1: Estimated CO_2 emission equivalent by selected cement-producing countries.

Country	**Cement capacity(Mt/annum)**	**CO_2 emission estimated ($MtCO_{2eq}$ /annum)**	**Reference**
China	1367.00	1170.10	[7]
India	324.60	276.30	[7]
USA	120.80	112.40	[7]
Russia	110.80	95.20	[7]
Vietnam	105.60	89.80	[7]
South Africa	-	5.20	[16]

Burning SB leaves 3 % SCBA, which is disposed of as industrial waste in landfills or stockpiling [2], [4], [17], [18]. These wastes may undermine air quality besides obstructing storm water runoff, causing stagnant water bodies that become breeding grounds for diseases, [19]. However, with a significant amount of silica available in SCBA, [20], [21], and its minimum preparation to qualify as a pozzolanic material [20], [22], its incorporation in concrete production may lead to reduced negative effects brought about by industrial SCBA waste dumping and the PC production chain. The SCBA pozzolanicity depends on its chemical constituents which rely on a specific geographical location of where sugar cane was grown [20], [23] as indicated in Table 1.2.

1.2 PROBLEM STATEMENT

Carbon mitigation and sustainable concrete have given rise to the use of SCMs. Currently, the annual production of concrete is 10 billion tons, by 2050 the estimated production will be 18 billion tons [24]. 1 ton of PC produces 1 ton of carbon dioxide (CO_2), which increases the GHG effect and accelerates global warming [2]. The East Africa, readily available SCMs are natural kamafugites and carbonatites in Uganda besides pumice and diatomite in Kenya [25]. However, their resource productivity is not guaranteed. Companies have therefore resorted to artificial SCM like GGCS and fly ash (FA). These artificial SCMs' availability is subject to constraints (e.g. decline of steel). On the other hand, FA is an environmental hazard. Its production emits GHGs. Hence, the search for alternative locally available and eco-friendly unconventional SCMs [6]. These unconventional SCMs are majorly agricultural by-products rich in silica such as SCBA [26], which are mostly dumped in open fields, staining air quality [27], besides possible leaching of toxic heavy metal into the soil [9]. Therefore utilizing SCBA in concrete production may lead to a sustainable PC production chain (e.g. reduction of CO_2 in PC production chain, reduction in raw mineral excavation), concrete affordability and mitigate the negative effects of SCBA waste disposal.

Table 1. 2: Chemical Constituents of SCBA from different geographical locations.

Country	Thailand	Sudan	India	Mexico	Brazil	Pakistan	Pakistan	Mauritius	China	South Africa	Kenya
Ref.	[20]	[20]	[20]	[20]	[20]	[20]	[28]	[20]	[20]	[20]	[20]
Oxide											
SiO_2	65.00	77.25	72.95	66.10	63.10	66.70	74.14	30.27	62.44	75.98	76.18
Al_2O_3	4.80	6.37	1.68	15.00	7.56	9.24	4.55	23.80	12.1	3.55	3.62
Fe_2O_3	0.90	4.21	1.89	7.60	4.59	1.53	4.60	4.87	9.44	2.71	8.71
CaO	3.90	4.05	7.77	2.57	8.28	10.07	2.05	1.69	2.52	3.70	2.88
K_2O	2.00	2.34	9.28	3.52	5.43	2.51	1.26	-	4.84	1.83	5.495
MgO	-	2.61	1.98	1.19	4.54	4.60	0.77	1.37	1.97	-	0.00
Na_2O	-	1.38	0.02	0.54	1.24	1.30	0.32	-	0.64	0.07	0.00
P_2O_3	-	0.59	-	1.14	2.13	1.55	-	-	1.30	2.83	1.422
TiO_2	-	0.58	-	1.13	-	0.25	-	-	1.24	0.14	0.937
MnO	-	0.27	-	0.22	-	0.05	0.69	-	-	-	0.456
SO_3	0.90	0.11	0.17	0.26	1.92	-	-	-	0.02	-	0.00
LOI	10.70	1.40	21.00	9.00	3.10	2.21	11.22	5.43	26.04	7.94	5.82
SAI	70.70	87.83	76.52	88.70	75.25	77.47	83.29	58.94	83.98	82.84	88.51

1.3 RESEARCH OBJECTIVES

1.3.1 General Objectives

The main objective of this research work is to investigate the mechanical properties of concrete developed from a binder composite of sugar cane bagasse ash and Portland cement.

1.3.2 Specific Objectives

These are as follows:

i. To evaluate the chemical constituents and surface morphology of SCBA and PC.

ii. To determine the structural properties of SCBA and PC.

iii. To examine structural, flexural and compressive strength properties of the developed concrete from varying SCBA doses.

1.4 JUSTIFICATION FOR THE STUDY

The cement production chain has grave environmental challenges, from loss of biodiversity to emission of GHGs. SCBA disposal harms air, water and land. More natural resources are depleted due to PC production. SCBA, a pozzolanic material, can be employed as a SCM to partly replace PC. This will reduce the negative impacts of SCBA disposal, the excavation of natural materials for PC production, and GHG emissions. It can also be used as an alternative SCM to fly ash and ground granulated corex slag. In line with this, the achievement of SDG 11 (sustainable cities and communities) and 13 (climate action) are attainable.

1.5 SCOPE OF WORK

The SCBA samples were obtained from Kenya at Kwale International Sugar Company Limited, located in Kwale County, Lungalunga along the coastal area, GPS 4°31'34.1"S 39°23'49.6" E as in the sketch, Figure 1.1.

XRD, XRF and SEM/EDX characterization were carried out on Portland cement, sugarcane bagasse ash and developed concrete. The partial replacement of Portland cement with sugarcane bagasse ash was 0, 10, 20, and 30%. Tests were done after twenty-eight days of concrete curing. The class of concrete developed was M25.

Figure 1. 1: Kwale International Sugar Company Limited (KISCOL) location.

CHAPTER TWO: LITERATURE REVIEW

2.1 INTRODUCTION

The investigations on alternative SCM to mitigate the negative effects of PC production are increasing. Several methodologies and models are being studied e.g. Limestone Clinker Calcined Clay Cement (LC3), to curb these effects. Additionally, researchers have considered alternatives such as artificial SCM, GGCS and FA, while others have embarked on natural SCM like volcanic ash (Kamafugites and phonolites). However, the literature under review is those of agricultural by-products such as SCM and more so SCBA. The scope of this review will be limited to published works from researchers investigating on use of SCBA as a potential SCM. The review will not explore how CO_2 is captured and measured while using SCBA as the SCM, but rather the conventional PC production and its challenges, concrete mechanical properties made from varying the doses of SCBA, and finally material characterization of SCBA (pozzolanicity).

2.2 CEMENT PRODUCTION AND CHALLENGES

Portland cement production consumes a lot of energy and its production units are categorised into three parts; virgin material processing, pyro-processing (production of clinker) and mixing and grinding. Raw materials are crushed, ground to a powder of 50 mm and mixed [29]. The typical mineral composition of Portland cement is as per Table 2.1.

The powdered feed is taken to pyro-processing where it is heated using flue gas from the calciner. Here magnesium carbonate and limestone decompose to MgO, $CaCO_3$, and CO_2 with complete decomposition at 960.0 ^oC [29]. From 900.0 to 1,200.0 ^oC, C_2S is formed, 1,200.0 to 1,280.0 ^oC production of C_4AF, C_3A, and C_3S, is realised [30]. Finally between 1,280.0 ^oC to 1,450.0 ^oC nodular clinker is produced. Clinker is finally cooled at 100.0 ^oC for mixing and grinding to produce PC [29].

Table 2. 1: Typical mineral composition for Portland cement.

Composition (wt %)											Ref.
SiO_2	CaO	Fe_2O_3	Al_2O_3	Na_2O	MgO	K_2O	SO_3	organics	H_2O	LOI	
14.03	41.51	2.54	3.39	0.24	2.59	0.57	0.30	0.00	0.00	34.83	[29]
13.55	40.74	2.60	4.10	0.08	2.07	0.30	0.56	0.90	0.50	34.60	[30]
13.55	41.95	2.55	3.31	0.00	1.98	0.41	0.00	0.00	0.00	35.12	[31]

Approximately 90 % of the energy needed in PC production is utilized in pyro-processing [29]. The emission of CO_2 during production could be summarized from the following sources: Fossil fuels combustion during clinker production 40 %; Transport of raw materials 10 %; Magnesium carbonate and calcium carbonate decomposition to magnesium oxide and calcium oxide respectively, 50 % [29]. Emission of CO_2 and consumption of high energy are the major problems associated with PC production. In solving these, the main mitigation approaches have been: savings on energy and fuel; separating carbon and storing it and using alternative cementitious materials [29].

Fuel and energy savings have been achieved by process modification and integration (e.g. wet, or dry cement production process), and plant optimization and maintenance. Furthermore, in carbon separation and storage, a model which separates, captures and stops CO_2 from being released to the atmosphere through storage in geological and deep saline formations has been utilized [29].

Lastly, utilizing alternative raw materials (e.g. SCMs) and substitution of clinker has also mitigated these emissions. These conventional raw materials have been substituted with industrial by-products. These include fly ash and GGCS which are majorly aluminate, silicates and calcium composites. Due to high CO_2 emissions, and heavy energy consumption associated with the production of clinker, introducing SCMs such as fly ash, GGCS or SCBA, leads to clinker reduction in PC production hence

mitigating these problems [29]. Thus, it has been realised that using alternative SCM in cement production reduces the clinker ratio in PC production. This ratio is called the clinker factor (CF). The lower the CF the lower the carbon footprint [29].

The utilization of the SCM in PC production has led to a gradual decrease in the CF ratio [29]. In the year 2003, 0.85 was the global CF average [29]. Additionally, in the year 2010, the global CF average reduced further to 0.77 [29]. Agricultural by-products such as rice husk ash, coffee husk ash and SCBA can be used as alternative SCM to bring this CF ratio further down and consequently reduce the global carbon footprints and at the same time improve concrete mechanical properties. However, SCBA is preferred due to the quantity of its siliceous content [20], [21]. Table 2.2 shows various reactions which take place during cement production [29].

Table 2. 2: Cement production reactions and heat evolution.

Reaction Name	**Temp (ºC)**	**Reaction**	**Reaction Heat (Δ Hg)**
De-calcination	550.0-960.0	$CaCO_3 \rightarrow CaO+CO_2$	+179.40 KJ/mol
$MgCO_3$ decomposition	550.0-960.0	$MgCO_3 \rightarrow CO_2 + MgO$	+117.610 KJ/mol
β-C_2S formation	900.0-1200.0	$2CaO+SiO_2 \rightarrow bC_2S$	-127.60 KJ/mol
C_3S formation	1200.0-1280.0	β-C_2S+CaO $\rightarrow$ C_3S	+16.00 KJ/mol
C_3A formulation	1200.0-1280.0	$3CaO+Al_2O_3 \rightarrow C_3A$	+21.80 KJ/mol
C_4AF formulation	1200.0-1280.0	$4CaO+ Al_2O_3+Fe_2O_3 \rightarrow C_4AF$	-41.30 KJ/mol
Formulation of liquid clinker	>1280.0	Solid clinker – Liquid clinker	+600.00 KJ/mol

2.3 CHEMICAL CONSTITUENTS OF SUGARCANE BAGASSE ASH

2.3.1 Mineral composition

A comprehensive study of the SCBA entails proper analysis of its mineral constituents. From mineral composition one could be able to optimise and predict concrete hydration trends and its properties in terms of its hardened and fresh state besides the toxicity and environmental hazards it may pose to the environment. Mineral constituent analysis on SCBA has been carried out using different techniques.

XRF, EDX, and XRD techniques have been employed [8]. This has accentuated the distinct features of SCBA that qualify it to be used as an SCM. Mineral constituents of SCBA vary reasonably with chorography [23], this variance relies on several factors, such as calcination temperature, soil type, crop type and underground water [1]. The percentile variation is shown in Table 2.3.

Table 2. 3: Percentile range of SCBA minerals constituents' variations from different nations.

SCBA Mineral Constituent	**% Range of Mineral Constituents**
Ref	[20] [28]
Silicon dioxide	30.27 - 77.25
Aluminium oxide	1.68 - 23.80
Iron oxide	0.90 - 9.44
Calcium oxide	1.69 - 10.07
Magnesium oxide	0.00 - 2.61
Manganese oxide	0.00 - 0.69
Sodium oxide	0.00 - 1.38
Potassium oxide	0.00 - 9.28
Phosphorus trioxide	0.00 - 2.83
Titanium dioxide	0.00 - 1.24
Sulphur trioxide	0.00 - 1.92
LOI	1.40 - 26.40

Table 2. 4: Chemical composition requirement for natural pozzolan.

Reference		**Class**	
[32]	**N**	**F**	**C**
Min % ; Silicon dioxide + aluminium oxide + iron oxide	70	70	50
Max %; Sulphur trioxide	4	5	5
Max %; Moisture content	3	3	3
Max %; LOI	10	6*	6

Major SCBA chemical constituents are SiO_2, Al_2O_3, and Fe_2O_3 which vary from 58.94 – 88.70 % as illustrated in Table 1.2 hence qualifying SCBA as natural pozzolan as per the ASTM-C 618 standard specification in Table 2.4 [32].

Some researchers reported that SCBA is a class F fly ash, with its reactive silica varying from 56.70 - 58.02 % [33]. This contradicted what other researchers also identified, Jagadesh *et al*. [34] classified SCBA as class N and so did Abdalla *et al.* [20]**.** Silica can be lower than 56.70 % as in the case of Mauritius at 30.27 % and higher than 58.02 % as in the case of Brazil, China, India, Mexico, Thailand, Pakistan, South Africa, and Sudan at 63.1, 62.44, 72.5, 66.1, 65, 66.7, 75.98, 77.25 % respectively, as indicated in Table 1.2. Hence SCBA silica percentile range cannot be conclusively stated as it is subject to variations.

The mineral analysis of Pakistan SCBA as reported by Abdalla *et al.* [20] and Khawaja *et al.* [28] in Table 1.2 differs. SiO_2, Fe_3O_2, MnO and LOI are lower in Abdalla *et al.* [20] than in Khawaja *et al.* [28] studies. Al_2O_3, CaO, K_2O, MgO, and Na_2O, are higher in Abdalla *et al*. [20] than in Khawaja *et al*. [28]. P_2O_3 and TiO_2 are only found in Abdalla *et al*. [20]. This comparison asserts that within a geomorphology, the SCBA mineral formation may vary greatly. Similarly, XRD can be employed in determining the hydrated cement paste powder mineral components. Indeed Girma and Asteray [35],

observed ettringite, okenite, portlandite and quartz from SCBA concrete besides other elements which would hydrate over time. Furthermore, XRD makes it possible to confirm if projected phases are produced, if additional, non-projected phases are being formed or if there are unreacted raw materials left in the sample [36].

From the mineral composition analysis from different SCBA, oxide composition varies so might the properties of SCBA concrete as minerals composition play a pivotal role in cement hydration process. This is indicative that SCBA in Kenya, which is the country of interest for this study may vary depending on the sampling area.

2.3.2 Pozzolanicity

Pozzolanicity refers to the ability of certain materials to react chemically with calcium hydroxide (portlandite) at ambient temperature and in the presence of water to form compounds with cement-like properties [37]. These materials, known as pozzolans, can enhance the properties of concrete when used as supplementary cementitious materials (SCMs). Pozzolans include materials like fly ash, silica fume, rice husk ash, sugar cane bagasse ash, and natural pozzolans such as volcanic ash. When pozzolans react with calcium hydroxide produced during the hydration of Portland cement, compounds, such as calcium silicate hydrates (C-S-H), which contribute to the strength and durability of concrete are produced [33]. The incorporation of pozzolans in concrete can lead to various benefits, including improved strength, reduced permeability, increased resistance to chemical attack, and enhanced long-term durability [38].

During SCBA concrete production, portladite realised on hydration, reacts with silica and alumina in the SCBA to give, calcium aluminium hydrate, calcium silicate hydrate, and calcium aluminium silicon hydrate [1], as shown in Equations (2.1) to (2.3). These reactions lead to improved paste and aggregate

interlocking. Hence, fewer pores in the material lead to increased mechanical properties [1], [9]. Therefore, indicating the potential of SCBA as a pozzolan.

$$Al_2O_3 + Ca(OH)_2 + H_2O = C\text{-}A\text{-}H \quad (2.1)$$

$$Ca(OH)_2 + H_2O + SiO_2 = C\text{-}S\text{-}H \quad (2.2)$$

$$SiO_2 + H_2O + Ca(OH)_2 + Al_2O_3 = C\text{-}A\text{-}S\text{-}H \quad (2.3)$$

Portland cement commonly used as hydraulic binder is a heterogeneous fine grain made up of four main phases; alite, belite, celite and brown-millerite. On hydration, phases such as calcium silicate hydrate, calcium monosulfate (AFm), ettringite and portlandite are initiated [39]. Alite and belite are responsible for early and late-age mechanical strength, respectively [39]. Therefore, incorporation of SCBA (whose major chemical oxides are silica dioxide, aluminium oxide and iron II oxide) in concrete production may vary the alite and belite ratios varying setting time and hence strength development. The cement hydration reactions involving these phases are as in Equations (2.4) to (2.7) [39].

$$\underset{\text{(Alite)}}{2(3CaO \cdot SiO_2)} + \underset{\text{(Water)}}{6H_2O} \longrightarrow \underset{\text{(C-S-H)}}{3CaO \cdot 2SiO_2 \cdot 3H_2O} + \underset{\text{(Portlandite)}}{3Ca(OH)_2} \quad (2.4)$$

$$\underset{\text{(Belite)}}{2(2CaO \cdot SiO_2)} + \underset{\text{(Water)}}{4H_2O} \longrightarrow \underset{\text{(C-S-H)}}{3CaO \cdot 2SiO_2 \cdot 3H_2O} + \underset{\text{(Portlandite)}}{Ca(OH)_2} \quad (2.5)$$

$$\underset{\text{(Celite)}}{3CaO \cdot Al_2O_3} + \underset{\text{(Gypsum)}}{3CaSO_4} + \underset{\text{(Water)}}{32H_2O} \longrightarrow \underset{\text{(Ettringite)}}{3Ca_6Al_2(SO_4)_3(OH)_{12} \cdot 26H_2O} \quad (2.6)$$

Ettringite further transforms to calcium monosulphoaluminate

$$Ca_6Al_2(SO_4)_3(OH)_{12} \cdot 26H_2O + 2(3CaO \cdot Al_2O_3) + 4H_2O \longrightarrow \underset{\text{(Calcium monosulphoaluminate)}}{CaO \cdot Al_2O_3 \cdot CaSO_4 \cdot 12H_2O} \quad (2.7)$$

2.4 SURFACE MORPHOLOGY OF SUGARCANE BAGASSE ASH

2.4.1 Microstructure morphology

SEM techniques are used to study morphological shapes, sizes and surface structures of SCM. SEM analysis of SCBA shows varied particle shapes, sizes and surface structure[9], [20]. Abdalla *et al.* [20] observed, elongated, fibrous, round, and irregular flakes of capillary pores. However, when subjected to calcination, particles became round. Additionally, Thomas *et al.* [9], realised that raw SCBA has particles of different morphology, fibrous, spherical, irregular and prismatic due to different calcination temperatures at the sugar factory furnace, ranging from 350 to 400 ^{o}C. Moreover, Xu *et al.* [27], realised that the fine particles of raw SCBA are rich in silica while the fibrous particles are more rich in carbon. The burnt (fine) particles displayed distinctively four shapes; spherical, prismatic, irregular and fibrous. Silicon-rich particles were prismatic and irregular while spherical particles contained mainly, P, Si, K, Mg, Fe, and Na elements. Carbon-rich particles were fibrous and rough in appearance. Similarly, Amin *et al.* [40], at an SCBA magnification range of X500 to X2000 realised the ground SCBA contained different particles, rounded, elongated, needle-shaped and elliptical which ranged from 10-50 µm. Following these current morphology studies, SCBA has diverse particle shapes, sizes and surface structure. The typical SCBA microstructure is illustrated in Figure 2.1 [1].

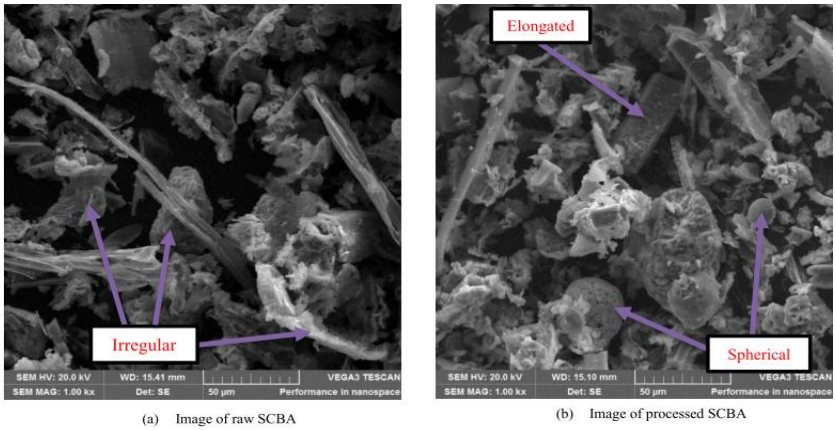

(a) Image of raw SCBA

(b) Image of processed SCBA

Figure 2. 1: Microstructure morphology of raw and processed SCBA.

(Produced with permission from Civil Engineering Journal (C.E.J)-Iran, Appendix E)

2.5 STRENGTH OF DEVELOPED CONCRETE FROM VARYING SUGARCANE BAGASSE ASH DOSE

2.5.1 Compressive strength

SCBA concrete compressive strength differs greatly from several researchers and with optimised strengths at different SCBA dosages. Subramaniyan and Sivaraja [23], researching the assessment of SCBA concrete on mechanical properties obtained optimum compressive strength at 5 % cement replacement, further increase of SCBA lowered compressive strength. Similarly Akil *et al.* [4], in studying SCBA as partial cement replacement showed that blended mix had higher compressive strength against control mix. Moreover, cement substitution was possible to 10 % with optimal SCBA concrete strength achieved at 6 %. Likewise Jagadesh *et al.* [34], on evaluating SCBA concrete mechanical properties concluded, that for cylindrical specimens the compressive strength was higher by 28 % compared to the control mix of 10 % cement substitution. In addition, up to 20 % cement replacement was possible.

Correspondingly, Praveenkumar and Sankarasubramanian [41], when investigating SCBA-blended concrete performance determined that 10 % of cement substitution optimised the concrete strength at day twenty-eight of curing. Similarly, studies carried out by Cordeiro *et al.* [18], on investigating the pozzolanic properties of ultrafine SCBA produced by controlled burning, determined that SCBA burnt at 600 ^{o}C had lower compressive strength on day one, moderate at day three and maximum at day twenty-eight of curing. This observation of delays in strength development in early ages and a significant increase in late ages was also confirmed by [41], [42]. Moreover, Amin *et al.* [40], working on developing a sustainable engineered cementitious composite, found that in addition to SCBA, the compressive strength was lowered on day fourteen of curing and significantly enhanced at later days with 10 % SCBA exhibiting maximum strength among all at 3 % higher on day twenty-eight.

Bersisa and Zekaria [33], working on the assessment of mechanical properties of SCBA concrete determined that SCBA reduces early-age mechanical performance. Furthermore, on compressive strength, the concrete containing SCBA dosages of 6.50 % and 13.0 % exceeded those of the control mix by 3.46 % and 6.64 %, respectively. The maximum strength gain was realised at 13 % of the SCBA dose. However, on replacing cement with SCBA up to 20 % concrete strength development was reduced. Similarly, Girma and Asteray [35], researching high-strength concrete made from SCBA concluded that SCBA dosages increase compressive strength at an early age of curing. This is in contrast with Bersisa and Zekaria, [33]. However, at day twenty-eight of curing, up to 10 % SCBA was noted to improve the compressive strength, contrasting the findings of Bersisa and Zekaria, [33], which stood at 13 %. Correspondingly, Tarekegn [43], researching blended SCBA concrete, established that compressive strength decreases as the replacement percentage increases, with optimised compressive strength at 10 % cement replacement on day twenty-eight of concrete curing.

Bheel *et al.* [24], realised the optimum compressive strength at 10 % SCBA which was greater than the control mix by 9.43 % at day twenty-eight of curing. Their study further showed that the addition of SCBA lowered the strength. Abdalla *et al.* [1], working on properties of SCBA blended with silica fumes, realised a significant increase in compressive strength at lower SCBA dosages with an increase of 6 % in strength at day twenty-eight. However, higher dosages led to strength decrease. A high early strength of 25 MPa was obtained on day three with up to 30 % SCBA addition. The optimum compressive strength above 60 MPa was observed at day twenty-eight with 10 % SCBA inclusion.

2.5.2 Flexural strength

Flexural strength could be defined as the resistance to bending of a material on pressure application. This helps to ascertain the product's area of application, longevity and safety of the end user. SCBA

improve the cement paste density by acting as a micro-filler. The paste and aggregate bond is therefore enhanced to improve the strength of concrete and hence its ability to resist bending [41].

Rebari *et al.* [26], showed that the addition of SCBA to concrete consistently decreased its flexural strength. This was in great contrast with other researchers. Firstly, Praveenkumar and Sankarasubramanian [41], observed that flexural strength increased gradually from 2.09 to 3.08 % for SCBA dosage of 5 to 10 % respectively with optimised flexural strength at 10 % SCBA. Secondly, Amin *et al.* [40], noted 10% SCBA dosage demonstrated higher flexural strength with results indicating 6.6 % higher flexural strengths at day twenty-eight of curing. Thirdly, Bersisa and Zekaria [33], reported that early-day flexural strength increased significantly for 6.5 % and 13 % SCBA dosage by 6.38 % and 17 % respectively on day twenty-eight of curing.

Further, Tarekegn *et al.* [43], observed that at 5 % SCBA dosage, the flexural strength was optimised at day fourteen and twenty-eighth day of curing and a further increase of SCBA drastically reduced the strength. Finally, Abdalla *et al.* [1], noted that after day twenty-eight of curing, 10 % SCBA showed the highest flexural strength of 8 % greater than the control. However, 20 % SCBA indicated lower flexural strength and mixes with 30 % and 40 % SCBA indicated the lowest strengths of 23 % and 28 %, respectively.

Hence, SCBA increases the flexural strength at different dosages and depending on the mineral compositions or mix design ingredients. However, it may also lower the flexural strength as was noted by Rebari *et al*. [26], depending on other additives to the mix design. The SCBA dosage for optimum strength and the maximum allowable dosage for both flexural and compressive strength are indicated in Table 2.5.

Table 2. 5: SCBA dosage for optimum strength and the maximum allowable dosage.

SCBA dosage for optimum strength (%)	Maximum allowable SCBA dosage (%)	Reference
6	10	[4]
10	30	[20]
5	-	[23]
10	-	[24]
15	25	[26]
13	-	[33]
10	20	[34]
10	-	[35]
10	-	[40]
10	-	[41]
10	-	[43]

In Kenya, SCBA is available in the western and coastal regions of the country. Abdalla *et al.* [1], [20] studied heat insulation and mechanical strength of concrete made from SCBA sampled at Ndhiwa (Kenya Western Region), with SCBA chemical constituents shown in Table 1.2. In their study, which focussed on the replacement of PC with the incorporation of SCBA and silica fumes (SF) as the SCMs, they partially replaced PC with SCBA from 10 to 50 % in steps of 10 with the incorporation of 25 % SF and super-plasticizer in the mix design. Good heat insulation and stability at temperatures of up to 600 ^{o}C at 50 % PC replacement and optimal concrete strength at 10 % PC replacement were observed. Therefore improving on the scope of study of the Kenya SCBA as an alternative SCM, this study focussed on mechanical properties of concrete containing SCBA as the only SCM in the mix design. Since SCBA is relatively rich in silicon dioxide [18], which is abundantly found naturally as quartz in the coastal areas, the sugarcane milling plants located along the Kenya coast were of interest to this study.

Considering the above studies, flexural and compressive strength show similar trends in strength development as indicated in Table 2.5. For optimum flexural and compressive strength, SCBA dosage varies with researchers. Therefore it could be concluded that flexural and compressive strength experience the same hydration process. These hydration processes are affected by the mineral compositions of the SCBA. These mineral compositions are affected by geographical locations, calcination temperature, type of soil used to farm sugarcane, crop type, and underground water.

2.6 SUMMARY OF LITERATURE REVIEWED

SCBA concrete strength could be influenced by various factors such as shape and size of SCBA, adopted design mix, materials' composition, SCBA dosage and curing methods. The literature reviewed showed that the optimum SCBA concrete mechanical properties (compressive and flexural strength) are realised at SCBA dosages of 5 %, 6 %, 10 %, 13 %, 15 % and 30 %. This difference is attributed to the mineral constituents leading to different hydration products whose quality (strength and durability) differs. Moreover, SCBA has been vouched as an alternative SCM owing to the good quality of its concrete. However, to qualify it as a pozzolan (SCM) it needs to be subjected to further preparations to maximize its silica, aluminium and iron content.

These preparations to increase its pozzolanicity have differed in several aspects from one researcher to another. These are as follows:

i. Pre-heating (calcining) to a certain temperature before incorporation into the mix design.
ii. Grinding and grading to a particular particle size before incorporation in the mix design.
iii. Pre-heating (calcining) and then grinding before incorporation in the mix design.
iv. Mixing SCBA with some additives such as silica fumes and waste products of organic nature, coffee husk ash, and rice husk ash, before incorporation into the mix design.

v. As collected SCBA incorporated into the mix design without any pre-treatment.

All these pre-treatments brought out concrete products with optimised properties at different SCBA dosages in the concrete design mix. Therefore, results obtained while using SCBA as an alternative SCM depend on myriads of variables hence one cannot conclusively state what may evolve from SCBA as an alternative SCM.

CHAPTER THREE: METHODOLOGY

3.1 INTRODUCTION

The chapter shows the way this research was conducted. The standards used were Indian Standard (IS), British Standards (BS) and the American Society for Testing and Materials (ASTM). The investigation consisted of materials description of the test methods conducted, such as specific gravity, flexural and compressive strength. The tests were divided into three subclasses, as per the specific objectives, chemical composition investigations, microstructure morphology and hardened concrete properties.

3.2 RESEARCH DESIGN

This research design involved experimental methods for data collection and hence their quantitative analysis using Origin-pro 2024b graphing and analysis software. The research design in Figure 3.1 was adopted.

3.3 MATERIALS SAMPLING

3.3.1 Fine aggregates

The fine aggregates here refer to the small-sized particles of sand, usually passing through a 4.75 mm sieve and retained on a 75-micron sieve **IS 10262-2009** [44]. The sand used was from the Kitui River bed, in Kenya. The physical properties are shown in Table 3.1.

3.3.2 Coarse aggregate

The CA used in this project was crushed stones from Ndarugo Quarry Kiambu, Kenya. The physical properties, were as indicated in Table 3.1.

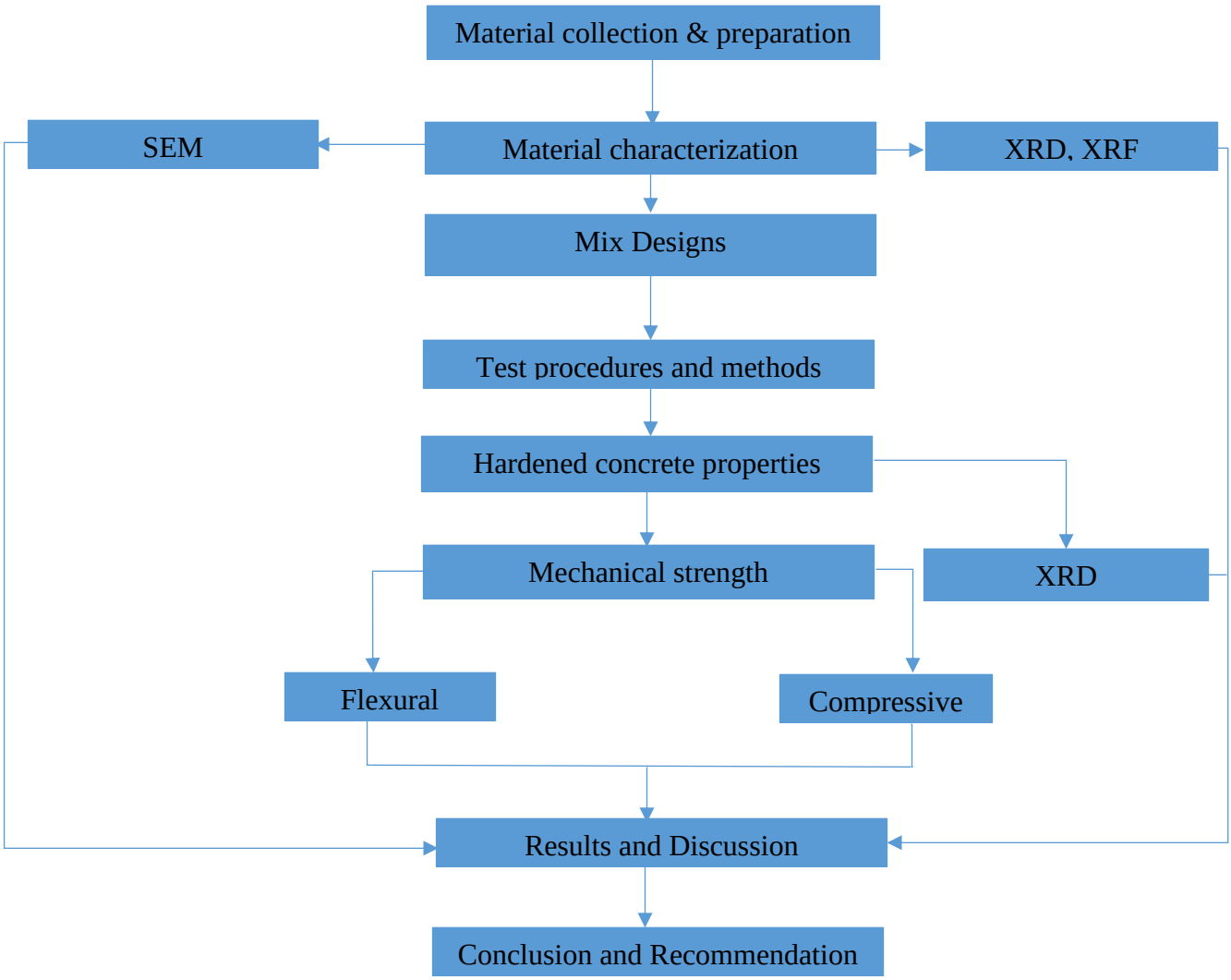

Figure 3. 1: Simplified flow chart of methodology.

Table 3. 1: Physical properties of fine and coarse aggregates.

Name	**Standard**	**Fine aggregate**	**Coarse aggregate**
Colour and texture	-	Caramel and texture	Grey and smooth
Shape of particles		rounded	angular
Specific gravity	IS 2386-(1) and (3)	2.64	2.84
Max. Nominal aggregate size	IS 383-2016	4.75 mm	20 mm

3.3.3 Mixture water and Portland cement

Figure 3. 2: The photo camera image of the as-received Bamburi Powerplus CEM I/42.5N.

The mixture water used in casting and curing was tap water unless otherwise specified by the standard.

Bamburi Powerplus CEM I/42.5N is a common Portland cement used in Kenya and based in the Athi River. It is the cement which was used in this study since it's made of pure clinker, 95 - 100 %. The physical properties, chemical properties/mineral compositions, hydration phases analysis and microstructure morphology of this cement were determined in this project and are as presented in Table 3.2, Table 4.2, Figure 4.16 and Figure 4.4 respectively. The image of the as-received cement used in this project is shown in Figure 3.2. The cement used did not undergo any further processing.

3.3.4 Sugarcane bagasse ash

The SCBA used in this study was sampled at KISCOL along the coastal area of Kenya. It was the bottom furnace ash. It is an inert material which does not take part in any reaction on itself unless mixed with other compounds [33]. The sampled SCBA was sieved using a 1.18 mm sieve as per BS 410-1:200 as

indicated in Figure 3.3(a). This removed the sand which had mixed with SCBA at the factory furnace bottom, the sand may have been generally picked with the sugarcane plants from the sugarcane plantation fields. The sieved SCBA was oven-dried for 24 hrs at 105 ^{o}C, using GenLab Materials Testing Oven, MTO /200F, with an element rating of 2,250 W and fan-assisted circulation. This pre-heating treatment was done since;

i. Oven-drying the SCBA, ensured that the SCBA material was in a dry state by removing moisture, hence preventing any undesired side reactions during subsequent heating in the Barnstead Thermolyne muffle furnace.

ii. On moisture removal due to pre-heating in the oven, it was ensured that the SCBA initial conditions were standardized by achieving a consistent starting condition for all particles within the sample. This was to allow for more reproducible and more accurate results thereafter.

iii. Explosive reactions do happen in furnaces, hence this was done to allow for gradual removal of any volatile substance which may have been introduced into the SCBA either at the factory through the factory sugar processing stages or in transit to the laboratory. Hence pre-heat treatment reduces the risk of explosive reactions during furnace treatment.

iv. Dry samples generally have better heat transfer characteristics than wet or moist samples [45], [46], [47]. This ensured that the furnace was more effective in uniformly heating the SCBA samples hence leading to a better control of the heating process and improved heat transfer within the SCBA samples.

The oven-dried SCBA was then loaded into the steel muffle furnace tray, Figure 3.3 (b) and then re-calcined at 600 ^{o}C for 3 hrs in a Barnstead Thermolyne furnace, model F85930*, 240 V, 20A, 6379 W element rating. The re-calcination was done in two stages;

i. The SCBA was calcined for 1 hr (Figure 3.3 (c)) cooled to room temperature (Figure 3.3 (d)) and thoroughly mixed to expose the SCBA which was lying on the bottom tray (Figure 3.3 (e)).
ii. The resulting mix was then re-calcined at the same temperature (600 ^{o}C) for the remaining 2 hrs (Figure 3.3 (f)). The re-calcined SCBA was then left to cool to room temperature.

Thereafter the already cooled SCBA was re-sieved at 75 μm to get processed SCBA which was tagged SCBA-600 as indicated in Figure 3.3(g). The SCBA-600 is light brown. This is properly illustrated in the schematic diagram in Figure 3.4.

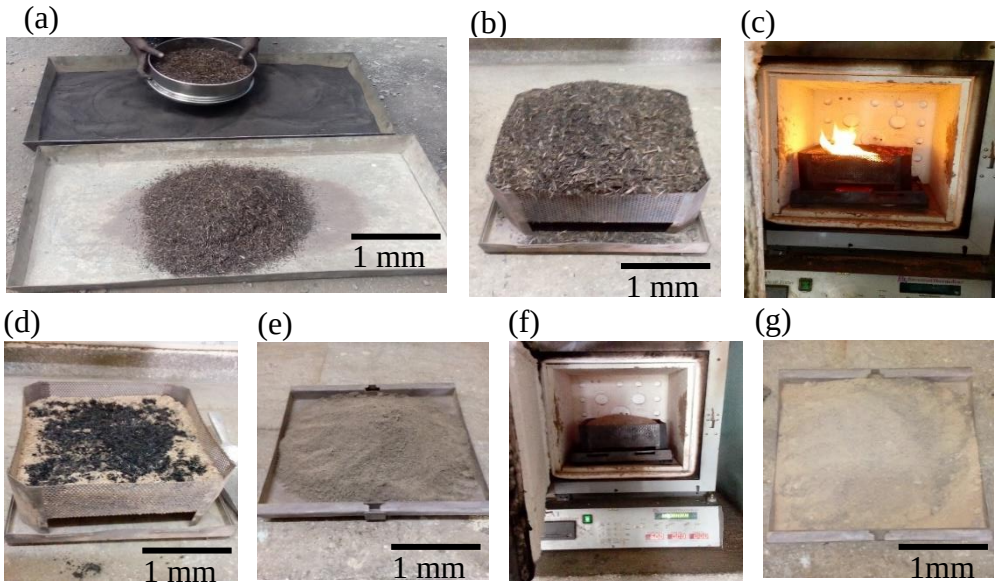

Figure 3. 3: The photo camera images showing different stages in SCBA processing.
(a) Sieving as received SCBA at 1.18mm, (b) Loading raw SCBA to the tray ready for calcination, (c) Calcining raw SCBA in a muffle furnace at 600 ^{o}C, (d) Calcined raw SCBA for 1 hr allowed to cool at room temperature, (e) Thoroughly mixed calcined raw SCBA, (f) Re-calcining raw SCBA for the remaining 2 hrs, (g) Processed SCBA (SCBA-600) allowed to cool at room temperature after 2 hrs.

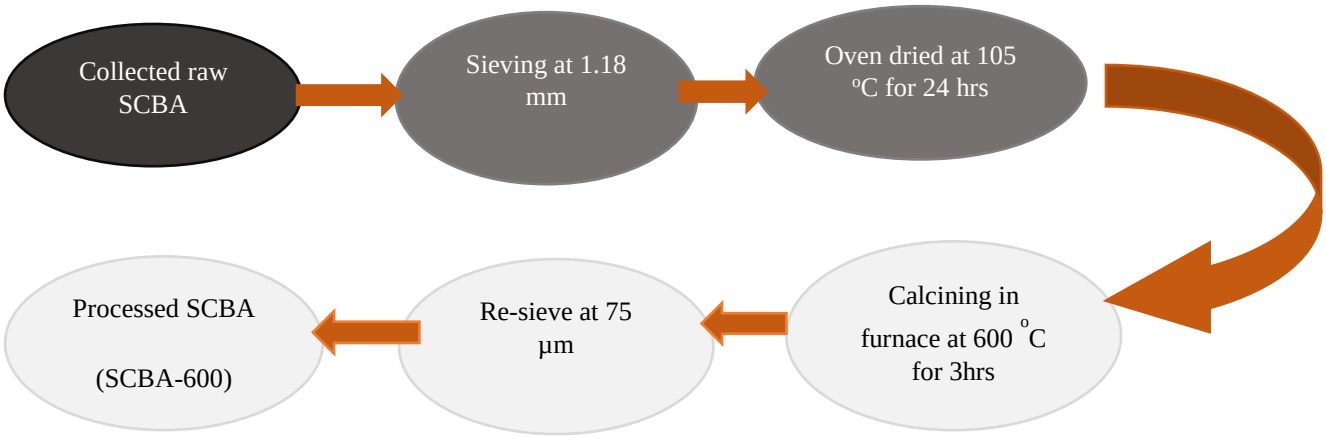

Figure 3. 4: SCBA sample preparation.

Table 3. 2: The physical properties of SCBA-600 and Bamburi Powerplus CEM I/42.5N cement.

Name	Standard	As received SCBA	SCBA-600	CEM I/42.5N
Colour	-	Black	Light off white	Grey
Specific gravity	IS 4031-(11)	-	2.31	3.15

The physical properties of SCBA-600 are as in Table 3.2. The chemical properties are as in Figure 4.6. The colour of SCBA changed from black to brown as indicated in Figure 3.4 due to carbon content reduction on calcination in the muffle furnace at 600 ºC.

3.4 MIX DESIGN

In designing this mix, **IS 10262-2009** [44] and **IS 456** [48] was adopted. The aggregates and binders' physical properties were as determined in Tables 3.1 and 3.2. The water binder ratio was kept constant in all the mixes, at 0.5. Standard strength concrete of characteristic strength (f_{ck}) M25 was designed for a mild exposure environment. The quantity of the mixed materials is shown in Tables 3.3 to 3.5. The mix design was for four cubes and 1.25 % to compensate for any wastage of materials.

Table 3. 3: Mix proportion for control mix (SCBA-0).

Concrete mass (kg/m^3)		Concrete mass in kg per 0.016878 m^3 (4 cubes + 1.25% waste)	
Cement	372.00	372.00 x 0.016878	6.28
Water	186.00	186.00 x 0.016878	3.14
CA	1225.52	1225.52 x 0.016878	20.68
FA	698.23	698.23 x 0.016878	11.78
W/C		0.5	

Table 3. 4: Mix Proportion with SCBA doses (kg/m^3).

Mix Id	% replacement	SCBA	Cement	Water	FAg	CA	W/C
SCBA-0	0.0	0.00	372.00	186.00	698.23	1225.52	0.50
SCBA-10	10.0	37.20	334.80	186.00	694.21	1218.47	0.50
SCBA-20	20.0	74.40	297.60	186.00	690.20	1211.43	0.50
SCBA-30	30.0	111.6	260.40	186.00	686.19	1204.39	0.50

Table 3. 5: Mix proportion with SCBA dose kg/ 0.016878 m^3.

Mixt Id	% replacement	SCBA	Cement	Water	FAg	CA	W/C
SCBA-0	0.0	0.00	6.28	3.14	11.78	20.68	0.50
SCBA-10	10.0	0.63	5.65	3.14	11.71	20.57	0.50
SCBA-20	20.0	1.26	5.02	3.14	11.64	20.45	0.50
SCBA-30	30.0	1.90	4.39	3.14	11.58	20.32	0.50

3.5 TEST SETUP AND PROCEDURE

3.5.1 Mixing, vibrating, casting and curing

These were carried out as per ASTM C-192 [49]. Machine mixing was done in four batches by the percentage of the SCBA dose, each batch had a different dose of SCBA (0, 10, 20 and 30 %). The processed SCBA (SCBA-600) was first dry-mixed with Portland cement until a homogenous blend was

obtained. The shovel was used to thoroughly blend the dry components. This pre-mixing step helped in breaking up clumps and ensured an even distribution of the SCBA within the Portland cement. This homogenous blend constituted the binder material.

Lubrication of the mixer, (Figure 3.5 (a)), was done using additional water, to prevent the machine from absorbing the calculated mixture water. Coarse aggregate and some of the calculated mixing water were then added and the rotation of the mixer started. This rotation was done for 5 mins until all the course aggregates were moist. Fine aggregates (sand), binder (a dry blend of Portland cement and SCBA dose) and water were then added, and mixed for 4 mins. The composite was then allowed to rest for 4 mins, after that, a final rotation was done for 3 mins to get mixed concrete. The mixed concrete was then deposited in a damp and clean mixing pan and a trowel was used in remixing it to uniformity. The slump was then determined using the ASTM C 143 standard method. Using a scoop, concrete was then placed into the moulds (150 mm cubes and 500 x 100 x 100 mm prisms) to half level and consolidated using an external vibration Table (Figure 3.5 (b)). The placing was then done to the top level and vibration was done up to when the specimen's top level became smooth, with no air bubbles breaking the top surface. Moulds were then covered with plastic to prevent moisture loss, and demoulded after 24 hrs. The specimens were then moist cured at room temperature and pressure (RTP) by using water curing tanks (Figure 3.5 (c)). The specimens (Figure 3.5 (d)) were then removed from the tank 1 day before conducting the tests.

After twenty-eight days of curing, the hardened concrete was tested for the hardened concrete physical properties, mainly; compressive strength and flexural strength. This was done according to ASTM C-39 [50], and ASTM C78-00 [51] standard procedures respectively. The total concrete cast was thirty-two concretes. The sixteen cubes of 150 mm were for compressive strength determination and sixteen prisms measuring 500 × 100 × 100 mm for flexural strength determination.

Figure 3. 5: The photo camera images showing the test set-up and procedure.
(a) Concrete mixer, (b) Ready oiled moulds on the vibrating table, (c) Cubes inside a curing tank (twenty-eight days curing), (d) Cubes ready for compressive test.

3.5.2 Compressive strength

The compressive strength was carried out as per ASTM C-39 [50] and BS EN 12390- 03 [52]. The control group Universal Tensile Machine (UTM) was used. The model of the control group UTM used for compressive was 50-C34L2. The illustration is indicated in Figure 3.6. The guiding equation is shown in Equation (3.1) [50].

$$\delta = \frac{\text{ultimate load } (\mu)}{\text{cross-sectional area } (a)} \quad N/mm^2 \qquad (3.1)$$

Where; δ – Compressive strength

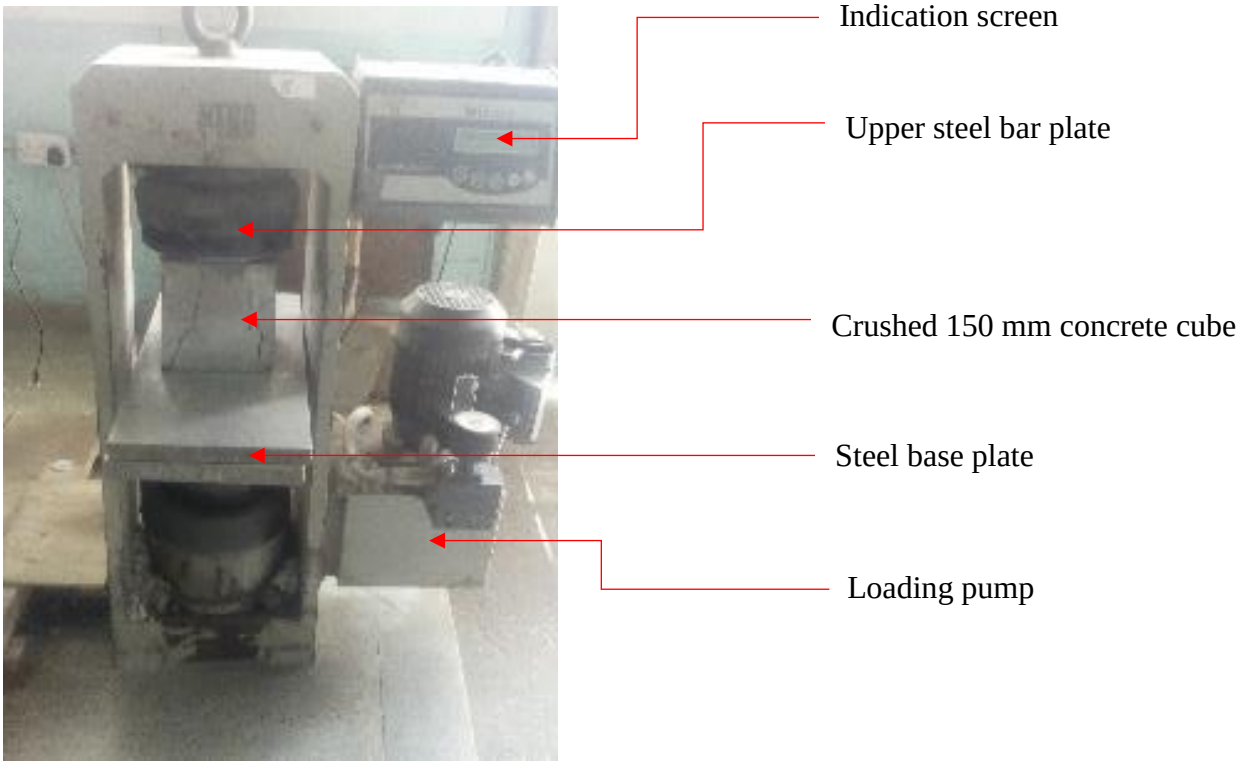

Figure 3. 6: The photo camera image of UTM assembly for compressive strength test.

3.5.3 Flexural strength

The flexural strength was carried out as per the procedure in ASTM C78-00 [51]. The UTM model 50-C3012 of high stiffness flexural frame of 350 kN cap was used. The test illustration is shown in Figure 3.7. This is a three-point bending test with the guiding Equation (3.2) [51].

$$\delta = \frac{3FL}{2WD^2} \quad N/mm^2 \tag{3.2}$$

Where;

F- Failure load, L- Specimen length, W- Specimen width and D- specimen depth

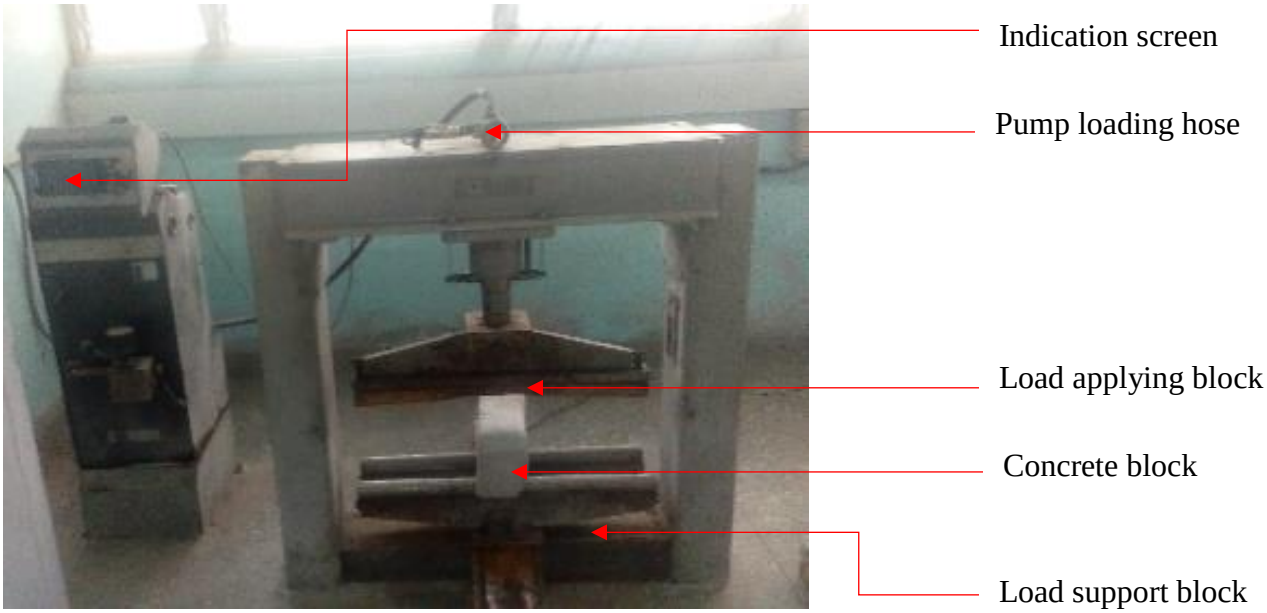

Figure 3. 7: The photo camera image of UTM assembly for flexural strength test.

3.6 CHARACTERIZATION METHODS

Three pieces of equipment were used in characterizing the sampled materials depending on the properties of focus, XRD, SEM/EDX and XRF.

3.6.1 X-Ray Diffraction

For the XRD analysis, the Shimadzu RD-7000 X-Ray Diffractometer of Makerere University was used. The X-ray radiation used was CuKα, λ=1.54 Å. The machine was operated at a continuous scan mode with a scan angle (2θ) range of 10-90 º at a step size of 0.02 º and a scanning speed of 2.00 º/min. The energy was selected at 40 kV with a current of 30 mA. The sample holder configurations, the divergence slit (DS), scattering slit (SS) and receiving slit (RS) were positioned at 1.0 º, 1.0 º and 0.3 mm, respectively. Powdered samples of raw SCBA, processed SCBA, cement and developed SCBA concrete were used. These gave different diffraction peaks indicating different minerals composition.

The diffraction peaks in XRD were typically observed due to the nature of X-ray interaction with the crystal lattice. The phenomenon is governed by Bragg's law indicated in Equation (3.3), which describes the conditions for constructive interference of X-rays scattered by crystal planes.

$$2d\sin(\theta) = n\lambda \tag{3.3}$$

Where;

- d is the inter-planar spacing of crystal planes,
- θ is the angle of incidence (and reflection) of the X-ray beam,
- n is an integer (the order of reflection),
- λ is the wavelength of the X-ray.

3.6.2 Scanning Electron Microscope

For microstructure morphology, of raw SCBA, processed SCBA, cement and developed concrete, a scanning electron microscope (SEM) of Zeiss sigma series, sigma 300VP of Makerere University was used (Figure 3.8). The samples were first chromium coated for conductivity at a thickness of 0.2 nm (Figure 3.8a). The SEM was then de-vacuumed (Figure 3.8b) and the sample was loaded (Figure 3.8c). The EHT was set to 10.0 kV and the secondary electron (SE) detector was selected since it provides a good signal-to-noise ratio even at long working distances (WD).

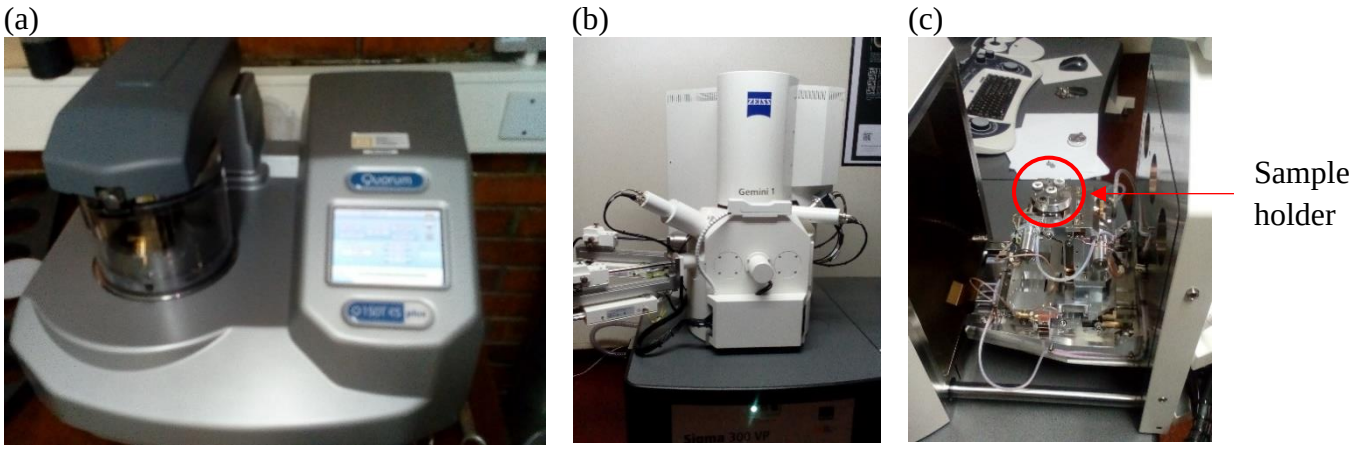

Figure 3. 8: Sample coating and loading into the SEM, camera images.
(a) Sample coating at 0.2 nm, (b) Venting SEM, Zeiss sigma 300VP, to atmospheric pressure (vacuum release) to allow sample loading, (c) Loading sample to SEM.

3.6.3 Energy Dispersive X-ray

EDX is an analytical method, that is used to determine elemental composition and operates on the concept that, each voltage pulse directly relates to the energy of the incoming X-ray photon [20]. The SE detector was used for getting the EDX images. The detector collector base was set to 300 V. The EDX detector was coupled with SEM, Zeiss sigma 300VP at the same operating conditions described in Figure 3.8 (a), (b) and (c).

3.6.4 X-Ray Fluorescence

The oxide composition of SCBA-600 and Portland cement was determined by an Energy Dispersive X-ray Fluorescence Spectrometer, Shimadzu EDXRF 800HS, Kyoto- Japan and Bruker XRF spectrometer. This XRF machine was sourced from Kenya at the Ministry of Roads and Transport, Materials Testing and Research Division laboratory. The powdered samples were placed in an open-end X sample cell with an outer diameter of 31.6 mm. The X-ray tube used was fitted with the rhodium (Rh) as the target. The detector type was a Si(Li) semiconductor detector. The XRF machine used is shown in Figure 3.9

Figure 3. 9: Energy dispersive X-ray fluorescence spectrometer.

The characterization of sugarcane bagasse ash was carried out in two phases;

i. Raw sugar cane bagasse ash, this is the as-received/collected SCBA from the KISCOL furnace bottom, without any pre-treatment, which was subjected to characterization, through XRD and SEM/EDX.
ii. Processed sugar cane bagasse ash. The raw SCBA was undertaken through some pre-treatment as specified in the methodology, with illustrations in Figure 3.3 (a-g) and Figure 3.4. Thereafter subjected to characterization through, XRD, SEM/EDX and XRF

CHAPTER 4: RESULTS AND DISCUSSION

4.0 INTRODUCTION

The chapter majorly focuses on the analysis of data obtained from the methods followed in chapter three and the discussion of these results. This is aimed at meeting the specific objectives stated and their comparison with the literature reviewed. And hence finding the solutions to the gaps identified from the literature reviewed. The chapter has been categorized into the following sections; materials characterizations, pozzolanicity and hardened concrete physical properties.

4.1 MATERIALS CHARACTERIZATION

4.1.1 Portland cement phase identification

Cement phases are typically identified and quantified through techniques such as X-ray diffraction (XRD) as was done in this project. The XRD patterns found were compared against the standard Inorganic Crystal Structure Database (ICSD) and different corresponding cement phases were identified when the diffraction peaks coincided. Each peak corresponded to a specific crystal plane, and the positions and intensities of these peaks were used to identify the different phases present in the Bamburi Powerplus CEM I/42.5N.

Cement is a complex matrix, and its composition varies depending on the class of cement and the specific manufacturing process, wet or dry [29]. The major cement phases as established by different researchers are alite, belite celite and millerite [39]. The Portland cement received was compared against the ICSD standards, 162744, 79551, 963, 40053, 2058, 15840,90144,26410,15325, 9863, and 16331. These correspond to various cement phases, alite, belite, celite, millerite, gypsum, hematite, illite, magnetite, moissanite, periclase, and quartz respectively. These phases were positively identified at different peak angles as indicated in Figures 4.1 and 4.2.

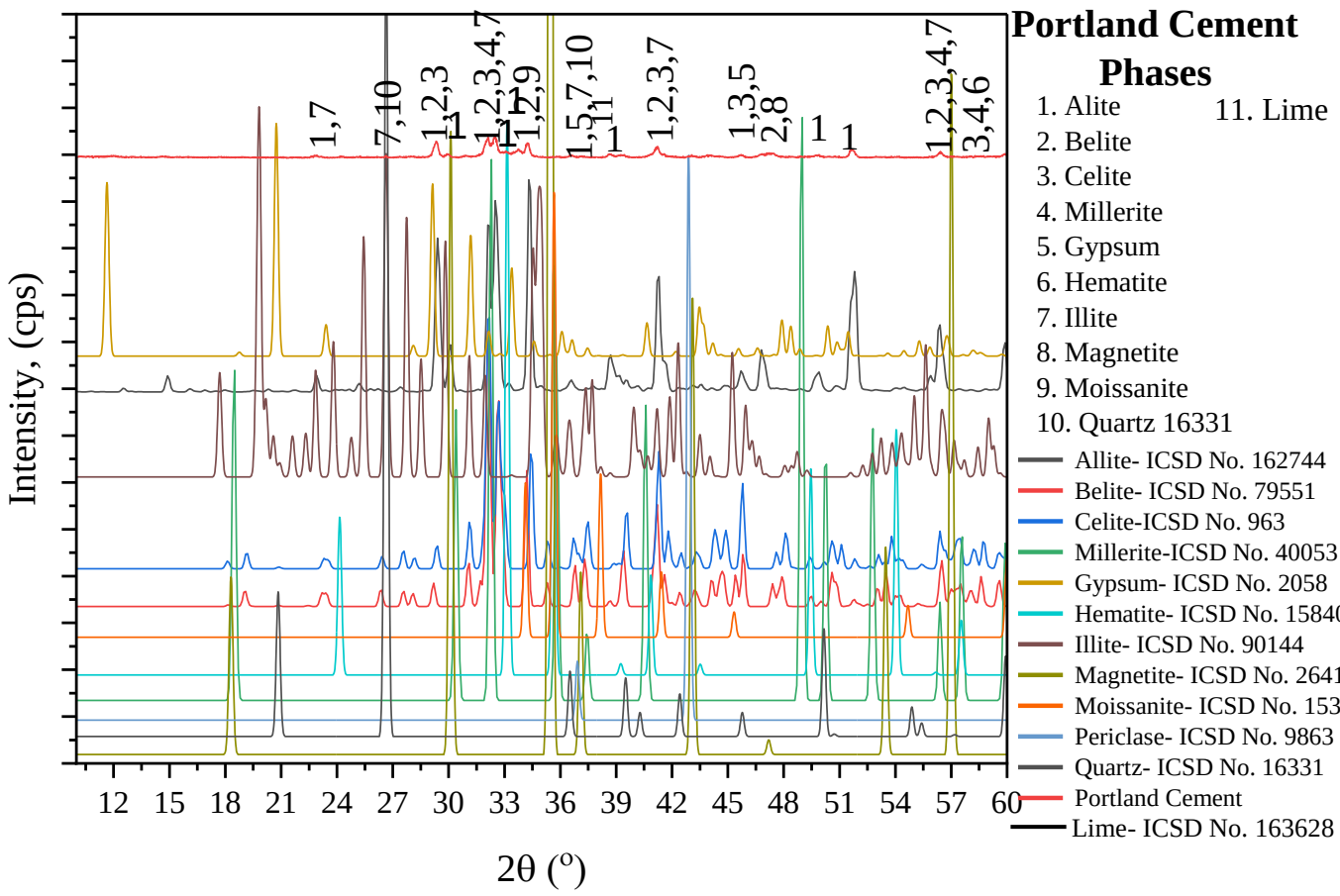

Figure 4. 1: Bamburi Powerplus CEM I/42.5N, XRD phase identification using ICSD standards.

A total of eleven cement mineral phases were identified at different peak angles as indicated in Figure 4.2. These phases are tricalcium silicate (alite) space group C1m1, dicalcium silicate (belite) space group $P12_{1/n}1$, tricalcium aluminate (celite) space group Pa-3, tetra-calcium aluminoferrite (millerite) space group Ibm2, calcium sulphate (gypsum) space group I 12/c1, calcium oxide (lime) space group Fm3m, ferric iron oxide (hematite) space group R-3/cH, clay compound(illite) space group C12/C1, ferrous-ferric oxide (magnetite) space group Fd3m, silicon carbide (moissanite) space group R3mH, and silicon dioxide (quartz) space group $P3_121$. The XRD graphs (Figures 4.1 and 4.2), indicated the presence of major and minor peaks showing major and minor mineral phases respectively.

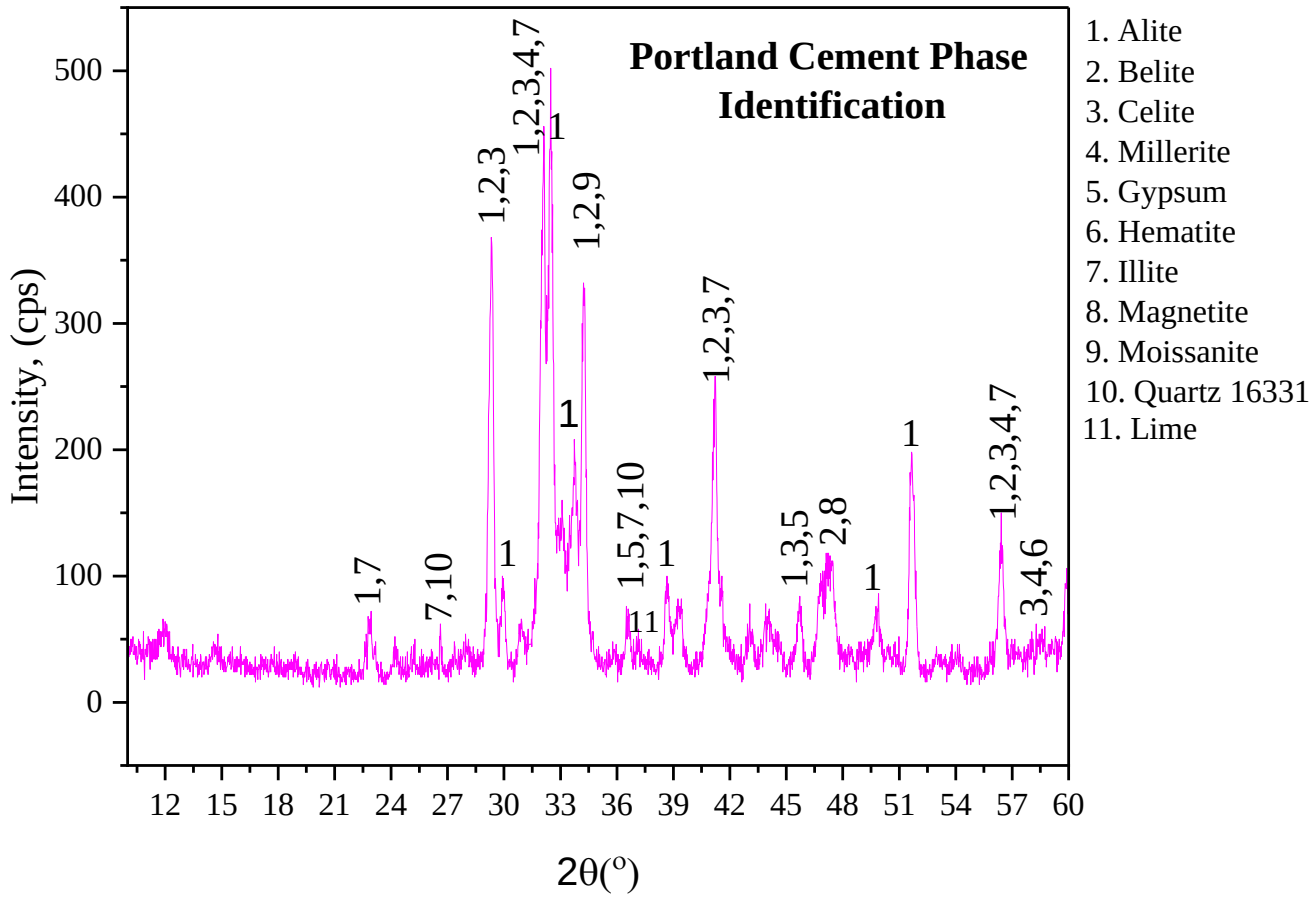

Figure 4. 2: Enlarged graph of XRD-identified phases of Bamburi Powerplus CEM I/42.5N.

The major phases are; alite at major peak angles of, 29.36, 32.08, 32.46, 34.22, 41.2, 51.66, 56.42, and belite at major peak angles of 29.36, 32.08, 34.22, 41.2, and 56.42. These are closely followed by celite at major peak angles, 29.36, 32.08, 41.2, 56.42, illite at major peak angles 32.08, 41.2, 56.42 and millerite at major peak angles 32.08, 56.42. A similar observation on the cement phases was also made in research conducted on 'observation of phase transformations in cement during hydration' [39], and transition and decomposition temperatures of cement phases – a collection of thermal analysis data, [53]. The full illustration of the Bamburi Powerplus CEM I/42.5N Portland cement mineral phases, space groups, common name, cement chemist notation (CCN), chemical formula, and phases peak angles both major and minor peaks are in Table 4.1.

Table 4. 1: Bamburi Powerplus CEM I/42.5N Portland cement XRD identified mineral phases.

Mineral phase	Space group	Name	Cement Chemist Notation (CCN)	Chemical Formula	Phase angle (2θ °)	
					Major	Minor
Alite	C1m1	Tricalcium Silicate	C_3S	$3CaO.SiO_2$	29.36, 32.08, 32.46, 34.22, 41.2, 51.66, 56.42	22.96, 29.94, 33.72, 36.54, 38.68, 45.64, 49.92,
Belite	$P12_{1/n}1$	Dicalcium Silicate	C_2S	$2CaO.SiO_2$	29.36, 32.08, 34.22, 41.2, 56.42	47.22,
Celite	Pa-3	Tricalcium Aluminate	C_3A	$3CaO.Al_2O_3$	29.36, 32.08, 41.2, 56.42	45.64, 58.26
millerite	Ibm2	Tetra-calcium Aluminoferrite	C_4AF	$4CaO.Al_2O_3.Fe_2O_3$	32.08, 56.42	58.26
Gypsum	I 12/c1	Calcium Sulphate	-	Ca_2SO_4	-	36.54, 45.64
Hematite	R-3/cH	Ferric iron oxide	-	Fe_2O_3	-	58.26
Illite	C12/C1	hydromuscovite	-	$(K,H_3O)(Al,Mg,Fe)_2(Si,Al)_4O_{10}[(OH)_2\cdot(H_2O)]$	32.08,41.2, 56.42	22.96, 26.64,36.54
Magnetite	Fd3m	Ferrous-ferric oxide	-	Fe_3O_4	-	47.22
Moissanite	R3mH	Silicon carbide	-	SiC	34.22	
Quartz	$P3_121$	Silicon dioxide	-	SiO_2	-	26.64, 36.54
Lime	Fm-3m	Calcium oxide	-	CaO	36.6	-

From the number of peaks realised on performing the XRD, Table 4.1, it can be clearly stated that minor peaks are mostly realised as the phase angles increase, and mostly after 37 ^{o} and major peaks are realised mostly below 37^{o}, at lower diffraction angles. However, we have some outliers from both cases. This observation can be mainly attributed to;

i. **Inter-planar Spacing (d):** For a given crystal lattice, the inter-planar spacing (d) is a fixed parameter. When X-rays interact with the crystal, the condition for constructive interference **(2dsin (θ) = nλ)** requires that the angle (θ) be relatively small for higher diffraction orders.

ii. **Wavelength (λ):** X-rays have short wavelengths (typically in the range of 0.01 to 10 nm). The short wavelength allows them to interact with the closely spaced crystal lattice planes, resulting in diffraction patterns at relatively small angles.

iii. **Order of Reflection (n):** In many XRD analyses, the first-order reflection (n=1) is commonly used. This means that the condition for constructive interference is satisfied at smaller angles.

Generally, in the XRD analyses, the angle at which a peak occurs is related to the spacing between crystal lattice planes, and the intensity of the peak is related to the abundance and arrangement of atoms in those planes. Therefore the major peaks identified indicate these mineral phases are in abundance in the sample analysed.

4.1.2 Portland cement elemental composition

EDX is an analytical method, that is used to determine elemental composition and operates on the concept that, each voltage pulse directly relates to the energy of the incoming X-ray photon [20]. Using the EDX detector mounted on the scanning electron microscope (SEM) of the Zeiss sigma series, sigma 300VP, the Bamburi Powerplus CEM I/42.5N matrix elements were investigated. The sample composition was found to have the absolute concentration of; oxygen (O), calcium (Ca), carbon (C),

silicon (Si), neodymium (Nd), and aluminium (Al), at 38.99, 27.33, 23, 3.31, 2.85, and 1.20 % respectively as the major elements. The minor/ trace elements were, sulphur (S), potassium (K), magnesium (Mg), strontium (Sn), tellurium (Te), manganese (Mn), iron (Fe), rubidium (Rb), titanium (Ti), sodium (Na), and zirconium (Zr) at an absolute concentration of; 0.87, 0.79, 0.34, 0.29, 0.24, 0.23, 0.23, 0.21, 0.05, 0.05 and 0.02 % respectively. This is well illustrated in Figure 4.3 and Appendix A (Table A1).

From the XRD analysis of Bamburi Powerplus CEM I/42.5N from Figure 4.1 and Table 4.1 where, silicates, ferrites, sulphates, and aluminates were identified in their different compounds, the same were also identified in their elemental nature as indicated from Figure 4.3, hence the validation of these analytical techniques employed in this study.

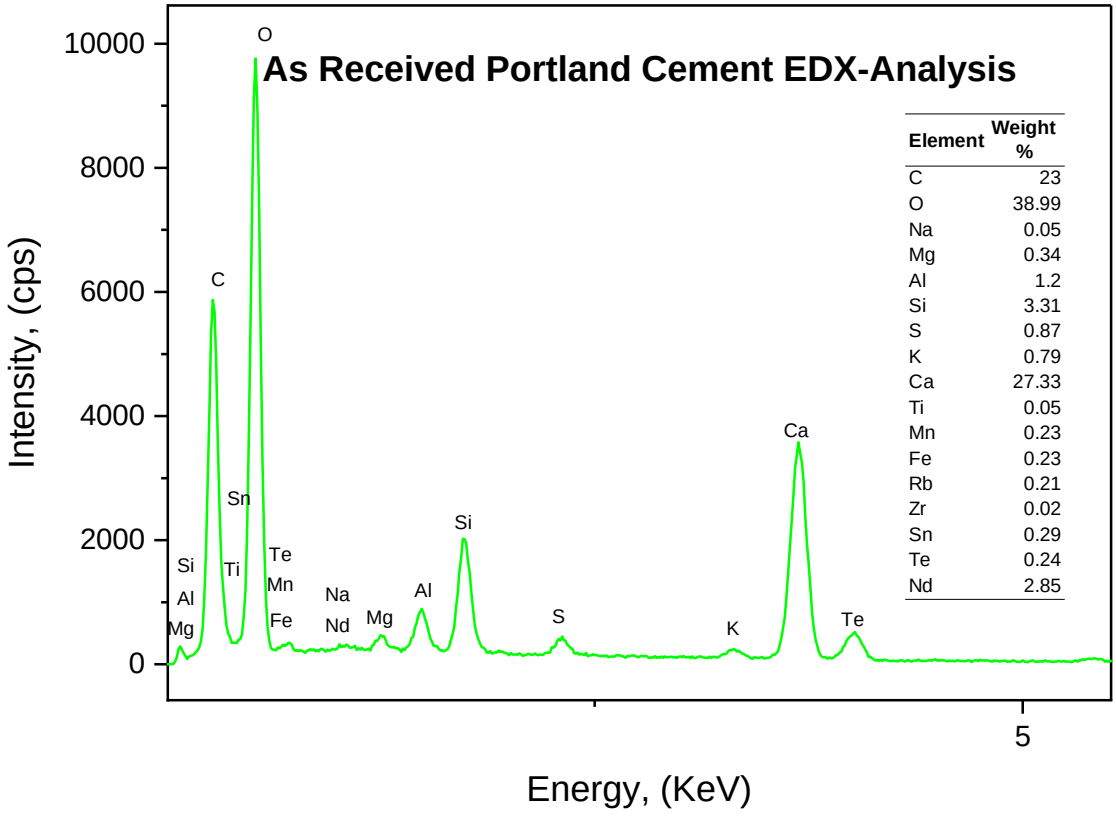

Figure 4. 3: Bamburi Powerplus CEM I/42.5N Portland cement EDX elemental analysis.

4.1.3 Portland cement microstructure morphology

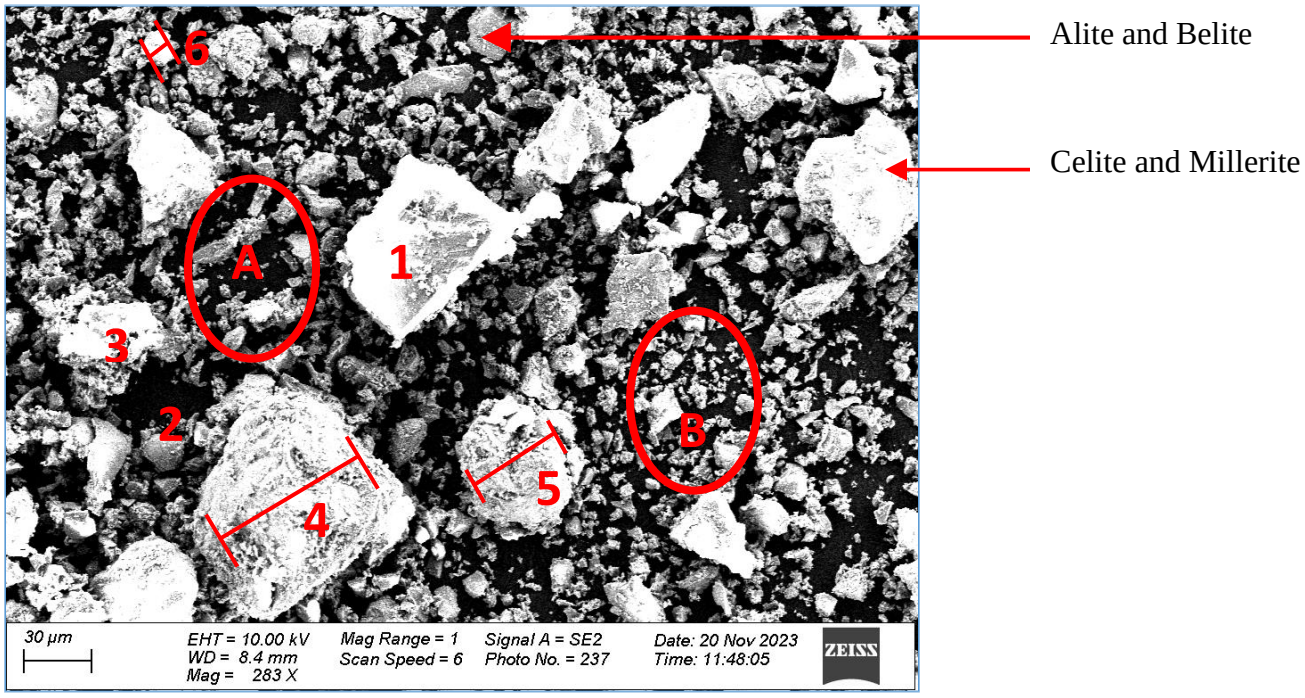

Figure 4. 4: Bamburi Powerplus CEM I/42.5N Portland cement SEM microstructure morphology.

Figure 4.4 indicates that the cement particles do not have homogenous shapes as observed at a magnification of X287. The cement particle shapes are varied, rectangular as seen in particles tagged 1, round as in 2, and irregular as in 3.

The particle sizes also differ. Particles 4, 5, and 6 are approximately, 60, 45 and 15 µm respectively. This estimation was done using image j software. The particle distribution density is not uniform. The particles along area A, are sparsely distributed while the particles along area B are densely distributed, giving an unequal inter-particle distance. The size distribution also varies widely, the bigger particles are sparsely distributed, while the smaller particles are densely distributed within the specific locality of focus. This is also evidenced by area A and area B respectively. This unequal distribution in density necessitates the need to thoroughly mix the cement particles before use.

Most of the particles are characterised by rough surface texture as can be indicated by particles 4 and 5. However, some particles such as particle 2 have smooth surfaces. The rough surfaces are associated with the voids and pores characterizing the particles' surfaces as indicated by particles 4 and 5. These rough particle surfaces can lead to good interlocking within the particles when properly mixed hence increasing the physical binding properties of cement as a material, enhancing concrete strength.

There is variation in brightness within the particles. Some particles are dull, while others are bright for example particles 2 and 1 respectively. The dull particles are most likely to be tricalcium silicates, alite and dicalcium silicates, and belite. The bright particles are most likely to be tricalcium aluminate, celite, tetra-calcium alumina-ferrite, and millerite and also since they can be easily seen to occur between the silicate phases. This confirms the observations made by researchers, Black and Brooker, working on a combined SEM - raman spectrometer for analysis of OPC clinker and Stutzman working on phase composition analysis of the NIST reference clinkers by optical microscopy and X-ray powder diffraction reference clinkers by optical diffraction [54], [55].

Since from Figure 4.4, the dull particles are more in comparison to the bright particles, and their identification as alite and belite for the dull areas and celite and millerite for the bright areas, this confirms the observation realised in Table 4.1 for XRD analysis indicating that alite and belite are more followed by celite and millerite in a given cement sample. The very large particles are most likely to be of celite and millerite phases, as we have identified these phases amount to the least number as indicated by the number of peaks realised from the XRD examination. The smaller size particles are most likely to be alite and belite phases, as they make the most number of particles in the sample as evidenced from the most XRD peaks angles observed.

4.1.4 Chemical composition for Portland cement

X-Ray Fluorescence (XRF), was used in the investigation of the Bamburi Powerplus CEM I/42.5N Portland cement chemical compositions. The machine uses the technique of polarised energy dispersion. The major chemical oxides observed were; calcium oxide (CaO), silicon dioxide (SiO_2), aluminium oxide (Al_2O_3) and iron oxide (Fe_2O_3) at the absolute concentration (wt %) of 71.592, 17.068, 3.695 and 3.095 % respectively. The minor/ trace chemical oxides observed were; potassium oxide (K_2O) as an alkali, manganese oxide (MnO), titanium oxide (TiO_2), sulphur triode (SO_3), zirconium dioxide (ZrO_2), strontium oxide (SrO), rubidium oxide (RbO_2) and Niobium oxide (NbO) at an absolute concentration of 0.371, 0.054, 0.225, 2.644, 0.033, 0.115, 0.003 and 0.005 %, respectively. These and other trace oxides are well illustrated in Table 4.2 and Appendix B (Table B1).

Table 4. 2: Bamburi Powerplus CEM I/42.5N Portland cement Chemical oxides composition.

Chemical composition	**Weight % m/m**
Silicon dioxide, SiO_2	17.068
Aluminium oxide, Al_2O_3	3.695
Iron oxide, Fe_2O_3	3.095
Potassium oxide, K_2O	0.371
Calcium oxide, CaO	71.592
Manganese oxide, Mn	0.054
Titanium oxide, Ti_2O	0.225
Sulphur trioxide, SO_3	2.644
Zirconium dioxide, ZrO_2	0.033
Strontium oxide, SrO	0.115
Rubidium oxide, RbO_2	0.003
Niobium oxide, NbO	0.005

The observation of the calcium oxide (CaO), silicon dioxide (SiO_2), aluminium oxide (Al_2O_3) and iron oxide (Fe_2O_3) as the major chemical oxides in Bamburi Powerplus CEM I/42.5N Portland, is in concurrence with the XRD analysis from Figure 4.1 and Table 4.1 as these are the major oxides which make up the major cement mineral phases identified, alite (C_3S), belite (C_2S), celite (C_3A) and millerite (C_4AF). This is illustrated in the Equations (4.2) to (4.5). These reactions take place at different clinker calcination temperatures during cement manufacturing [29].

$$2CaO+SiO_2 \longrightarrow \beta C_2S \quad (4.2)$$

$$\beta\text{-}C_2S+CaO \longrightarrow C_3S \quad (4.3)$$

$$3CaO+Al_2O_3 \longrightarrow C_3A \quad (4.4)$$

$$4CaO+ Al_2O_3+Fe_2O_3 \longrightarrow C_4AF \quad (4.5)$$

4.2 SUGARCANE BAGASSE ASH MATERIAL CHARACTERIZATION

The characterization of sugarcane bagasse ash was carried out in two phases; raw sugar cane bagasse ash, and processed sugar cane bagasse ash.

4.2.1 Raw sugarcane bagasse ash mineral composition analysis

The expected major mineral phases as observed by Abdala *et al.* [1] are quartz, cristobalite, potassium carbonate, calcium phosphate, hematite and mullite [1]. The raw SCBA used in this research was subjected to XRD characterization and XRD graphs with different peaks were obtained. These peaks corresponded to different mineral phases present.

The peaks were then matched against the ICSD standards XRD graphs to precisely identify the minerals' names.

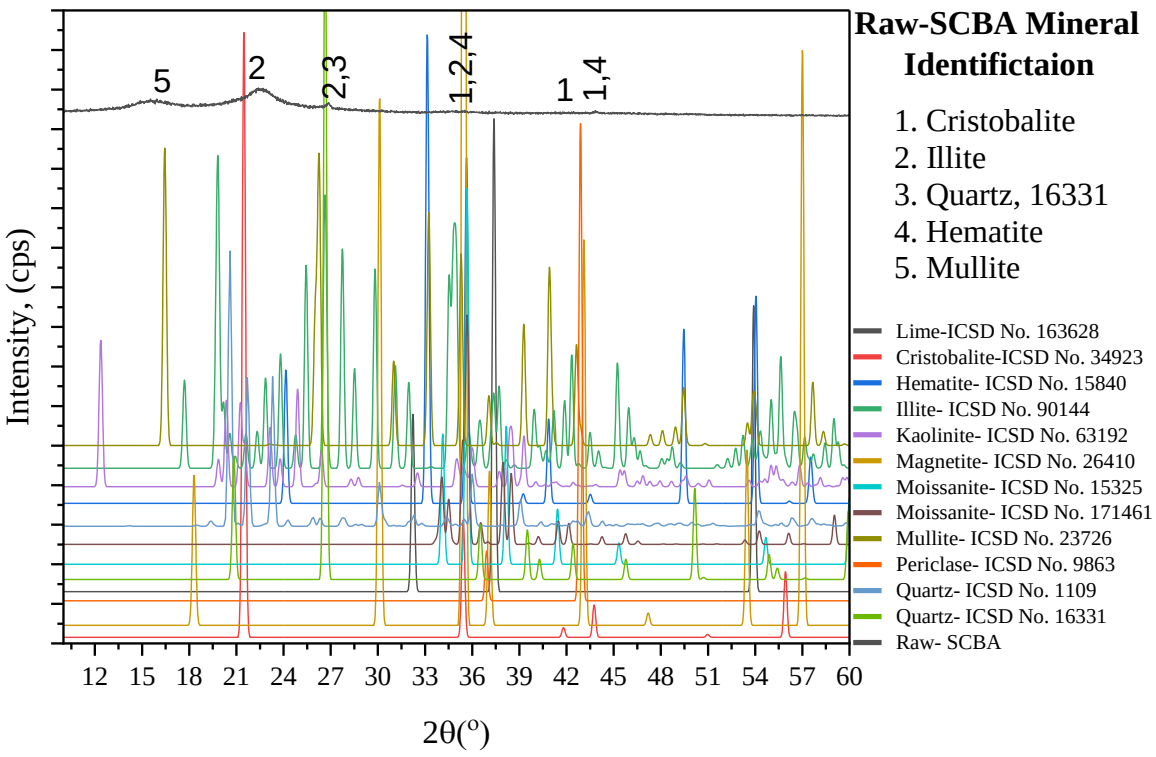

Figure 4. 5: Raw SCBA XRD phases identification using ICSD standards.

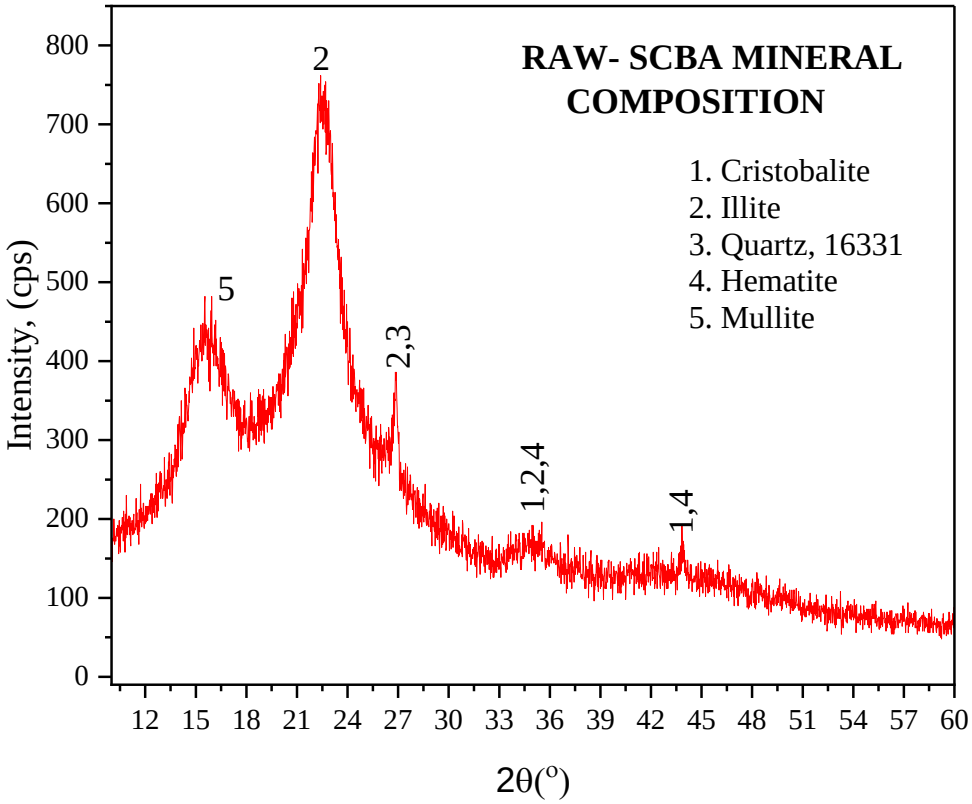

Figure 4. 6: Enlarged XRD graph showing crystallization phases of raw SCBA, mineral composition.

The ICSD No. of the standard graphs used were; 163628, 34923, 15840, 90144, 63192, 26410, 15325, 17146, 23726, 9863 and 16331; which corresponded to the mineral phases; lime, cristobalite, hematite, illite, kaolinite, magnetite, moissanite, moissanite, mullite, periclase and quartz respectively.

Some of these phases were positively identified in the raw SCBA as indicated in Figure 4.5 and Figure 4.6.

Following the XRD characterization, five major peaks were realised from the raw SCBA. These peaks showed that five major mineral phases were present in the raw SCBA. The peaks were identified as cristobalite (silica) space group Fd3-mz, illite (hydromuscovite) space group C12/C1, quartz (silicon dioxide) space group $P3_121$, hematite (Ferric iron oxide) space group R-3/cH, and mullite (porcelainite) space group Pbam. These corresponded to ICSD XRD standards, 34923, 90144, 16331, 15840 and 23726, respectively.

Illite corresponding to peak angles, 22.38, 26.84, and 35.32, was found to be a major mineral phase of raw SCBA. This was followed closely by cristobalite and hematite with similar peak angles at 35.52 and 43.84. Finally, the least phases in raw SCBA were found in quartz and mullite at the peak angles of 26.84 and 16.38, respectively.

These findings were synonymous with the observation of various researchers; Sultana and Rahman [56], when looking at the ‘characterization of calcined sugarcane bagasse sugarcane waste ash for industrial use’ and, Abdala *et al.* [1], while researching ‘mechanical properties of eco-friendly concrete made with sugarcane bagasse ash’. The raw SCBA research findings are well illustrated in Table 4.3.

According to Table 4.3, the presence of silica in the mineral phase of cristobalite and quartz, the presence of iron oxide in the mineral phase of hematite and the presence of aluminium oxide in the mineral phase of mullite and illite as the major minerals' composition of the raw SCBA, clearly indicates that SCBA

has semi cementitious properties hence pozzolanic. These three mineral phases indicate the materials' pozzolanicity [32].

Table 4. 3: The raw sugarcane bagasse ash mineral composition at different peak angles.

Mineral phase	Space group	Name	Chemical Formula	Peaks angle (2θ º)
Cristobalite	Fd3-mz	silica	SiO_2	35.52, 43.84
Illite	C12/C1	hydromuscovite	$(KH_3O)(Al,Mg,Fe)_2(SiAl)_4O_{10}[(OH)_2(H_2O)]$	22.38, 26.84, 35.32
Quartz	$P3_121$	Silicon dioxide	SiO_2	26.84
Hematite	R-3/cH	Ferric iron oxide	Fe_2O_3	35.52,43.84
Mullite	Pbam	porcelainite	$3Al_2O_3.2SiO_2$	16.38

4.2.1.2 Elemental composition for raw sugarcane bagasse ash

The EDX analysis of raw SCBA carried out using, the EDX detector of scanning electron microscope (SEM) of Zeiss sigma series, sigma 300VP, is shown in Figure 4.7 and Appendix A (Table A2). The major elements found in raw SCBA are carbon (C) and oxygen (O) at the absolute concentration of 85.75 and 10.26 %. The minor/trace elements identified are; sodium (Na), magnesium (Mg), aluminium (Al), silicon (Si), sulphur (S), potassium (K), titanium (Ti), manganese (Mn), iron (Fe), rubidium (Rb), zirconium (Zr), tin (Sn), tellurium (Te) and Neodymium (Nd) at absolute concentration of; 0.09, 0.19, 0.16, 0.13, 0.07, 0.77, 0.14, 0.18, 0.07, 0.12, 0.1, 0.3, 0.28, and 1.43 % respectively.

The elemental analysis also showed the presence of silicon, aluminium, and iron elements which were similar to the XRD data analysis. The silicon, aluminium and iron elements were at very small absolute weight concentration percentages. This indicates the need to subject the raw SCBA to further heat treatment to maximize its properties. The factory boiler furnace temperature of about 400 - 500 ºC at which they were calcined has been proved by this EDX analysis, not to be enough to optimise its materials' quality.

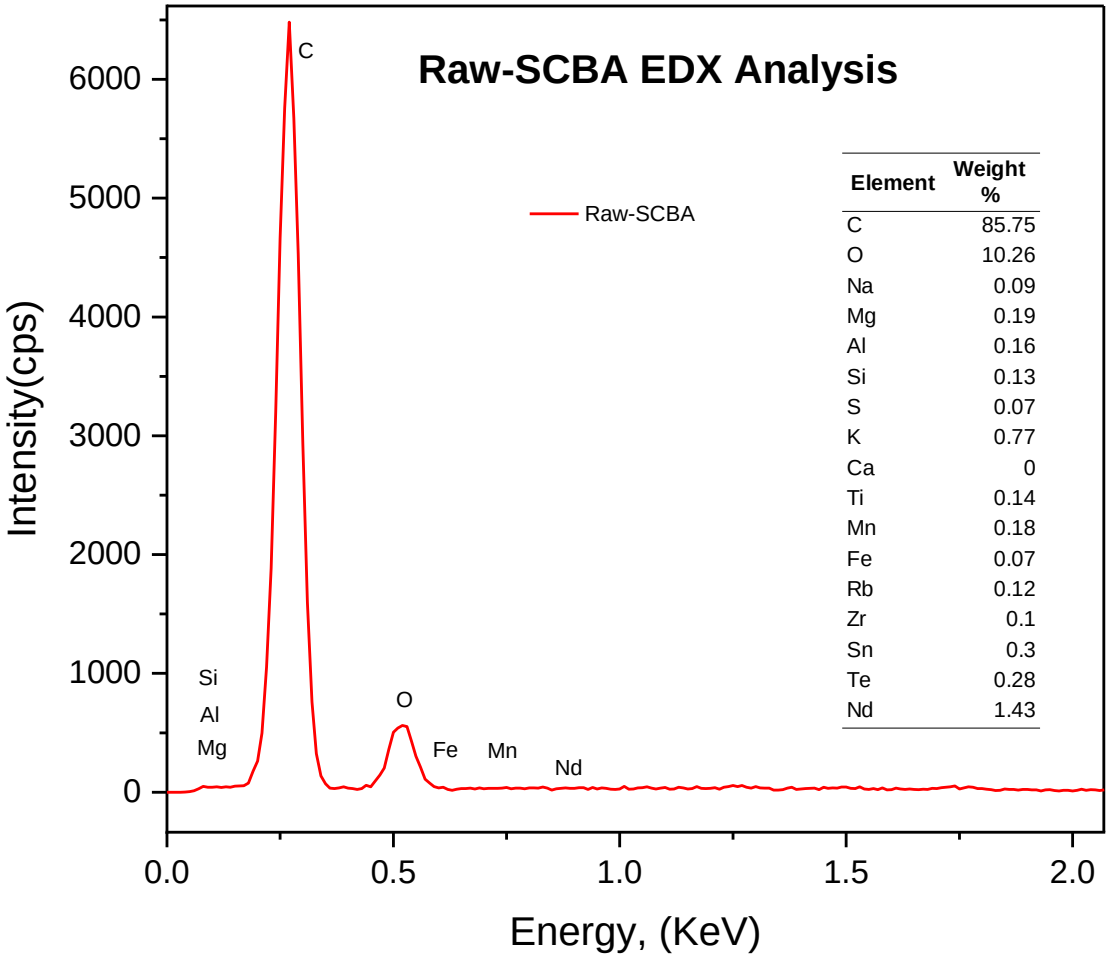

Figure 4. 7: Elemental composition of raw SCBA.

Carbon had the highest percentage weight, during this analysis. This also indicated the possibility of incomplete combustion of the SCBA in the boiler furnace at the sugarcane plant factory. Therefore, a need for further re-calcination at higher temperatures for particle properties optimization. This is similar to the suggestion made by Cordeiro *et al.* [18] while looking at the pozzolanic activity of SCBA about calcining temperature.

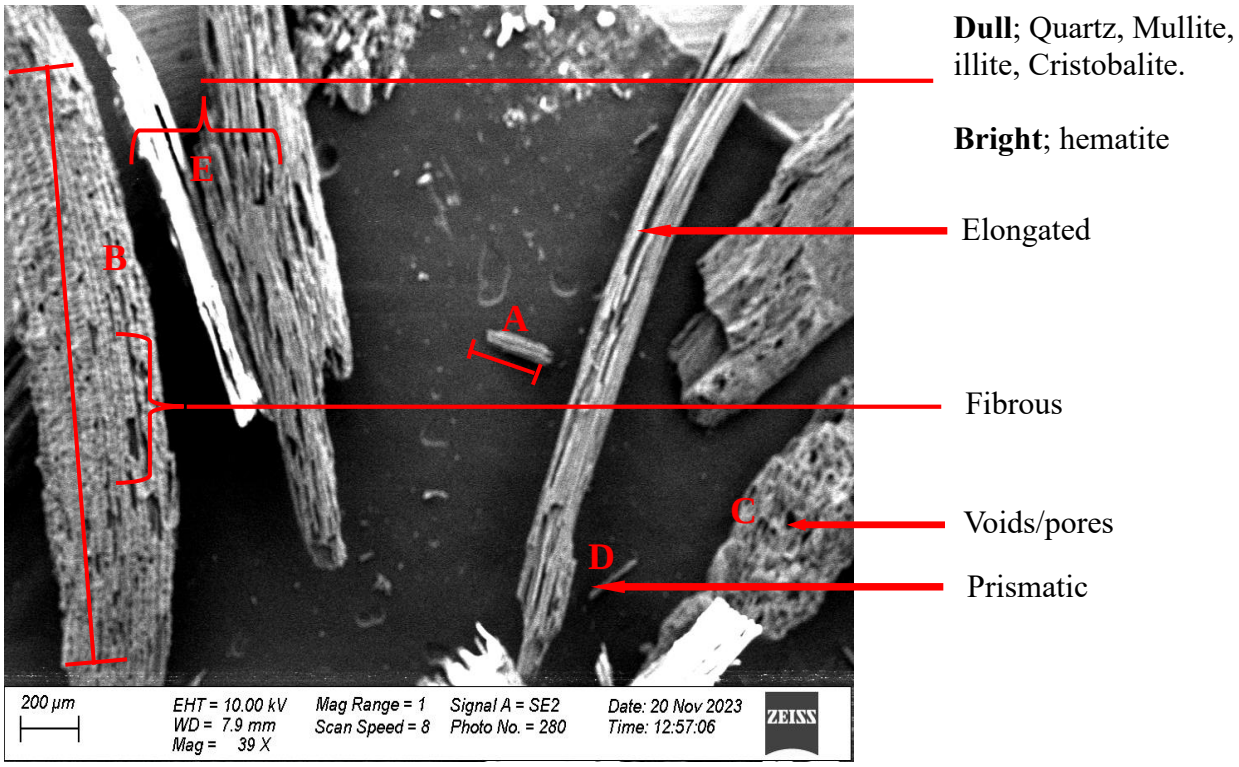

Figure 4. 8: SEM microstructure morphology and elemental composition for raw SCBA.

4.2.1.3 Microstructure morphology for raw sugarcane bagasse ash

The SEM analysis of the raw SCBA (Figure 4.8) taken at a magnification of 39X, revealed, the fibrous (particle B) and prismatic (particle D) nature of the particles with various particle size distributions. There are bigger and longer particles approximately 2,000 µm so are smaller particles approximately 200 µm as indicated by particles B and A respectively. Summarily, these particles are fibrous in nature with various shapes, elongated, prismatic and irregular.

The fibrous nature shows that they are carbonaceous [57], this has been validated by the EDX analysis as the carbon element had the highest absolute concentration 85.75 wt %. This showed they are the most common particles in the raw SCBA. The prismatic particle shows the siliceous nature of the raw SCBA [57]. From the EDX analysis, the silicon element was at 0.13 % of the total sample absolute weight concentration. This indicates that the quantity of the siliceous particles in the raw SCBA is very small.

Looking at the SEM image, the prismatic particles which are silica in nature are countable, hence this is similar to the EDX analysis and so is the XRD Table 4.3. Payá *et al.* [57] realised a similar observation as they carried out research on the properties of sugar cane bagasse ash for concrete production.

The particles' surface textures are rough since they have the appearance of pores/voids inducing air locks as indicated in particle C. There is also variation in particle brightness, indicating a difference in particle composition. The dull areas of the particles contain the mineral phases of quartz, mullite, illite, and cristobalite, and the bright particle areas contain hematite.

4.2.2 Processed sugarcane bagasse ash

The raw SCBA was calcinated at 600 ^{o}C to activate its pozzolanic properties, enhance its reactivity and remove any organic matter. This process was to ensure its suitability as an SCM in concrete and improve product strength.

The processed SCBA (SCBA-600) was subjected to XRD analysis as shown in Figures 4.9 and 4.10. The mineral phases of SCBA-600 identified were; cristobalite space group, Fd3-mz, hematite space group R-3/cH, illite space group C12/C1, kaolinite space group C1, magnetite space group Fd3m, moissanite space group R3mH, mullite space group Pbam, periclase space group Fm-3m and quartz space group $P3_121$, corresponding to the standard ICSD graphs No. 34923, 15840, 90144, 63192, 26410, 171461, 23726, 9863 and 16331, respectively. These phases had peaks at different angles.

The major mineral phases were silicon, iron and aluminium. The silicon phase was realised in cristobalite at peak angles of 35.38 and 43.62, moissanite at peak angles of 35.38, 36.44, 40.14, and 41.58, and quartz at peak angles of 20.72, 26.54, 36.44, 39.34, 40.14, 42.26 45.76, 50.02, 54.76, and 59.92. The aluminium phase was realised in illite, at peak angles of 20.72, 26.54, 27.72, 30.14, 36.44, 42.26, 43.62, 48.08, 48.38, and 57.1, kaolinite at peak angles of 23.24, 26.54, 35.38, 39.34, 45.76, and

46.82, and mullite at peak angles of 35.38, 39.34, 48.08, and 42.62. Finally, the iron phase was realised in hematite at peak angles 39.34, and 43.62, and magnetite at peak angles 30.14, 43.24, and 57.1. This is well illustrated in Table 4.4.

4.2.2.1 Processed Sugarcane bagasse ash mineral phases identification

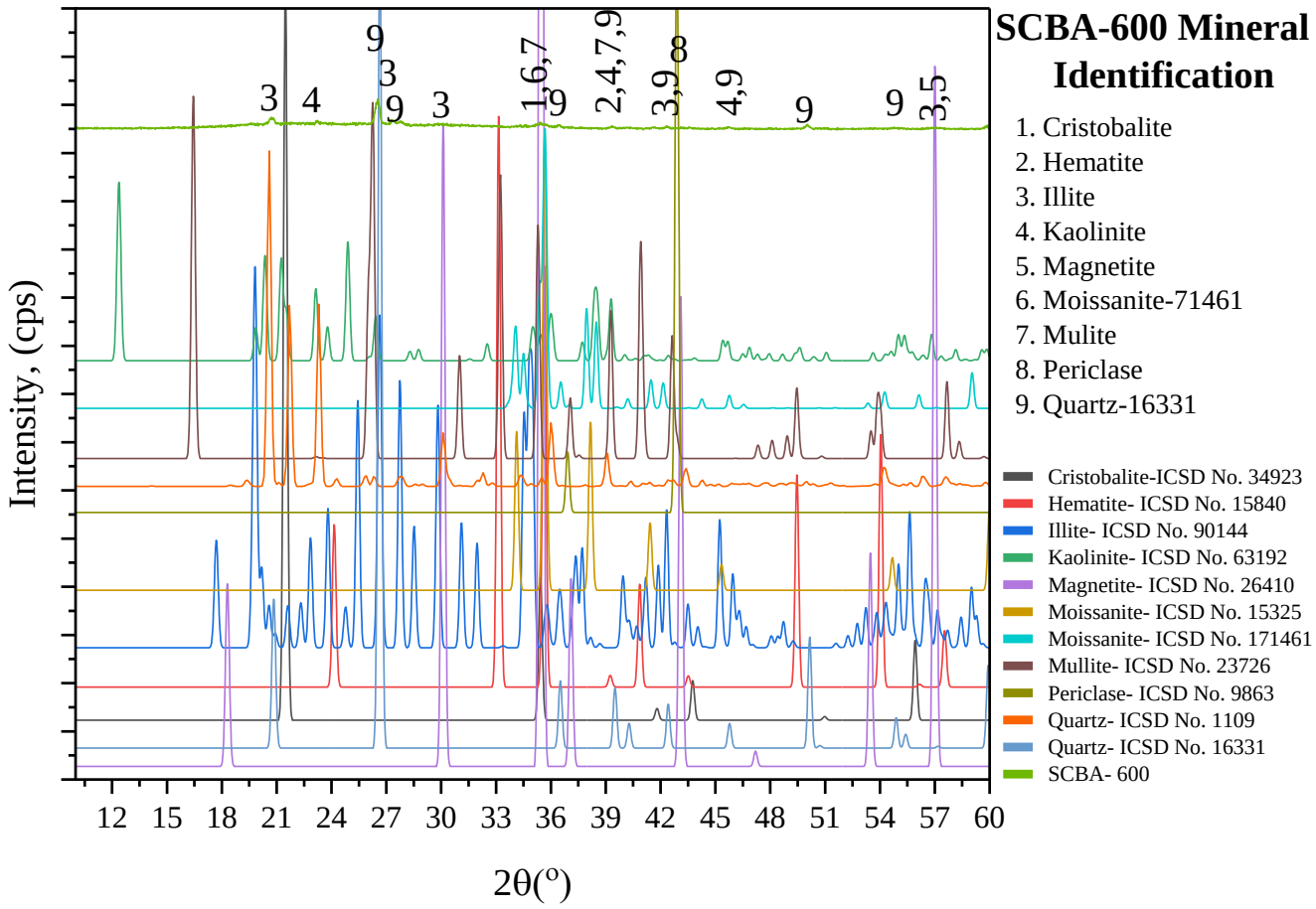

Figure 4. 9: XRD spectra of the processed sugarcane bagasse ash using ICSD standards.

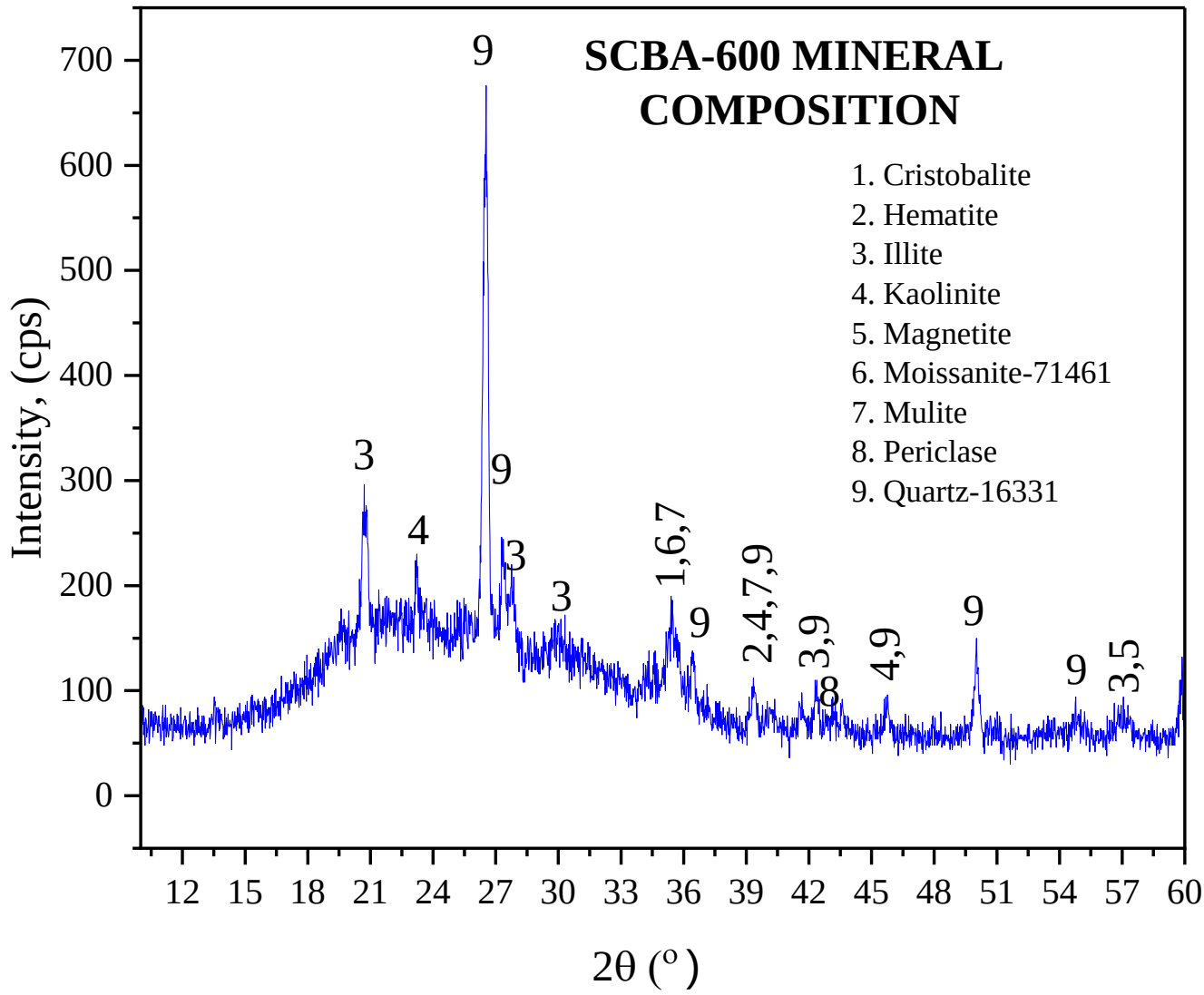

Figure 4. 10: XRD spectra of the SCBA-600 using ICSD standards.

Table 4. 4: The SCBA-600 mineral composition at different peak angles.

Mineral phase	Space group	Name	Chemical Formula	Peaks angle (2θ °)
Cristobalite	Fd3-mz	Silica	SiO_2	35.38, 43.62
Hematite	R-3/cH	Ferric iron oxide	Fe_2O_3	39.34, 43.62
Illite	C12/C1	Hydromuscovite	$(KH_3O)(Al,Mg,Fe)_2(SiAl)_4O_{10}[(OH)_2(H_2O)]$	20.72, 26.54, 27.72, 30.14, 36.44, 42.26, 43.62, 48.08, 48.38, 57.1.
kaolinite	C1	Kaolin	$Al_2Si_2O_5(OH)_4$	23.24, 26.54, 35.38, 39.34, 45.76, 46.82
Magnetite	Fd3m	Ferrous-ferric oxide	Fe_3O_4	30.14, 43.24, 57.1
Moissanite, 71461	R3mH	Silicon carbide	SiC	35.38, 36.44, 40.14, 41.58,
Mullite	Pbam	Porcelainite	$3Al_2O_3.2SiO_2$	35.38, 39.34, 48.08, 42.62
Periclase	Fm-3m	Magnesium oxide	MgO	42.62
Quartz, 16331	$P3_121$	Silicon dioxide	SiO_2	20.72, 26.54, 27.22, 36.44, 39.34, 40.14, 42.26 45.76, 50.02, 54.76, 59.92

4.2.2.2 Elemental composition for processed sugarcane bagasse ash

This was carried out using EDX. The elements present in the SCBA-600, after re-calcination in the muffle furnace at a temperature of 600 ^oC, were found to be; oxygen (O), carbon (C), silicon (Si), aluminium (Al), calcium (Ca), iron (Fe) and neodymium (Nd) as major elements at an absolute concentration by weight per cent (wt %) of 40.56, 33.4, 12.12, 1.81, 1.13, 0.93 and 3.84 %, respectively. The minor/trace elements; sodium (Na), magnesium (Mg), sulphur (S), titanium (Ti), manganese (Mn), rubidium (Rb), zirconium (Zr), tin (Sn) and tellurium (Te) were found at absolute concentration by weight percent (wt %) of 0.08, 0.49, 0.11, 0.37, 0.62, 0.21, 0.46, 0.18, 0.67 %, respectively. This analysis is well illustrated in Figure 4.11 and Appendix A (Table A3).

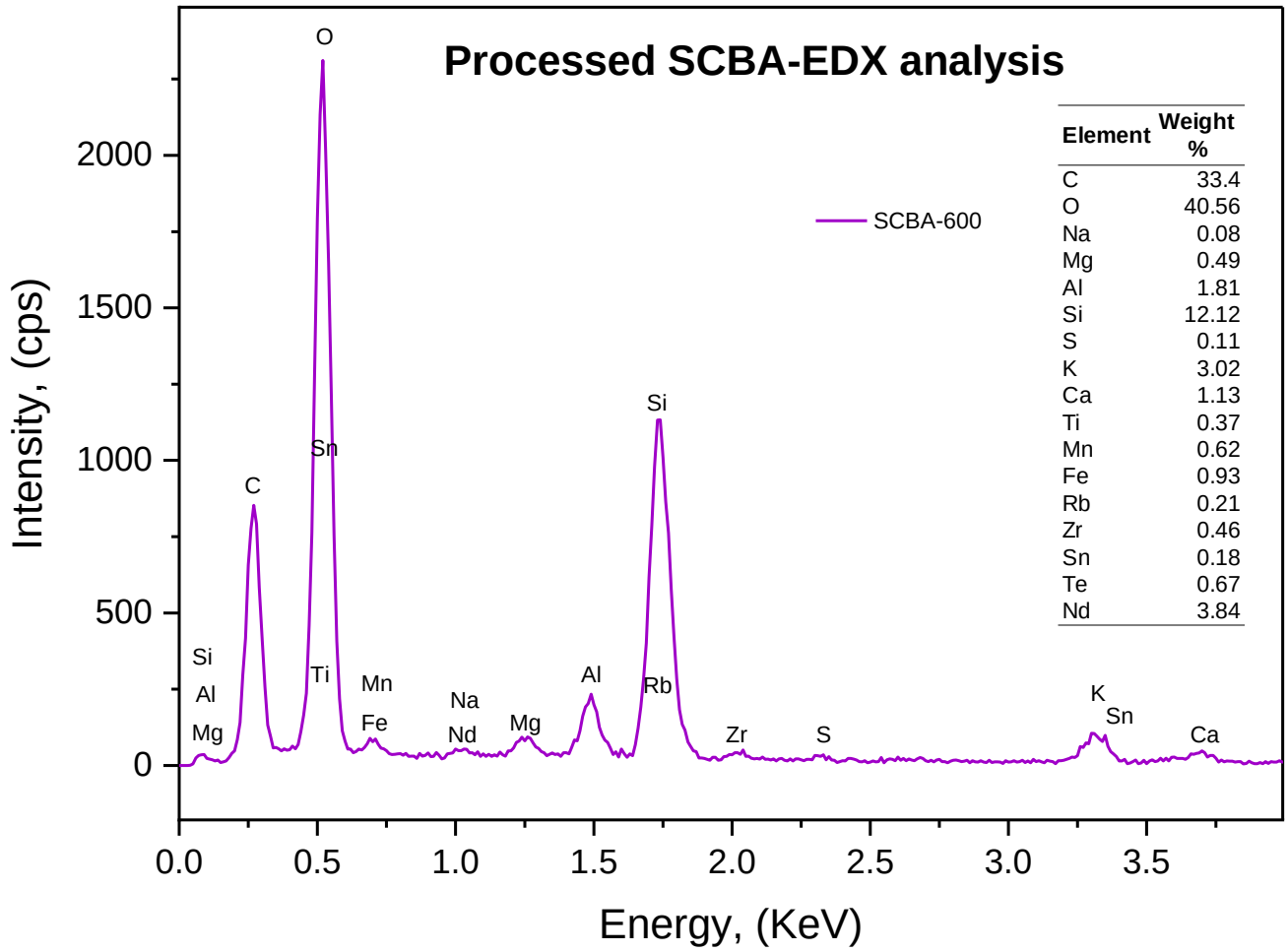

Figure 4. 11: The EDX spectra for SCBA-600.

The weight per cent (Wt %) of silicon, aluminium and iron increased from 0.13, 0.16 and 0.17 % in raw SCBA to 12.12, 1.81, and 0.93 %, respectively in SCBA-600. This shows the amorphous nature of raw SCBA and the crystalline nature of the SCBA-600. Hence calcination of the raw SCBA increases its crystallinity being in agreement with the observation made by Cordeiro *et al* [18], that calcining SCBA at high temperature increases its properties.

The elemental analysis of the SCBA-600 is similar to the XRD analysis in Figures 4.9, 4.10 and Table 4.4 as the SAI elements are conspicuously visible.

4.2.2.3 Microstructure morphology for processed sugarcane bagasse ash

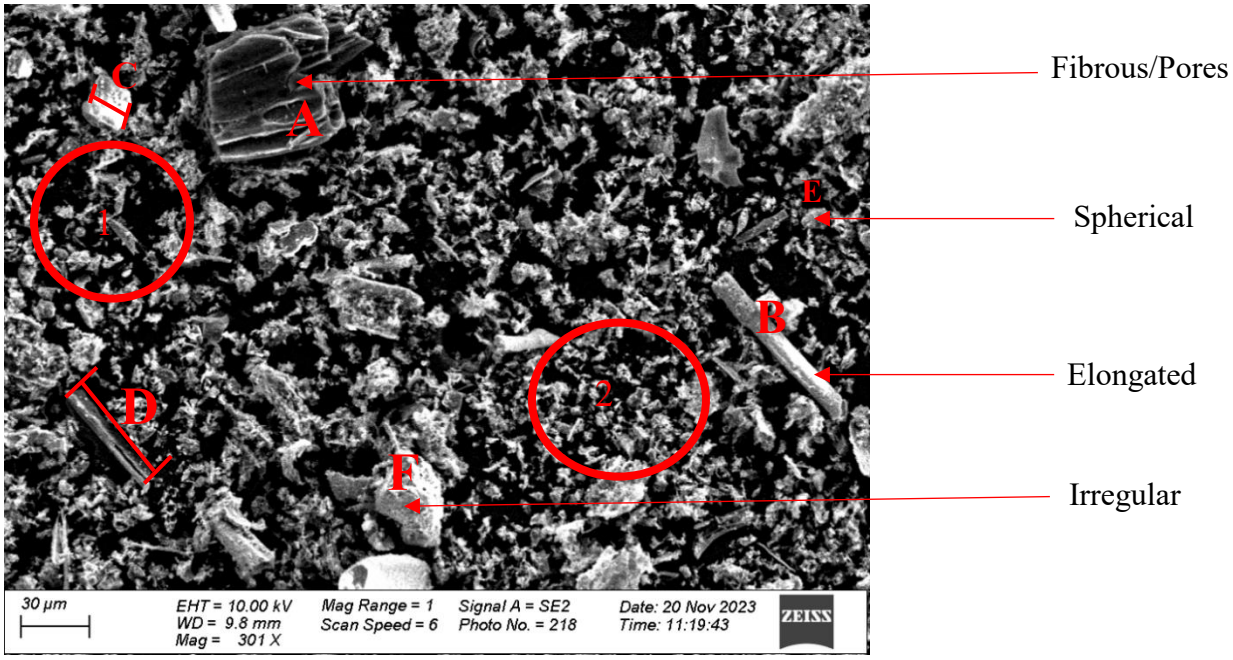

Figure 4. 12: SEM microstructure morphology for processed SCBA (SCBA-600).

Particles shape, of SCBA-600 were found to be spherical (particle E), elongated (particle B), irregular (particle F) and fibrous (particle A). A similar observation was also made by Abdala *et al.* [20] while looking at the mechanical and durability properties of SCBA concrete. The variation in particle sizes was also observed. Some particles were elongated and prismatic measuring approximately 60 µm (particle D) while others had sizes measuring approximately, 15 µm. This showed the non-uniformity of particle size distribution within the SCBA sample. The particle's surface texture was generally rough as indicated in particles A and F. This is mostly due to the porous nature of the SCBA particle. Through SEM analysis as shown in Figure 4.12, some particles were bright (particle F) and others were dull (particle D). This is most likely due to the variation in the mineral composition of these particles, as some minerals are believed to exhibit a bright nature in the SEM analysis and others a dull nature. The bight particles are mostly likely to be, hematite, magnetite, and periclase, and the dull particles; are kaolinite, illite, mullite, quartz and moissanite. This is mostly because, hematite, magnetite, and

periclase, elements in these compounds have relatively high atomic numbers, iron (Fe) atomic number 26, and magnesium (Mg) atomic number 12. Hence have high electron backscatter characteristics. This leads to brighter images on the detector. Cristobalite, illite, kaolinite, moissanite, mullite and quartz show a dull nature since the elements in these compounds have moderate atomic numbers hence fewer backscattered electrons were realised during analysis [58].

4.2.2.4 Chemical composition for processed sugarcane bagasse ash

The X-ray fluorescence analysis was done on the SCBA-600. This was to determine the chemical oxides composition. The major oxide compositions realised were; silicon dioxide (SiO_2), potassium oxide (K_2O), iron oxide (Fe_2O_3), aluminium oxide (Al_2O_3), calcium oxide (CaO), phosphorus pentoxide (P_2O_5) and manganese oxide (MnO) at the absolute concentration, weight percent (wt% m/m) of 44.331, 21.623, 13.450, 12.819, 3.271, 2.225 and 1.072 % respectively. There were also trace/ minor compound oxides; titanium oxide (TiO), sulphur trioxide (SO_3), zirconium dioxide (ZrO_2), zinc oxide (ZnO), strontium oxide (SrO), nickel oxide (NiO), rubidium oxide (RbO_2), copper oxide (CuO), and niobium oxide (NbO), at the absolute concentration, weight per cent (wt % m/m) of 0.833, 0.124, 0.104, 0.042, 0.035, 0.020, 0.020, 0.018, and 0.012 %, respectively.

This analysis also confirms the EDX and XRD analysis showing SAI as the major composites of SCBA at 44.331, 12.819 and 13.450 %, respectively. The total summation weight per cent of the silicon dioxide, aluminium oxide, and iron oxide compounds is 70.6 %. The ASTM standard C618-12a, dealing with the chemical composition required for calcined natural pozzolan, gives three classes N, F and C, depending on the silicon dioxide, aluminium oxide and iron oxide total mineral oxide composition. This is well illustrated in Table 2.4 [32]. Using this standard as a guide, the SCBA from the KISCOL sugar plant, located in the coastal areas of Kenya, can be classified as calcined natural pozzolan under class F

and N. Table 4.5 and Appendix B (Table B2), illustrate the mineral oxides composition of the SCBA - 600.

Table 4. 5: Mineral oxides composition of the SCBA-600.

Chemical composition	**Weight % m/m**
Silicon dioxide, SiO_2	44.331
Potassium oxide, K_2O	21.623
iron oxide, Fe_2O_3	13.450
Aluminium oxide, Al_2O_3	12.819
Calcium oxide, CaO	3.271
Phosphorous pentoxide, P_2O_5	2.225
Manganese oxide, MnO	1.072
Titanium oxide, TiO	0.833
Sulphur trioxide, SO_3	0.124
Zirconium dioxide, ZrO_2	0.104
Zinc oxide, ZnO	0.042
Strontium oxide, SrO	0.035
Nickel oxide, NiO	0.020
Rubidium oxide, RbO_2	0.020
Copper Oxide, CuO	0.018
Niobium oxide, NbO	0.012

4.3 POZZOLANICITY

4.3.1 Introduction

The hardened concrete hydration properties are of interest. The XRD, EDX and SEM analyses were carried out on the concrete product which exhibited the highest compressive and flexural strength characteristics. The improvement of the SCBA material on calcination was also investigated.

4.3.2 Hydration products analysis for SCBA-600 concrete

The concrete mix design was carried out with SCBA-600 partially replacing cement at different SCBA dosages, 0, 10, 20 and 30 %. The concrete mix obtained for testing was tagged, SCBA-0 (control mix), SCBA-10, SCBA-20, and SCBA-30. The compressive and flexural strength tests were then done in all the concrete mixes after twenty-eight days of concrete curing. The control mix had a compressive and flexural strength at 36.25 and 7.68 N/mm^2, respectively. The concrete mix with 20 % SCBA-600 dose achieved the highest strength, 3.5 N/mm^2 and 0.5 N/mm^2 for compressive and flexural strengths respectively higher than the control mix. This is well illustrated in Tables 4.9 and 4.11. Since SCBA-20 emerged with the highest strengths, it became of interest to this study. It was subjected to X-ray diffraction analysis for the hydration products, specifically portlandite and ettringite. Figures 4.13 and 4.14 show these hydration products' identification using ICSD XRD standards graphs.

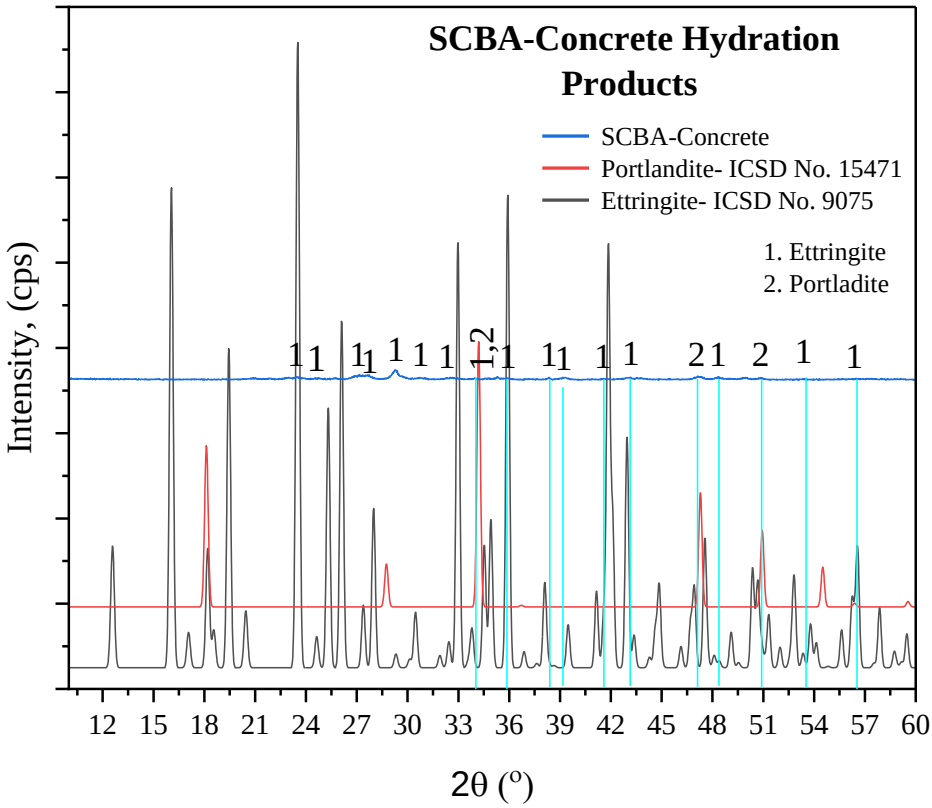

Figure 4. 13: XRD spectra of the powdered SCBA-600 concrete using ICSD standards.

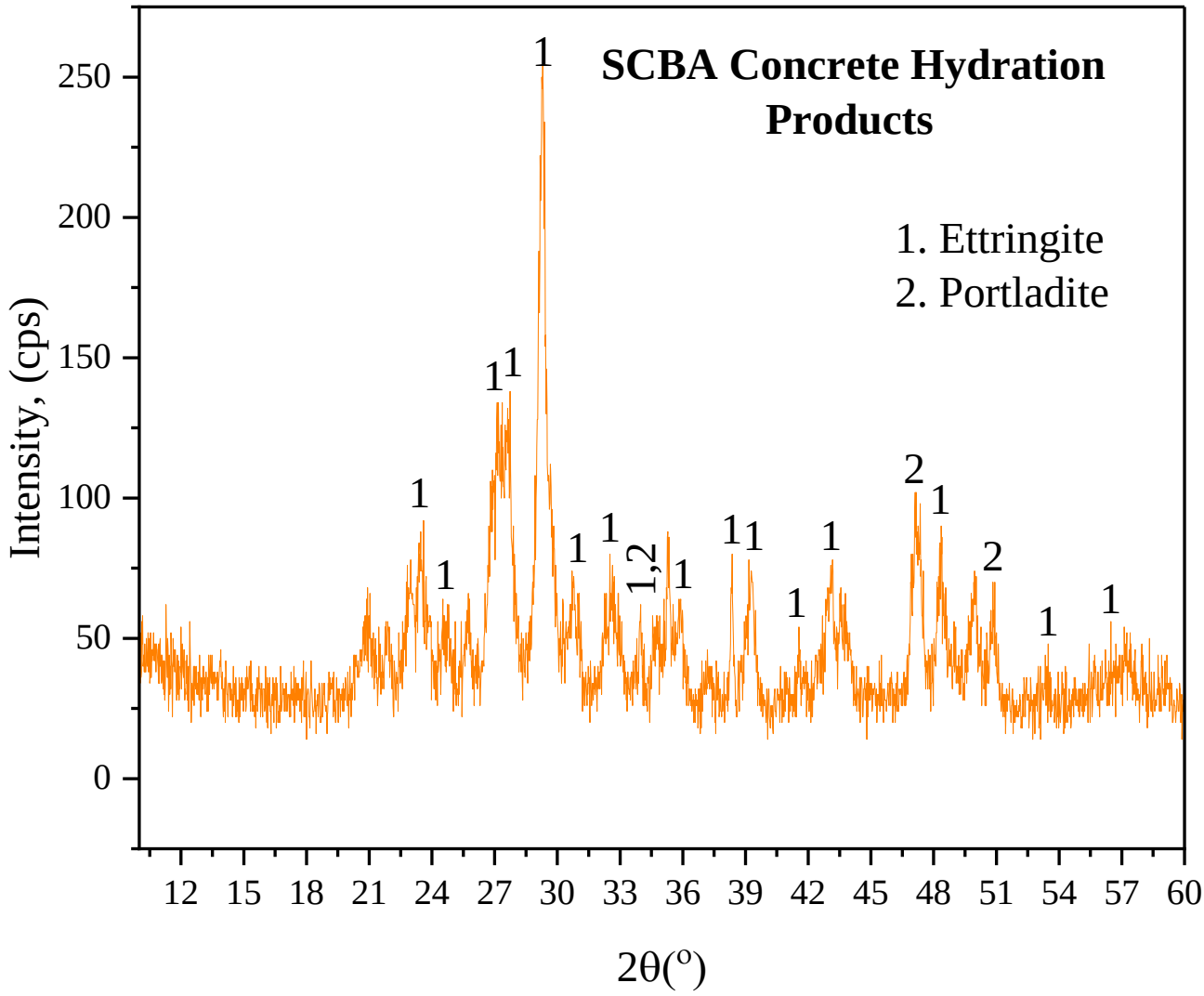

Figure 4. 14: XRD spectra for crystallization phases of hydrated powdered SCBA-600 concrete.

Identifying the mineral phases of the hydration products using standard ICSD graphs. On identification, the quantities of these mineral phases were analysed. This was done using the scanning electron microscope (SEM) and energy dispersive x-ray (EDX) to give a general view of their spread on the SCBA concrete surface.

The hydration products identified were hydrous calcium aluminium sulphate (ettringite), space group P63 calcium hydroxide (portlandite), and space group P3-m1, corresponding to standard ICSD No. 9075 and 15471, respectively.

Table 4. 6: Powdered SCBA-600 concrete hydration products at different peak angles.

Mineral phase	Space group	Name	Chemical Formula	Peaks angle (2θ ^{o})
Ettringite	P63	Hydrous calcium aluminium sulphate	$Ca_6Al_2(SO_4)3(OH)_{12}\cdot 26H_2O$	23.6, 24.74, 27.12, 27.74, 29.26, 30.7, 32.52, 33.98, 35.82, 38.36, 39.16, 41.56 ,43.16 ,48.36 ,53.48 ,56.48
Portlandite	P3-m1	Calcium hydroxide	$Ca(OH)_2$	33.98, 47.12, 50.92

These hydration products were identified at different peak angles as well indicated in Table 4.6. The hydrous calcium aluminium sulphate had its peak angles at 23.60, 24.74, 27.12, 27.74, 29.26, 30.70, 32.52, 33.98, 35.82, 38.36, 39.16, 41.56, 43.16, 48.36, 53.48 and 56.48, while calcium hydroxide had its peak angles at 33.98, 47.12, and 50.92.

The number of peaks of a particular mineral phase in a compound suggests the quantity of that mineral in that compound. The ettringite peaks were observed to be very many in comparison to the portlandite as shown in Figures 4.13 and 4.14. This indicated that in the concrete mix of 20 % SCBA dose, there was optimum hydration, leading to enhanced strength of the concrete product as indicated in Figures 4.18 and 4.19.

4.3.3 Elemental composition analysis for powdered SCBA-600 concrete

The elemental composition of powdered SCBA-20 concrete mix was carried out using EDX and the results are indicated in Figure 4.15 and Appendix A (Table A4). The major elements were; oxygen (O) carbon (C), calcium (Ca), silicon (Si), aluminium (Al), sodium (Na), and neodymium (Nd), at absolute concentrations of; 43.13, 27.37, 14.08, 6.33, 2.89, 1.88, and 1.21 % respectively. The minor elements were, potassium (K), tellurium (Te), rubidium (Rb), iron (Fe), sulphur (S), tin (Sn), magnesium (Mg),

manganese (Mn), titanium (Ti), and zirconium (Zr) at absolute concentration of; 0.66, 0.63, 0.46, 0.38, 0.3, 0.23, 0.21, 0.14, 0.1, and 0.03 %, respectively.

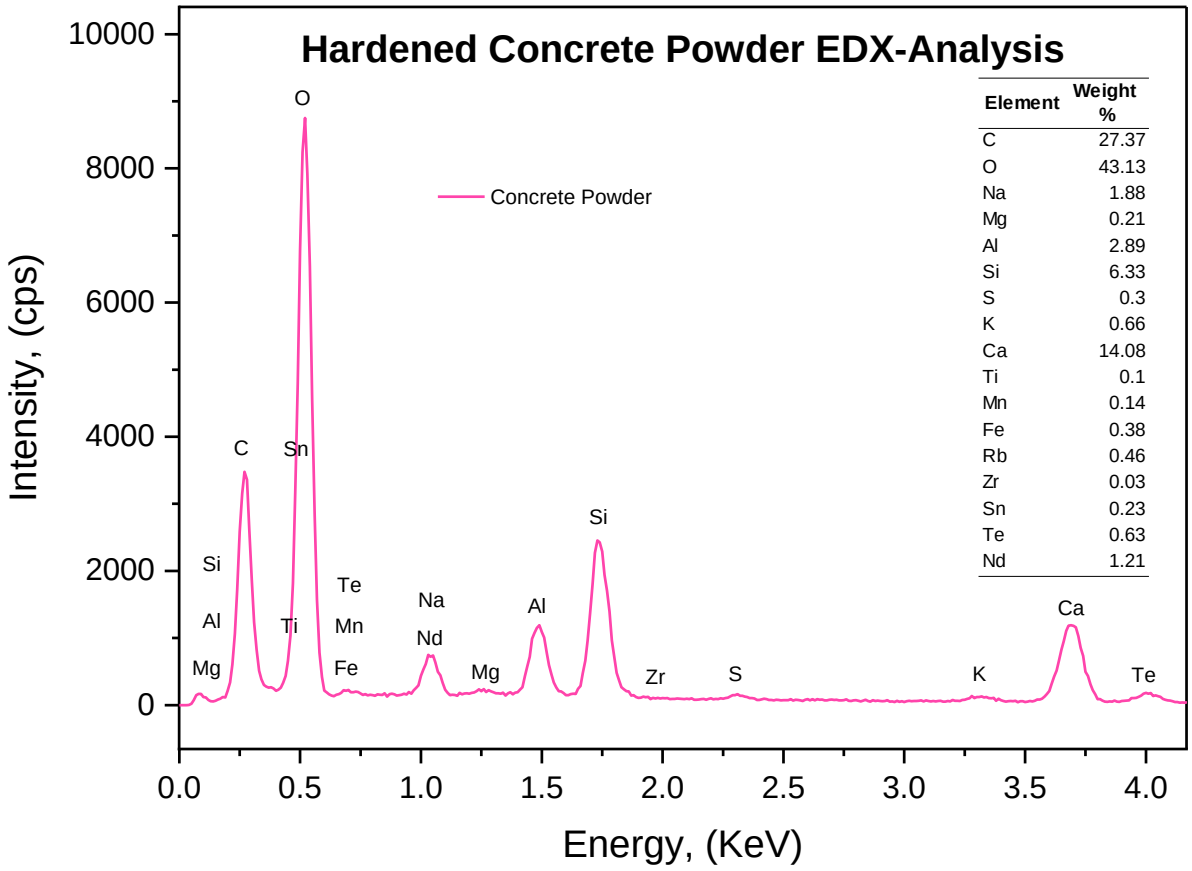

Figure 4. 15: Elemental composition of powdered SCBA-600 concrete.

The concentrations of the pozzolanic oxides, silicon dioxide, aluminium oxide, iron oxide and calcium oxide (SAIC) were; 6.33, 2.89, 0.38 and 14.08 % as tabulated in Table 4.7.

Table 4. 7: EDX SAIC elemental analysis.

EDX SAIC elemental analysis (wt %)				
	Silicon	Aluminium	Iron	Calcium
Bamburi Powerplus CEM I/42.5N Portland cement	3.31	1.2	0.23	27.33
SCBA-600	12.12	1.81	0.93	1.13
SCBA-20 concrete mix	**6.33**	**2.89**	**0.38**	**14.08**

There is a constant reduction in the measured wt % of all these SAI elements in the SCBA-20 concrete mix as illustrated in Table 4.7. This reduction can be attributed to;

i. Dilution effects; When the binder (SCBA-600 and Bamburi Powerplus CEM I/42.5N Portland cement) was mixed with other materials such as aggregates (fine and course) and water, the concentration of silicon, aluminium iron and calcium in the resulting concrete mixture decreased due to dilution effects [59].
ii. Chemical reactions and effects: These reactions consume silicon, aluminium, iron and calcium ions, reducing the overall concentrations of these elements in the SCBA-20 concrete mix. These chemical effects are the pozzolanic activities which take place during the hydration process. The hydration process occurred when water was added to the binder (SCBA-600 and Bamburi Powerplus CEM I/42.5N Portland cement), and aggregates (fine and coarse) to form concrete. These reactions involved, silicon, aluminium, iron and calcium compounds which were present in the binder material as was identified in Figures 4.3 and 4.11. Hence leading to the formation of new compounds and possibly the incorporation of calcium, silicon, aluminium and iron into the crystal lattice of hydrated products like calcium silicate hydrate (C-S-H), calcium aluminate hydrate (C-A-H), calcium aluminate silicon hydrate (C-A-S-H), calcium hydroxide (Ca(OH)2) and calcium aluminate sulphate (ettringite). These reactions are well illustrated in Equations (2.1) to (2.7) [1], [39].

The reduced silicon, aluminium, iron and calcium elements to 6.33, 2.89, 0.38, and 14.08 % is a clear indication of hydration reactions leading to the formation of portlandite and ettringite analysed from the XRD graphs in Figures 4.13 and 4.14.

4.3.4 Microstructure morphology for SCBA -600 concrete

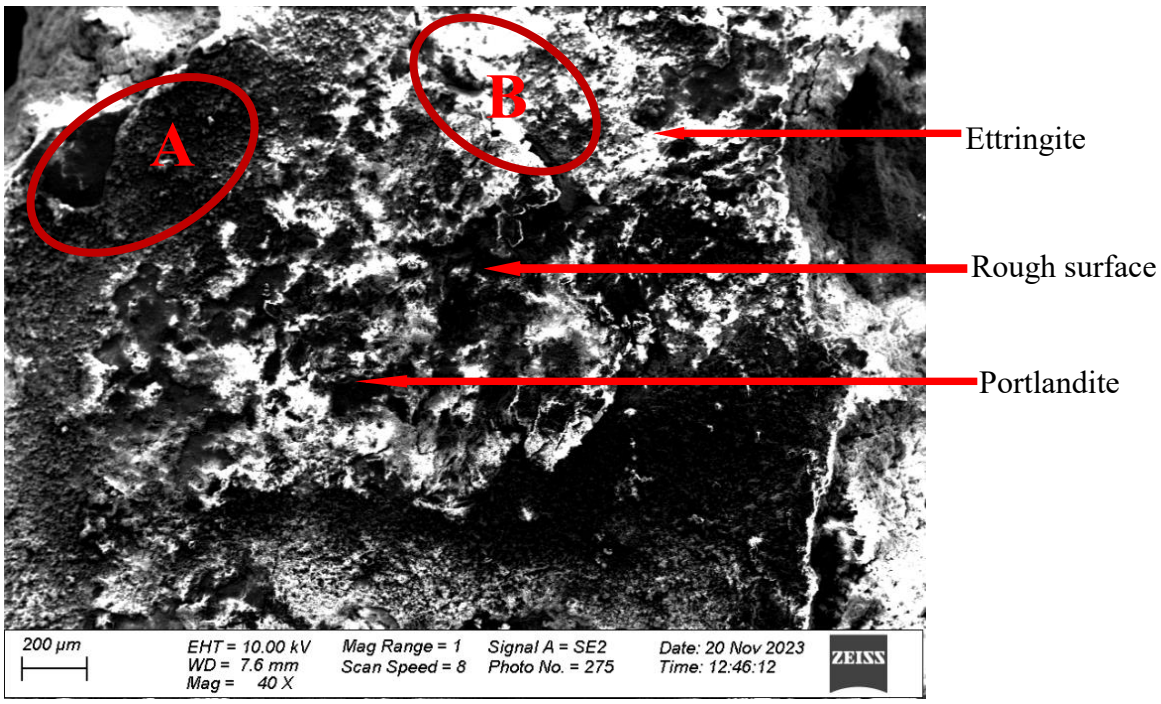

Figure 4. 16: SCBA-600 concrete, SEM, surface morphology and hydration products.

The SCBA-20 concrete mix was subjected to SEM surface morphology analysis at a magnification of 40X. The concrete surface texture appeared rough. This appearance could be attributed to aggregate distribution within the concrete matrix since both fine and coarse aggregates had different sizes (4.75 mm and 20 mm). Besides the surface texture, there was also variation in brightness as depicted in Figure 4.16.

The brightness distribution differs conspicuously. Looking at distribution areas A and B, area A looks darker compared to area B which looks brighter. This difference in brightness is attributed to mineral compounds (ettringite and portlandite) found on the concrete surface. Even though both ettringite and portlandite have a dull appearance on SEM images, ettringite appears brighter than portlandite when only these two compounds are compared. Hence on the SCBA-20 concrete mix surface, the brighter areas depict the presence of ettringite while the dull areas depict portlandite. This is so since the

portlandite elements have less atomic number than ettringite. The higher the atomic number, the higher the electron scatter and hence the brighter the SEM image and vice versa [58].

The SEM image depicts the ettringite particles as the majority of particles on the SCBA-20 concrete mix surface, this is synonymous with the XRD analysis in Figure 4.13 and Table 4.6.

4.3.5 Improvement of sugarcane bagasse ash pozzolanic properties on calcination

The raw SCBA was subjected to calcination in the muffle furnace at a temperature of 600 ^{o}C for 3 hrs. This is the temperature at which the SCBA pozzolanic elements begin to improve their cementitious properties [21]. Hence this was done to improve the pozzolanic properties of the SAI mineral phases as was identified in Figure 4.6 (crystallization phases of raw SCBA, mineral composition). The raw-SCBA was identified to have five major phases, cristobalite (SiO_2), hematite (Fe_2O_3), illite ($(KH_3O)(Al, Mg, Fe)_2(SiAl)_4O_{10}[(OH)_2(H_2O)]$), mullite ($3Al_2O_3.2SiO_2$) and quartz ($SiO_2$). On calcination, four additional mineral phases were identified; kaolinite ($Al_2Si_2O_5$ $(OH)_4$), magnetite (Fe_3O_4), moissanite (SiC) and periclase (MgO). The kaolinite changes to metakaolinite at this temperature [14]. Metakaolinite is a highly reactive pozzolana material. Hence having its particles in the SCBA-600 materials greatly improves its cementitious properties. The change of kaolinite to metakaolinite took place as illustrated in Equation (4.6) [14].

$$\underset{\text{Kaolinite}}{Al_2Si_2O_5(OH)_4} \xrightarrow{600\ ^{o}C} \underset{\text{Metakaolinite}}{Al_2O_3.2SiO_2} + 2H_2O \qquad (4.6)$$

Comparing the SAI phases in raw SCBA and SCBA-600 as indicated in Figure 4.17, the latter has more SAI elements indicative of good pozzolanicity, since SAI are the major pozzolan elements. Hence re-calcination of SCBA at 600 ^{o}C, improved its properties significantly.

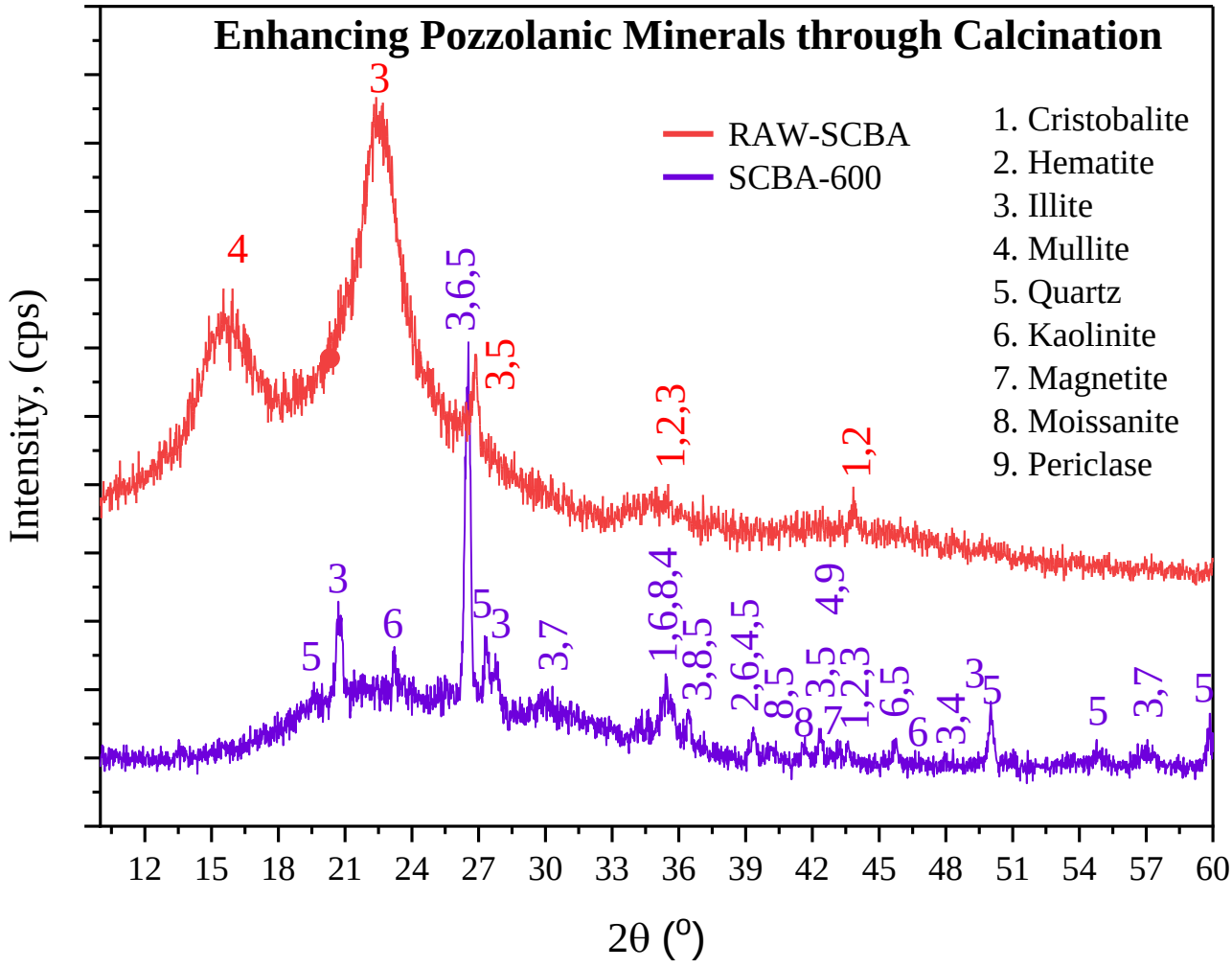

Figure 4. 17: The comparison of the pozzolanic mineral phases in Raw SCBA and SCBA-600.

The peaks of SCBA-600 as indicated in Figure 4.17 were sharper, indicating the crystalline nature of the particles on calcination at a temperature of 600 ^{o}C compared to raw SCBA which looked amorphous. This is a clear indication that calcining the SCBA at 600 ^{o}C improves its particle properties at the micro-level. Hence enhanced pozzolanic activity in the concrete matrix.

While amorphous materials generally exhibit higher pozzolanic activity, some crystalline phases formed during calcination can also contribute to pozzolanic reactions.

Table 4. 8: Enhancement of SCBA elemental properties upon heating- EDX analysis.

	EDX SAI Elemental Analysis (wt %)		
Elements	**Raw-SCBA**	**SCBA-600**	**Wt % increase**
Silicon	0.13	12.12	9, 223.07
Aluminium	0.16	1.81	1,031.25
Iron	0.07	0.93	1,228.57

The increase in absolute concentration weight per cent (wt %) of the pozzolanic elements such as SAI in SCBA-600 in comparison with the raw SCBA is indicated in Table 4.8. This is a clear indication that calcining SCBA material at high temperatures improves its particle properties. The elemental analysis of these SAI elements is indicated in Figures 4.7 and 4.11.

These (SCBA-600) crystalline phases upon calcination had reactive sites that participated in the formation of cementitious compounds, potentially enhancing the overall pozzolanic activity of the material. This was exhibited in the concrete mix with a 20 % SCBA dose. This mix had the highest strength (compressive and flexural) compared to the control mix after twenty-eight days of concrete curing.

4.4 HARDENED CONCRETE PROPERTIES

4.4.1 Introduction

Hardened concrete exemplifies several properties that are critical to its functionality and longevity. These properties are; strength, durability, and permeability. Strength indicators such as compressive, tensile, and flexural strengths are fundamental in assessing concrete's ability to withstand applied loads, while durability factors, such as resistance to environmental conditions and chemical attacks, ensure its long-term stability. Moreover, permeability properties such as water and gaseous ingress further contribute to concrete's overall integrity and performance. Additionally, the interfacial transition zone

(ITZ) in concrete refers to the region surrounding the aggregate particles, where the properties of the binder paste gradually transition to those of the aggregate [60]. Its presence and characteristics are critical since they significantly influence the concrete strength.

Understanding and managing these properties are essential for durable and sustainable concrete structures that can withstand the rigours of real-world applications. The strength property (compressive and flexural strength) of SCBA concrete made from SCBA collected from the coastal area of Kenya was determined in this project. A total of four different mixes, SCBA-0, SCBA-10, SCBA-20, and SCBA-30, with partial replacement of Portland cement at 0, 10, 20, and 30 % respectively, were designed for concrete class 25. The results are discussed in the following paragraphs.

4.4.2 Compressive strength

The concrete properties were investigated after twenty-eight days of casting and curing. This period is significant since by the end of twenty-eight days, most concrete mixes have reached a significant portion of their ultimate strength of about 96 -100 % [49], [59]. Hence testing at twenty-eight days provides a good indication of the concrete's strength potential and its suitability for its intended use. The results were as stipulated in Figure 4.18, Table 4.9 and Appendix D (Table D2).

The highest compressive strength was realised on the concrete mix (SCBA-20) with a 20 % SCBA dose. This was higher than the control mix (SCBA- 0) by 3.50 Nmm^{-2} which represents a 9.65 % strength gain above the control mix. The least strengths were realised from the mixes of SCBA-30, with 30% SCBA dose, and SCBA 10, with 10 % SCBA dose. These represented -5.68 and -2.30 Nmm^{-2} strength lower than the control mix, corresponding to 15.66 and 6.34 % strength loss from the control mix (SCBA-0) respectively.

Table 4. 9: Compressive strength after twenty-eight days of concrete curing.

Mix	Replacement level (%)	Compressive strength (Nmm^{-2})	Strength variation from control mix (Nmm^{-2})	Strength variation from control mix (%)	Remarks on strength
SCBA - 0	0	36.25	0.00	0	Constant
SCBA- 10	10	33.95	-2.30	-6.34	Lower
SCBA- 20	20	39.75	3.50	9.65	Higher
SCBA- 30	30	30.57	-5.68	-15.66	Lowest

Early strength development in concrete (days one and two) is always lower than late strength developments (days three, seven, and twenty-eight) [33], [18]. This observation has been confirmed in this study, whereby, after twenty-eight days of concrete curing, the compressive strength was tested and found to be high as expected, but with strength variations from the four mixes made.

Three distinct variations of the SCBA concrete strength from the control mix exist. These variations in strength are majorly attributed to the Bamburi Powerplus CEM I/42.5N Portland cement phases (alite, belite, celite, millerite, gypsum, hematite, illite, magnetite, moissanite, quartz, and lime), and the SCBA doses in the mix ratio**.** The major cement phases identified earlier are, alite, belite, celite and millerite with average composition by mass as indicated from earlier research shown in Table 4.10 [61].

Table 4. 10: Composition of major PC phases by mass.

Chemical Name	CCN	Chemical Formula	Approximate % in PC (mass)
Alite	C_3S	$3CaO{\cdot}SiO_2$	45.0 - 60.0
Belite	C_2S	$2CaO{\cdot}SiO_2$	15.0 - 25.0
Celite	C_3A	$3CaO{\cdot}Al_2O_3$	7.0 - 12.0
Millerite	C_4 AF	$4CaO{\cdot}Al_2O_3 \cdot Fe_2O_3$	6.0 - 10.0

Alite phases have the highest composition followed by belite, celite, and lastly millerite. This is similar to our findings on cement phase identification indicated in Table 4.1.

In a normal cement hydration process (PC with no pozzolan mixture), alite exothermically reacts with water to form calcium silicate hydrates (C-S-H) whereas celite reacts rapidly with water to form calcium aluminate hydrate (C-A-H). These contribute to early-stage concrete strength development [61]. Belite and millerite also react with water to form calcium silicate hydrate (C-S-H) and calcium ferrite hydrate (C-F-H), respectively. These former reactions are slow-paced and therefore contribute to the later stage of concrete strength development. Moreover, as these reactions take place, there is also the production of calcium hydroxide (portlandite). C_3S and C_2S produce more portlandite than C_3A and C_4AF as they are more in the cement sample. The chemical reactions are as shown in the following equations [61], [62]**;**

$$C_3S + H_2O \rightarrow C\text{-}S\text{-}H + Ca(OH)_2 \quad (4.7)$$

$$C_2S + H_2O \rightarrow C\text{-}S\text{-}H + Ca(OH)_2 \quad (4.8)$$

$$C_3A + H_2O \rightarrow C\text{-}A\text{-}H + Ca(OH)_2 \quad (4.9)$$

$$C_4AF + H_2O \rightarrow CFH + Ca(OH)_2 \quad (4.10)$$

The reactions of pozzolan in a cement matrix depend on the hydration products of the cement, more so portlandite. The SCBA-600 used in this research project has been classified as a natural pozzolan under class N or F. On cement hydration, calcium silicate hydrate, calcium monosulphate (ettringite), calcium ferrite hydrates and portladite are initiated as indicated in Equations (4.7) to (4.10). The total amount of these hydration products depends on the curing period, and hence the choice for twenty eight day curing period. Within this period almost all hydration products shall have been formed at 100 % [61].

SCBA being an inert material [33], its reaction depends on the portladite ($Ca(OH)_2$) from the cement hydration reaction. Normally, on reacting cement with water, without a pozzolan, the hydration product, portlandite, will always form some film around other slower-reacting cement compounds (such as C_2S and C_4AF) stopping further reaction [33]. When a pozzolan (such as SCBA-600 in our case) is added to the concrete mix to form part of the binder material, during the hydration reactions, it absorbs (reacts with) this film (portlandite) as indicated in Equation (4.11) [61], producing further calcium silicate hydrates gels (C-S-H). Moreover, paving the way for further hydration reactions of the slow-paced cement compound hence enhancing concrete strength developments in later stages.

$$3Ca(OH)_2 + 2(SiO_2) \rightarrow 3(CaO).2(SiO_2).3(H_2O) \quad (4.11)$$

As indicated in Table 4.9, the mix of SCBA-10 has a strength variation of -2.30 Nmm^{-2}, which is 6.30 % lower than the control mix (SCBA-0). This might be attributed to excess portlandite in the mix since all the SCBA introduced into the mix at a dosage of 10 % had all been depleted during the hydration reactions. The excess portlandite forms a cage/film around the remaining cement compounds stopping further formations of C-S-H gels which enhances concrete strength leading to a comparable weak concrete. The mix of SCBA-20 had a strength variation of 3.5 Nmm^{-2}, which is 9.65 % higher than the control mix. This mix depicted the optimum strength. This might be attributed to the optimum amount of SCBA present in the mix to dilute most of the portlandite formed during hydration reactions, exposing all the cement compounds to complete the hydration process, (optimum formation of C-S-H, C-A-H, and C-F-H). Finally, the mix of SCBA-30 with a strength variation of -5.68, which is 15.66 % lower than the control mix, had the least strength of all the mixes. This might be attributed to the following factors;

i. The SCBA present at 30 % partial replacement of cement, may have reacted with all the portlandite produced during the hydration process. The excess SCBA due to their inert nature could not take part in any further reaction and hence acted as filler elements within the concrete matrix. This might have led to poor interfacial bonding between the porous SCBA-600 particles (Figure 4.8), the cement matrix and the aggregates hence leading to weaker bonds in the concrete matrix.

ii. Porous materials like SCBA-600 (Figure 4.8) have a higher capacity to absorb water. When excess SCBA-600 is incorporated into the concrete matrix, it can absorb a significant amount of mixing water, leading to reduced hydration products such as C-S-H gels which enhances strength development and, hence weaker concrete strength.

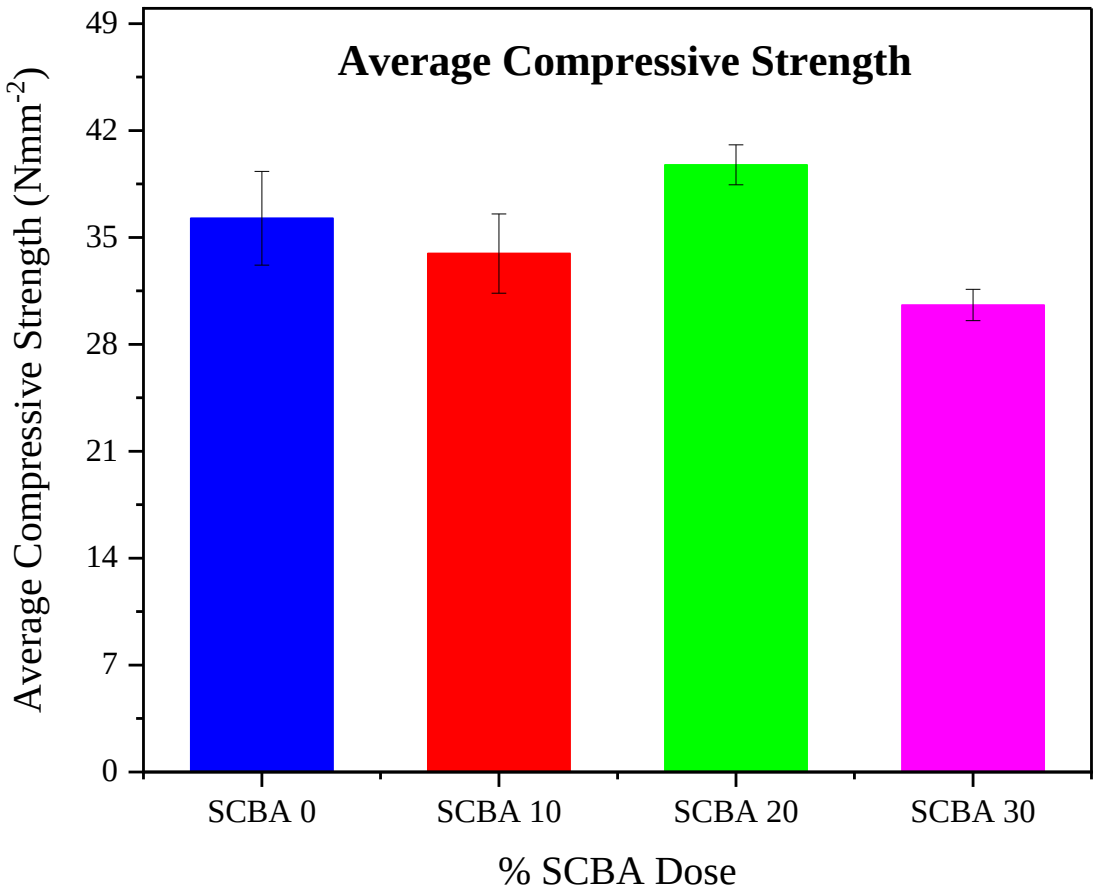

Figure 4. 18: Average compressive strength at twenty-eight days of concrete curing.

4.4.3 Flexural strength

Table 4. 11: Flexural strength after twenty-eight days of concrete curing.

Mix	Replacement level (%)	Flexural strength (Nmm^{-2})	Strength variation from control mix (Nmm^{-2})	Strength variation from control mix (%)	Remarks on strength
SCBA - 0	0	7.68	0.00	0	Constant
SCBA- 10	10	7.08	-0.6	-7.81	Lower
SCBA- 20	20	8.18	0.5	6.51	Higher
SCBA- 30	30	6.78	-0.9	-11.72	Lowest

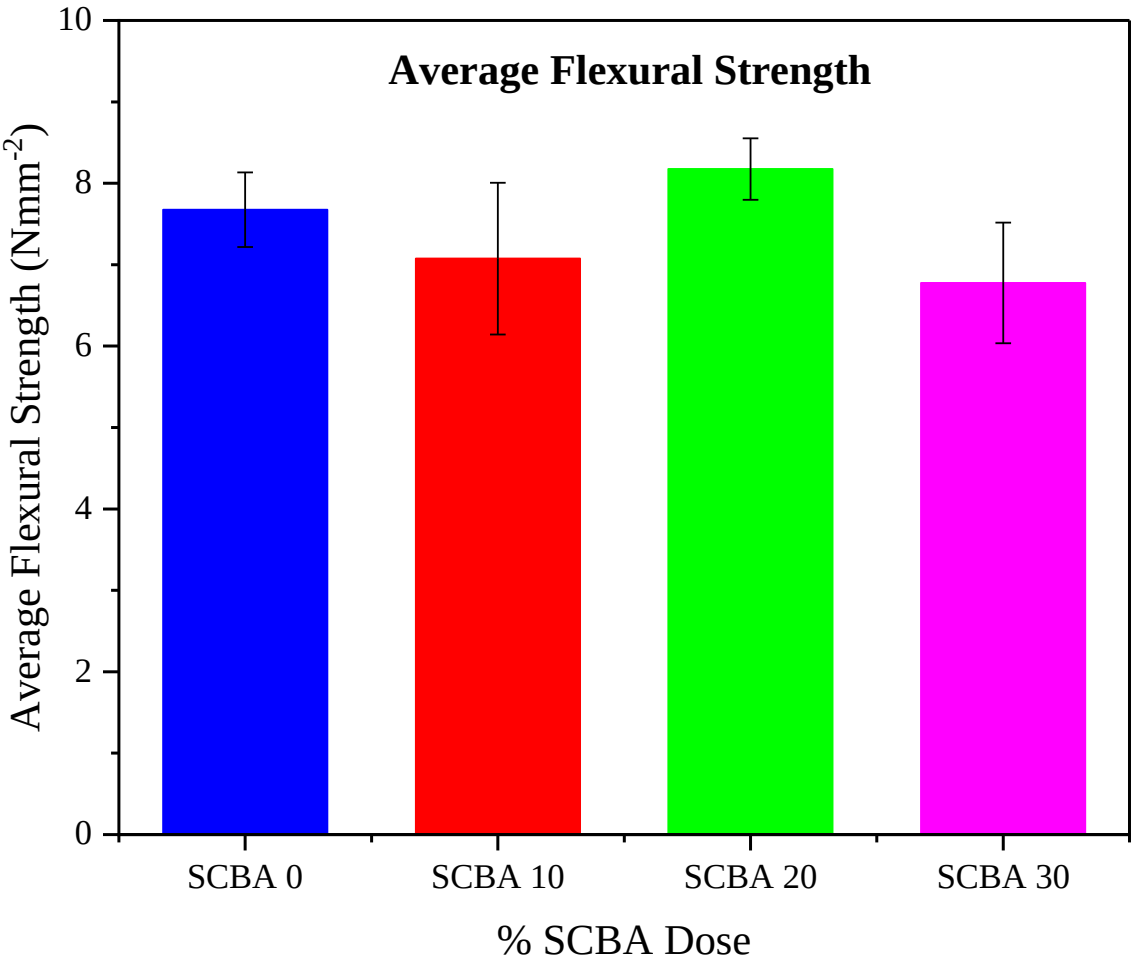

Figure 4. 19: Average flexural strength after twenty-eight days of concrete curing.

The flexural strength was also determined after twenty-eight days of concrete curing, and the results are as indicated in Table 4.11, Figure 4.19 and Appendix D (Table D1).

The concrete mix of SCBA-10, representing 10 % of the partial replacement of cement, had a strength variation of 0.6 Nmm^{-2}, corresponding to 7.81 % lower than the control mix (SCBA-0). The mix, SCBA-20, partially replacing cement by 20 %, had the highest flexural strength of all the mixes. This mix had a strength variation of 0.5 Nmm^{-2}, corresponding to 6.51 % greater than the control mix. The SCBA-30 mix, partially replacing cement by 30 %, had the least strength among all the mixes. This mix had a strength variation of 0.9 Nmm^{-2}, corresponding to 11.72 % lower than the control mix. These variations are further illustrated in Figure 4.19.

The variation of the flexural strength among the four mixes can be attributed to the bonding in the Interfacial Transition Zone (ITZ) of the concrete matrix. The ITZ often has a higher concentration of voids, micro-cracks, and weaker bonds compared to the bulk cement paste. Hence it's a zone of reduced strength, making it a potential weak link in the concrete matrix [60]. Moreover, if the ITZ is poorly formed or weakened due to inadequate bonding between the cement pastes and aggregate, it may contribute to reduced flexural strength. On the other hand, a well-bonded and strong ITZ can enhance the overall performance of the concrete in flexural loading.

The pozzolanic reactions (silicon dioxide present in the SCBA-600 and the portlandite) lead to the refinement of the microstructure in the ITZ. This happens by reducing the size of the pores and enhancing the density of the ITZ. This refinement results in a denser and less porous ITZ, hence improving the bond strength between aggregates and cement paste [60].

When the SCBA was mixed with cement paste, on hydration, C-A-H, C-S-H, C-A-SH and ettringite were formed, as indicated in Equations (2.1) to (2.7). The CSH gel and the ettringite formed influenced

the ITZ as filler effects at a nano/micro-level, reducing the thickness of the ITZ by filling in the pores and micro-cracks which might have developed during the rapid hydration process. The filling enhances the regional microstructures within these ITZs [63]. Hence influencing the concrete flexural strength.

In the mix of SCBA-10 where the variation of strength from the control mix was -7.81 %, the low strength could be attributed to less SCBA-600 present in the mix to enhance the production of enough C-S-H gel and ettringite which would enhance the ITZ to optimise the flexural strength. From the mix of SCBA-20, optimum flexural strength was achieved, which was 6.51 % above the control mix. This phenomenon can be attributed to having the right quantity of the SCBA-600 in this particular mix, which enhanced the optimum production of the C-S-H gel and ettringite leading to optimum flexural strength achieved. These C-S-H gels (These gels have cohesive properties and contribute to the overall strength) and ettringite filled the voids and micro-cracks substituting weaker calcium hydroxide (portlandite) layers and leading to stronger ITZ bonds between the cement paste and the aggregates. The mix having SCBA-30 had the least strength (-11.72 %) compared to the control mix (SCBA-0). This can be attributed to;

i. Increased porosity in the concrete matrix due to over-supply of the SCBA-600 in the mix design, this reduces the ITZ bonds.
ii. Excessive substitution of cement with SCBA up to 30 % resulted in a reduction of the overall amount of effective cementitious material in the concrete mix. Since SCBA-600 is an inert material under class N or F pozzolan (cannot self-harden as class C pozzolan), a decrease in the cement content leads to lower strength development [33].
iii. Incomplete pozzolanic reactions due to excess of SCBA in the mix design of SCBA-30, as the unreacted SCBA-600 particles act as inert fillers reducing the overall strength.

CHAPTER 5: CONCLUSION AND RECOMMENDATIONS

5.1 INTRODUCTION

After setting objectives and reviewing relevant literature to get the study gaps, this chapter draws conclusions based on the results obtained from this study. The goals of the study have been achieved. The specific objectives set (that is evaluating the chemical constituents and surface morphology of sugarcane bagasse ash and Portland cement, determining the structural properties of sugarcane bagasse ash and Portland cement, and examining the structural, flexural and compressive strength properties of the developed concrete from varying SCBA doses), have been achieved.

5.2 SPECIFIC CONCLUSION

The following are the discussions and conclusions of this study based on the specific objectives.

5.2.1 Evaluation of the surface morphology and chemical constituents of sugarcane bagasse ash and Portland cement

5.2.1.1 Surface morphology of sugarcane bagasse ash and Portland cement

The surface morphology of both raw-SCBA and processed SCBA (SCBA-600) and Bamburi Powerplus CEM I/42.5N, Portland cement were studied in this project as per the specific objective one, and the following observations were made;

At SEM magnification X287, the cement particles have no homogenous shape and are rectangular, round and irregular. The cement size distribution also varies widely, the bigger particles are sparsely distributed, while the smaller particles are densely distributed within the area of focus. The inter-particle distance is varied. The cement particles surface texture looks rough and rugged. This was seen as a way the particles may enhance their surface interlocking properties hence enhancing the binding properties

of cement as a material. There is variation in the brightness of the cement particles. This most likely indicated different phase compositions of the cement materials. The major phases identified were, alite, belite, celite and brown-millerite. Alite and belite correspond to dull SEM areas while celite and brown millerite correspond to the bright areas confirming the observations made by researchers, Black and Brooker [55], and Stutzman [54].

At SEM magnification of X39, the raw SCBA particle shapes were found to be elongated, fibrous and prismatic. The particles size distribution was varied so was the particle density. The particle surface area looked rough showing the presence of pores. There was a variation in particle brightness, a clear indication of different mineral phases present. The brighter areas showed the presence of hematite while the dull areas showed the presence of quartz, mullite, illite and cristobalite mineral phases.

At SEM magnification of X301, the processed SCBA (SCBA-600) particle shape, was found to be spherical, elongated and some irregular. The particle sizes were also different, and a combination of smaller and bigger particles was realised. Additionally, they had rough and fibrous surface texture, indicating the presence of pores and voids with a varied particle distribution density per area of focus. The variation in particle brightness was also realised indicating the different mineral phases present. The bright areas corresponded to hematite, magnetite and periclase mineral phases while the dull areas corresponded to kaolinite, illite, mullite, quartz, moissanite and cristobalite mineral phases. This is mostly due to the differences in the atomic numbers, as those with relatively high atomic numbers have high electron backscatter characteristics and those with relatively low atomic numbers have fewer backscatter electrons [58].

The literature reviewed had very little information on the use of SEM to identify chemical constituents as has been done in this study.

5.2.1.2 Chemical constituents of sugarcane bagasse ash and Portland cement

The chemical constituents of SCBA and PC were analysed using EDX and XRF equipment. The SCBA-600 was found to have sixteen chemical oxides from the XRF analysis. The major oxides were silicon dioxide, potassium oxide, aluminium oxide and iron oxide with percentage composition of 44.331 %, 21.623 %, 12.819 % and 13.450 %, respectively. The silicon dioxide, aluminium oxide and iron oxide make a composition of 70.6 % of total oxides compositions. This qualifies this SCBA-600 material used in this study as a natural pozzolan under class N or F as per ASTM C618-12a [32]. Hence the Kenya coastal area sugarcane bagasse ash when calcinated at the temperature of 600 ^{o}C and above can be used as a natural pozzolan of class N or F in pozzolana cement production. The SCBA-600 properties at this temperature are similar to that of class N or F fly ash.

The EDX elemental analysis of SCBA-600 revealed seventeen elements. The major elements were oxygen and carbon closely followed by silicon, aluminium and iron at 40.56, 33.40, 12.12, 1.81, and 0.93%, respectively. The least element was sodium at 0.08 %. From the EDX elemental analysis, it was possible to see that, silicon dioxide, aluminium oxide and iron oxide elements were present in the samples tested hence showing the potential use of SCBA-600 as an SCM. These EDX results confirmed the XRF results, confirming that the coastal Kenya SCBA given an appropriate pre-treatment, such as calcination at temperatures of 600 ^{o}C and above can be used as an alternative source of semi-cementitious materials such as fly ash.

The major oxides of Bamburi Powerplus CEM I/42.5N, Portland cement using XRF were; silicon dioxide, iron oxide, calcium oxide and sulphides. Their composition percentages were, 17.068, 3.069, 3.095, 71.592 and 2.644 %, respectively. The elemental analysis using EDX, the major Bamburi Powerplus CEM I/42.5N, Portland cement elements were, carbon, oxygen, calcium, silicon, and aluminium the least element by composition was nobelium. Their percentage composition was 23.00,

38.99, 27.33, 3.30, 1.20, 2.89 and 0.02 % respectively. These oxides' composition was as per the acceptable limits required as per Ugandan standard US EAS 18-1, criteria for common cements [64].

5.2.2 Determining the structural properties of sugarcane bagasse ash and Portland cement

5.2.2.1 Sugarcane bagasse ash and Portland cement mineral composition

The mineral composition for processed SCBA (SCBA-600) was determined using XRD and was found as follows; kaolinite, moissanite, magnetite, quartz, mullite, illite, hematite, cristobalite, periclase and lime, while Bamburi Powerplus CEM I/42.5N Portland cement these major mineral phases were observed; alite, belite, celite and brown – millerite. These minerals from SCBA-600 and Bamburi Powerplus CEM I/42.5N Portland cement, play major roles in pozzolanic and hydration reactions [20], [39] as they are made up of chemical oxides which increase pozzolanicity [21], [23].

5.2.2.3 Pore structure and refinement

The effect of processed SCBA (SCBA-600) in the interfacial transition zone (ITZ) was observed when it enhanced the flexural strength in the mix of 20 % Portland cement replacement. The SCBA-600 reduced the thickness of the ITZ by increasing the production of C-S-H, C-A-H, C-F-H, and C-A-S-H, which acted on the supposedly micro crack and pores within the ITZ refining and densifying it hence increasing the flexural strength [33]. The SCBA-600 reacted with the weaker bonds created by the portlandite from the hydration reactions. It facilitated the replacement of these weaker portlandite bonds in the ITZ with stronger and more cohesive bonds from the C-S-H, C-A-H, C-F-H, and C-A-S-H gels. This enhanced the bonds between the aggregates and the binder matrix. Therefore SCBA-600 increased the densification of the concrete matrix leading to greater flexural strengths.

5.2.3 Examining structural, flexural and compressive strength properties of the developed concrete from varying sugarcane bagasse ash dose

5.2.3.1 Structural properties

It was observed that the hardened concrete made from the mix of SCBA-20 had higher ettringite in comparison to the portlandite. This is a clear indication that the SCBA dose at 20 %, had the maximum hydration reaction. This led to most of the portlandite which causes weaker bonds at the ITZ to be absorbed. The absorption of these portlandite led to the formation of the finer ettringite which filled the micro-cracks of the ITZ leading to greater densification in these zones. The more the densification, the more enhanced the mechanical strength [33].

Sixteen phases of ettringite were realised against the three phases of portlandite as shown from the XRD spectre of Figure 4.14.

5.2.3.2 Compressive strength

The results obtained in this study showed that the compressive strength of sugarcane bagasse ash (SCBA) incorporated concrete is increased up to a particular SCBA dose, above which it begins to decrease. In this study, the mix SCBA-20, which had a SCBA dose of 20 % gave the optimum concrete strength. This was mostly attributed to the formation of C-S-H gel, C-A-H gel and C-A-S-H gel which increases the ITZ bonding with the aggregates due to high pozzolanic activity and acceleration of hydration reactions, occasioned by optimum SCBA at 20 % [33]. This mix had 9.65 % strength higher than the control mix (SCBA-0). When the SCBA was increased to 30 % as indicated by the mix SCBA-30, the compressive strength dropped and this was associated with the oversupply of the SCBA in the concrete mix, resulting in incomplete pozzolanic reactions, since unreacted SCBA particles act as inert fillers in the concrete matrix leading to weaker bond formation [60]. Hence it was concluded that SCBA

can improve concrete strength to a particular SCBA dose level, which was called the dose optimum or "optimum dosis." Above this optimum level, the compressive strength begins to reduce significantly.

5.2.3.3 Flexural strength

It was observed that the addition of SCBA in the concrete mix design also increased the flexural strength of the concrete under study. As the SCBA was increased from 10 - 30 % in the step size of 10 %, it was realised that a maximum strength was achieved at a mix of SCBA-20 having 20 % PC replacement. This was mostly attributed to reduced heat of hydration during the hydration process [18], formation of C-S-H, C-A-H, C-A-S-H gel and ettringite leading to no micro cracks as observed from Figure 4.12 [20], [33]. However, as the SCBA was increased above this level to 30 % as indicated from the mix of SCBA-30 in Table 4.11, the flexural strength reduced. The reduction of the flexural strength is mostly attributed to the oversupply of the inert SCBA-600 which leads to incomplete pozzolanic reactions making the ITZ bonds between aggregates and the binder matrix weak [60].

Hence, it was concluded that the addition of calcined SCBA to an optimum level in a concrete matrix increases both flexural and compressive strength. However, further addition of SCBA above this level will significantly reduce both strengths as the pozzolanic reactions are greatly compromised by higher doses of SCBA above the optimum level.

5.3 CONCLUSION SUMMARY

Sugarcane bagasse ash (SCBA) available along the Kenya coast can positively influence the mechanical properties of the hardened concrete. Hence, it can be concluded that;

i. Calcining SCBA above 600 ^{o}C, improves its pozzolanic properties, and increases SAI to above 70% of the total oxide components.
ii. The SCBA under study can be classified as class N or F natural pozzolan.

iii. SCBA can be partially used to replace PC but to a given/ particular percentage since SCBA is inert and cannot initiate any chemical reaction when it is the only cementitious material in the concrete mix.

iv. SCBA dose of 20 % Portland cement replacement gives the optimum strength for both compressive and flexural strength. Hence SCBA can be used to manufacture pozzolana cement as an alternative SCM.

v. This particular SCBA dose above 20 % will lead to a decrease in both compressive/flexural strength significantly and hence may lead to structural failure when the cement replacement is done above 20 %.

vi. The addition of SCBA in the cement matrix may reduce the heat of hydration as the heat of hydration releases micro-cracks into the concrete matrix, these micro cracks were not observed when the developed concrete was subjected to SEM analysis as indicated in Figure 4.12.

vii. SCBA increases portlandite consumption. This is because the more the SCBA was increased to the optimum dose, the ITZ bonds also increased as indicated by the increase in compressive and flexural strength. As reported by other researchers, portlandite increases weak ITZ bonds [33].

From EDX analysis of Bamburi Powerplus CEM I/42.5N Portland cement and processed sugarcane bagasse ash (SCBA-600) shows similar chemical composition but with variation in proportion. Hence SCBA-600 can be used as SCM in concrete production.

The influence of SCMs on the twenty-eight-day strength of mortar can be classified into three types: dilution effect, physical effect and chemical effect. The dilution effect usually results in a change in the water-cement ratio and leads to a reduction in strength. The physical effect is the filling effect and the heterogeneous nucleation effect arises from particle size refinement, which contributes to strength enhancement. The chemical effect refers to the pozzolanic activity and other cementitious properties

that stem from increased hydration products. This generalized classification scheme provides a useful framework for analysing the various mechanisms through which SCMs affect mortar strength [59].

This research focussed on characterizing the sugarcane bagasse ash produced by a local sugar mill along the Kenya coast, improved it by controlled calcination at a temperature of 600 ^{o}C, and finally used it independently to design a standard-strength concrete. These concrete properties were then studied in the hardened state. The findings are encouraging, these coastal SCBA-manufactured concrete showed excellent compressive and flexural strength. Hence when this study is adopted by the policymakers in the cement manufacturing industries, it will lead to the value addition of local SCBA waste as an SCM, reduce SCBA waste disposal in landfills and the GHGs associated with local PC production chain while at the same time increasing resource productivity and longevity (sustainability of natural resources).

The Kenya Coastal SCBA is the best SCBA which can be used as an SCM since the SCBA along the western side of Kenya needed SF to be added to the mix design to give the required results Abdalla *et al.* [1], [20]**.** Kenya coastal SCBA was the only SCM in the mix design but gave out very good results as portrayed in this study.

Therefore the scarcity of SCM, the CO_2 pollution and the improper SCBA waste disposal can be mitigated by the inclusion of the Kenya Coast SCBA in the concrete matrix.

5.4 RECOMMENDATIONS

A further study on the following areas is recommended for a full understanding of the Kenya coastal SCBA for pozzolana cement production. The highlighted areas were not the scope of this project, but the research on these areas is highly recommended for the full understanding and knowledge building on the Kenya coastal SCBA for cement production.

i. How Kenya coastal SCBA will alter concrete microstructure in terms of pore refinement and reduction, a deep study on the interfacial transition zones of SCBA-incorporated concrete is recommended.

ii. The influence of SCBA on concrete penetrability, in terms of gas permeability, absorption/sorptivity, and chloride ion penetration besides carbonation and carbonation prediction model. This is very important for reinforced concrete. The SCBA concrete produced has the capability of being used as reinforced concrete.

iii. Study on the sustainability and environmental effects of the Kenya coast SCBA, in terms of CO_2 mitigation (actuals CO_2 produced in preparation of the SCBA) and economic viability.

iv. The extent to which Kenya's coastal SCBA reduces the heat of hydration needs to be researched further. The heat of hydration leads to micro-cracks, these were not observed in the final concrete. Hence a need to investigate the reduction percentage of heat of hydration by this SCBA.

This study has added to the board of knowledge the use of the coastal SCBA as SCM. Hence, creating awareness in the cement manufacturing family, the possibility of using the coastal SCBA in the manufacture of the pozzolana cement.

6.0 REFERENCES

[1] T. A. Abdalla, D. O. Koteng, S. M. Shitote, and M. Matallah, "Mechanical Properties of Eco-friendly Concrete Made with Sugarcane Bagasse Ash," *Civ. Eng. J.*, vol. 8, no. 6, pp. 1227–1239, 2022, doi: 10.28991/CEJ-2022-08-06-010.

[2] B. Y. P. K. Mehta, "Reducing the Environmental Impact of Concrete," no. October, pp. 61–66, 2001.

[3] M. S. Eid and H. M. Saleh, "Characterizations of Cement and Modern Sustainable Concrete Incorporating Different Waste Additives," *Sustain. Concr. With Synth. Recycl. Aggregates*, no. November, 2022, doi: 10.5772/intechopen.100447.

[4] K. Akil, P. Parthasarathy, and D. S. Shankar, "International Journal of Engineering Research and Modern Education Experimental Studies on the Properties of Cement Concrete with Water Hyacinth Fibres International Journal of Engineering Research and Modern Education," no. April, pp. 61–62, 2017.

[5] H. Ganapathi and M. Phukan, *Environmental Hazards of Limestone Mining and Adaptive Practices for Environmental Management Plan*, no. February. Springer International Publishing, 2020. doi: 10.1007/978-3-030-38152-3.

[6] S. H. Channa, S. A. Mangi, N. Bheel, F. A. Soomro, and S. H. Khahro, "Short-term analysis on the combined use of sugarcane bagasse ash and rice husk ash as supplementary cementitious material in concrete production," *Environ. Sci. Pollut. Res.*, vol. 29, no. 3, pp. 3555–3564, Jan. 2022, doi: 10.1007/s11356-021-15877-0.

[7] J. Farfan, M. Fasihi, and C. Breyer, "Trends in the global cement industry and opportunities for

long-term sustainable CCU potential for Power-to-X," *J. Clean. Prod.*, vol. 217, pp. 821–835, 2019, doi: 10.1016/j.jclepro.2019.01.226.

[8] B. Zerihun, M. D. Yehualaw, and D. Vo, "Effect of Agricultural Crop Wastes as Partial Replacement of Cement in Concrete Production," vol. 2022, 2022.

[9] B. S. Thomas *et al.*, "Sugarcane bagasse ash as supplementary cementitious material in concrete – a review," *Materials Today Sustainability*, vol. 15. Elsevier Ltd, Nov. 01, 2021. doi: 10.1016/j.mtsust.2021.100086.

[10] Suthirat Kittipongvises, "Assessment of Environmental Impacts of Limestone Quarrying Operations in Thailand," vol. 20, pp. 67–83, 2017, doi: 10.1515/rtuect-2017-0011.

[11] K. Wang and Iowa State University. Center for Transportation Research and Education., *Proceedings of the International Workshop on Sustainable Development and Concrete Technology, Beijing, China, May 20-21, 2004*. Center for Transportation Research and Education, Iowa State University, 2004.

[12] S. Shankar, "Management and Remediation of Problem Soils, Solid Waste and Soil Pollution," no. October, 2017, doi: 10.1007/978-981-10-1866-4.

[13] R. Berenguer *et al.*, "Cement-based materials: Pozzolanic activities of mineral additions are compromised by the presence of reactive oxides," *J. Build. Eng.*, vol. 41, 2021, doi: 10.1016/j.jobe.2021.102358.

[14] A. T. Bakera and M. G. Alexander, "Properties of Western Cape Concretes with Metakaolin," vol. 11011, pp. 1–14, 2018.

[15] S. S. Muthu, *Assessment of Carbon Footprint in Different Industrial Sectors*, vol. 1. 2006.

[16] R. M. Andrew, “Global CO 2 emissions from cement production , 1928 – 2017 1 Introduction to Previous estimates of global cement emissions,” *Earth Syst. Sci. Data*, vol. 10, no. 4, pp. 1–20, 2021.

[17] S. A. Memon, U. Javed, M. I. Shah, and A. Hanif, “Use of Processed Sugarcane Bagasse Ash in Concrete as Partial Replacement of Cement : Mechanical and Durability Properties,” 2022.

[18] G. C. Cordeiro, P. V. Andreão, and L. M. Tavares, “Pozzolanic properties of ultrafine sugar cane bagasse ash produced by controlled burning,” *Heliyon*, vol. 5, no. 10, Oct. 2019, doi: 10.1016/j.heliyon.2019.e02566.

[19] Abul Salam, “Evironmental and Health Impact of Solid Waste Disposal at Mangwaneni Dumpsite In Manzini: Swaziland, Journal of Sustainable Development in Africa (Volume 12, No.7, 2010),” vol. 12, no. 7, pp. 64–78, 2010.

[20] T. A. Abdalla, D. O. Koteng, S. M. Shitote, and M. Matallah, “Mechanical and durability properties of concrete incorporating silica fume and a high volume of sugarcane bagasse ash,” *Results Eng.*, vol. 16, p. 100666, Dec. 2022, doi: 10.1016/j.rineng.2022.100666.

[21] E. M. R. Fairbairn, B. B. Americano, G. C. Cordeiro, T. P. Paula, R. D. Toledo, and M. M. Silvoso, “Cement replacement by sugar cane bagasse ash : CO 2 emissions reduction and potential for carbon credits,” *J. Environ. Manage.*, vol. 91, no. 9, pp. 1864–1871, 2010, doi: 10.1016/j.jenvman.2010.04.008.

[22] K. Lakshmi Priya and R.Ragupathy, “Effect of Sugarcane Bagasse Ash on Strength Properties of Concrete,” *Int. J. Res. Eng. Technol.*, vol. 05, no. 04, pp. 159–164, 2016, doi: 10.15623/ijret.2016.0504030.

[23] K. S. Subramaniyan and M. Sivaraja, “Assessment of Sugarcane Bagasse Ash Concrete on Mechanical and Durability Properties,” *Middle-East J. Sci. Res.*, vol. 24, no. S1, pp. 257–262, 2016.

[24] N. Bheel, M. O. A. Ali, Tafsirojjaman, S. H. Khahro, and M. A. Keerio, “Experimental study on fresh, mechanical properties and embodied carbon of concrete blended with sugarcane bagasse ash, metakaolin, and millet husk ash as ternary cementitious material,” *Environ. Sci. Pollut. Res.*, vol. 29, no. 4, pp. 5224–5239, Jan. 2022, doi: 10.1007/s11356-021-15954-4.

[25] A. Buregyeya, S. Nwaubani, W. Schmidt, A. G. Kerali, and U. Bagampadde, “supplementary cementitious materials in Portland cement Pozzolanic and hydration properties of kamafugites and carbonatitic lavas as supplementary cementitious materials in Portland cement,” no. November, 2018, doi: 10.1080/20421338.2018.1527539.

[26] M. Rebari, Y. Agrawal, T. Gupta, and R. Sharma, “Mechanical Properties of Sustainable Concrete Containing Sugarcane Bagasse Ash : A Review,” pp. 150–163, 2020.

[27] Q. Xu, T. Ji, S. J. Gao, Z. Yang, and N. Wu, “Characteristics and applications of sugar cane bagasse ash waste in cementitious materials,” *Materials*, vol. 12, no. 1. MDPI AG, Dec. 22, 2018. doi: 10.3390/ma12010039.

[28] S. A. Khawaja, U. Javed, T. Zafar, M. Riaz, M. S. Zafar, and M. K. Khan, “Eco-friendly incorporation of sugarcane bagasse ash as partial replacement of sand in foam concrete,” *Clean. Eng. Technol.*, vol. 4, Oct. 2021, doi: 10.1016/j.clet.2021.100164.

[29] E. Benhelal, G. Zahedi, E. Shamsaei, and A. Bahadori, “Global strategies and potentials to curb CO2 emissions in cement industry,” *J. Clean. Prod.*, vol. 51, pp. 142–161, 2013, doi:

10.1016/j.jclepro.2012.10.049.

[30] T. Engin and V. Ari, “Energy auditing and recovery for dry type cement rotary kiln systems - A case study,” *Energy Convers. Manag.*, vol. 46, no. 4, pp. 551–562, 2005, doi: 10.1016/j.enconman.2004.04.007.

[31] C.-T. Galbenis and S. Tsimas, “Use of construction and demolition wastes as raw materials in cement clinker production,” *China Particuology*, vol. 4, no. 2, pp. 83–85, 2006, doi: 10.1016/s1672-2515(07)60241-3.

[32] ASTM, “ASTM C618-12a: Standard Specification for Coal Fly Ash and Raw or Calcined Natural Pozzolan for Use,” pp. 1–5, 2014, doi: 10.1520/C0618.

[33] A. Bersisa and A. Zekaria, “Assessment of the Mechanical Properties of Bagasse Ash Concrete,” *Eng. Sci.*, vol. 6, no. 3, p. 39, 2021, doi: 10.11648/j.es.20210603.12.

[34] P. Jagadesh, A. Ramachandramurthy, and R. Murugesan, “Evaluation of mechanical properties of Sugar Cane Bagasse Ash concrete,” *Constr. Build. Mater.*, vol. 176, pp. 608–617, 2018, doi: 10.1016/j.conbuildmat.2018.05.037.

[35] M. Girma and B. Asteray, “Fresh, Mechanical, and Microstructural Properties Investigation on the Combined Effect of Biomedical Waste Incinerator Ash and Bagasse Ash for High-Strength Concrete,” *Adv. Mater. Sci. Eng.*, vol. 2022, 2022, doi: 10.1155/2022/5685372.

[36] A. Wesselsky and O. M. Jensen, “Synthesis of pure Portland cement phases,” *Cem. Concr. Res.*, vol. 39, no. 11, pp. 973–980, 2009, doi: 10.1016/j.cemconres.2009.07.013.

[37] P. Suraneni and J. Weiss, “Examining the pozzolanicity of supplementary cementitious materials using isothermal calorimetry and thermogravimetric analysis,” *Cem. Concr. Compos.*,

vol. 83, no. July, pp. 273–278, 2017, doi: 10.1016/j.cemconcomp.2017.07.009.

[38] A. Bahurudeen, K. Wani, M. A. Basit, and M. Santhanam, “Assesment of Pozzolanic Performance of Sugarcane Bagasse Ash,” *J. Mater. Civ. Eng.*, vol. 28, no. 2, pp. 1–11, 2016, doi: 10.1061/(asce)mt.1943-5533.0001361.

[39] H. K. Choudhary *et al.*, “Observation of phase transformations in cement during hydration,” *Constr. Build. Mater.*, vol. 101, pp. 122–129, 2015, doi: 10.1016/j.conbuildmat.2015.10.027.

[40] M. N. Amin *et al.*, “Role of Sugarcane Bagasse Ash in Developing Sustainable Engineered Cementitious Composites,” *Front. Mater.*, vol. 7, no. April, pp. 1–12, 2020, doi: 10.3389/fmats.2020.00065.

[41] S. Praveenkumar and G. Sankarasubramanian, “Mechanical and durability properties of bagasse ash-blended high-performance concrete,” *SN Appl. Sci.*, vol. 1, no. 12, pp. 1–7, 2019, doi: 10.1007/s42452-019-1711-x.

[42] B. Ribeiro, Y. Yamashiki, and T. Yamamoto, “A study on mechanical properties of mortar with sugarcane bagasse fiber and bagasse ash,” *J. Mater. Cycles Waste Manag.*, vol. 22, no. 6, pp. 1844–1851, 2020, doi: 10.1007/s10163-020-01071-w.

[43] M. Tarekegn, K. Getachew, and G. Kenea, “Experimental Investigation of Concrete Characteristics Strength with Partial Replacement of Cement by Hybrid Coffee Husk and Sugarcane Bagasse Ash,” *Adv. Mater. Sci. Eng.*, vol. 2022, 2022, doi: 10.1155/2022/5363766.

[44] IS 10262 (2009), “Guidelines for concrete mix design proportioning [CED 2: Cement and Concrete],” 2009.

[45] S. Chen, Y. Zheng, M. Wu, J. Hu, and W. Xiang, “Thermodynamic analysis of oxy-fuel

combustion integrated with the sCO2 Brayton cycle for combined heat and power production," *Energy Convers. Manag.*, vol. 232, no. x, p. 113869, 2021, doi: 10.1016/j.enconman.2021.113869.

[46] A. Hassn, A. Chiarelli, A. Dawson, and A. Garcia, "Thermal properties of asphalt pavements under dry and wet conditions," *Mater. Des.*, vol. 91, pp. 432–439, 2016, doi: 10.1016/j.matdes.2015.11.116.

[47] M. Hedayati-Dezfooli and W. H. Leong, "An experimental study of coupled heat and moisture transfer in soils at high temperature conditions for a medium coarse soil," *Int. J. Heat Mass Transf.*, vol. 137, pp. 372–389, 2019, doi: 10.1016/j.ijheatmasstransfer.2019.03.131.

[48] IS 456 : 2000, "Plain and Reinforced Concrete - Code of Practice (Fourth Revision," no. July, 2000.

[49] ASTM C 192/C 192M - 00, "Standard Practice for Making and Curing Concrete Test Specimens in the Laboratory," *Eng. Concr.*, vol. 04, pp. 107–108, 2009, doi: 10.1201/9781420091175-c23.

[50] ASTM C 39/C 39M – 14, "Standard Test Method for Compressive Strength of Cylindrical Concrete Specimens," pp. 3–9, 2014, doi: 10.1520/C0039.

[51] ASTMC 78 - 02, "Standard Test Method for Flexural Strength of Concrete (Using Simple Beam with Third-Point Loading)," *Annu. B. ASTM Standars*, vol. 04.02, pp. 1–3, 2002.

[52] BS EN 12390-3:2019, "Testing hardened concrete - Part 3: Compressive strength of test specimens," *BSI Stand. Publ.*, vol. 38, no. 10, p. 18, 2019.

[53] N. C. Collier, "Transition and decomposition temperatures of cement phases - a collection of

thermal analysis data," *Ceram. - Silikaty*, vol. 60, no. 4, pp. 338–343, 2016, doi: 10.13168/cs.2016.0050.

[54] P. Stutzman and S. Leigh, "Phase Composition Analysis of the NIST Reference Clinkers by Optical Microscopy and X-ray Powder Diffraction Reference Clinkers by Optical Diffraction," *NIST Tech. Note 1441*, no. May, p. 44, 2002.

[55] L. Black and A. Brooker, "SEM-SCA: Combined SEM - Raman spectrometer for analysis of OPC clinker," *Adv. Appl. Ceram.*, vol. 106, no. 6, pp. 327–334, 2007, doi: 10.1179/174367607X228052.

[56] M. S. Sultana and A. Rahman, "Characterization of calcined sugarcane bagasse sugarcane waste ash for industrial use," *Int. Conf. Mech. Ind. Mater. Eng. 2013*, vol. 2013, no. 1–3, pp. 508–513, 2013.

[57] J. Payá, J. Monzó, M. V. Borrachero, M. M. Tashima, and L. Soriano, *Bagasse ash*. 2018. doi: 10.1016/B978-0-08-102156-9.00017-1.

[58] L. M. Khaskhanova *et al.*, "Scanning Electron Microscopy," *J. Int. Dent. Med. Res.*, vol. 15, no. 1, pp. 107–110, 2022, doi: 10.21273/hortsci.9.5.414.

[59] C. Zhang *et al.*, "Activity quatifictaion of recycled concrete powder and its classification based on the dilution effect, physical effect and chemical effect," *J. Emerg. Technol. Innov. Res.*, vol. 06, no. 4, pp. 1–25, 2006.

[60] P. K. Mehta and P. J. M. Monteiro, *Concrete; Microstructure, Properties and Materials*, Third. New -York: McGraw- Hill, 2006. doi: DOI: 10.1036/0071462899.

[61] A. Ahmed, "Chemical Reactions in Pozzolanic Concrete," *Mod. Approaches Mater. Sci.*, vol. 1,

no. 4, pp. 128–133, 2019, doi: 10.32474/mams.2019.01.000120.

[62] A. N. Christensen, T. R. Jensen, and J. C. Hanson, “Formation of ettringite, Ca(6)Al(2)(SO4) 3(OH)(12)·26H2O, AFt, and monosulfate, Ca(4)Al(2)O(6)(SO4)·14H 2O, AFm-14, in hydrothermal hydration of Portland cement and of calcium aluminum oxide - Calcium sulfate dihydrate mixtures studied by in situ synchrot,” *J. Solid State Chem.*, vol. 177, no. 6, pp. 1944–1951, 2004, doi: 10.1016/j.jssc.2003.12.030.

[63] J. A. Rossignolo, M. S. Rodrigues, M. Frias, S. F. Santos, and H. S. Junior, “Improved interfacial transition zone between aggregate-cementitious matrix by addition sugarcane industrial ash,” *Cem. Concr. Compos.*, vol. 80, pp. 157–167, 2017, doi: 10.1016/j.cemconcomp.2017.03.011.

[64] US EAS 18-1:2017, *Cement — Part 1: Composition, specification and conformity criteria for common cements*. Kampala: Uganda National Bureau of Standards, 2019. [Online]. Available: www.unbs.go.ug%0A

APPENDIX A- EDX Analysis

A1: Bamburi Powerplus CEM I/42.5N Portland cement elemental composition- EDX analysis

Table A1: Bamburi Powerplus CEM I/42.5N Portland cement Elemental Composition- EDX Analysis

APEX eZAF Smart Quant Results

Project : New Project | New Sample | Area 762 | Live Map 1

QuantMethod : eZAF
KV : 10 Live Time (sec) : 317.44 AmpTime : 3.84 TakeOffAngle : 34.95 Resolution : 130.76

Element	Line	Weight %	Atomic %	Error %	Net Int.	R	A	F
C K	K	23.00	36.17	9.21	70.63	0.8991	0.3513	1.0000
O K	K	38.99	46.01	9.61	206.49	0.9123	0.2693	1.0000
Na K	K	0.05	0.04	86.25	0.55	0.9275	0.5705	1.0031
Mg K	K	0.34	0.27	13.33	5.12	0.9322	0.6998	1.0053
Al K	K	1.20	0.84	7.18	18.02	0.9367	0.7907	1.0087
Si K	K	3.31	2.22	4.98	49.46	0.9409	0.8531	1.0116
S K	K	0.87	0.51	10.83	9.18	0.9490	0.9233	1.0295
K K	K	0.79	0.38	14.08	5.14	0.9606	0.9726	1.1150
Ca K	K	27.33	12.87	3.80	125.10	0.9644	0.9795	1.0145
Ti K	K	0.05	0.02	84.22	0.16	0.9722	0.9682	1.0274
Mn K	K	0.23	0.08	77.80	0.27	0.9844	0.9878	1.0458
Fe L	L	0.23	0.08	65.85	0.65	0.9183	0.3008	1.0000
Rb L	L	0.21	0.05	31.10	1.50	0.9409	0.8456	1.0048
Zr L	L	0.02	0.01	99.99	0.14	0.9466	0.8958	1.0086
Sn L	L	0.29	0.05	52.09	0.67	0.9647	0.9763	1.0094
Te L	L	0.24	0.04	84.83	0.41	0.9684	0.9765	1.0046
Nd L	L	2.85	0.37	37.01	1.84	0.9840	0.9847	1.0086

A2: Raw SCBA elemental composition - EDX analysis

Table A2: Raw SCBA Elemental composition - EDX analysis

APEX eZAF Smart
Quant Results

Project : New Project | New Sample | Area 766

| Live Map 1QuantMethod : eZAF
KV : 10 Live Time (sec) : 40.96 AmpTime : 3.84 TakeOffAngle : 35.83 Resolution : 130.76

Element	Line	Weight %	Atomic %	Error %	Net Int.	R	A	F
C K	K	85.71	90.95	6.75	800.61	0.9405	0.5628	1.0000
O K	K	10.26	8.17	11.55	91.79	0.9495	0.2403	1.0000
Na K	K	0.09	0.05	69.30	2.21	0.9595	0.6883	1.0018
Mg K	K	0.19	0.10	21.14	6.16	0.9626	0.7970	1.0029
Al K	K	0.16	0.08	27.46	4.97	0.9654	0.8669	1.0045
Si K	K	0.13	0.06	39.78	3.81	0.9681	0.9129	1.0065
S K	K	0.07	0.03	65.50	1.46	0.9732	0.9618	1.0141
K K	K	0.77	0.25	17.88	8.92	0.9801	0.9879	1.0324
Ca K	K	0.00	0.00	99.99	0.02	0.9823	0.9908	1.0408
Ti K	K	0.14	0.04	69.43	0.84	0.9865	0.9954	1.0713
Mn K	K	0.18	0.04	86.13	0.42	0.9927	0.9998	1.1064
Fe L	L	0.07	0.02	76.87	0.51	0.9535	0.4018	1.0000
Rb L	L	0.12	0.02	66.71	1.78	0.9681	0.9078	1.0019
Zr L	L	0.10	0.01	66.74	1.09	0.9717	0.9465	1.0031
Sn L	L	0.30	0.03	62.69	1.32	0.9825	0.9902	1.0096
Te L	L	0.28	0.03	65.82	0.92	0.9845	0.9925	1.0122
Nd L	L	1.43	0.13	57.28	1.77	0.9925	0.9967	1.0201

A3: Processed SCBA (SCBA-600) - EDX analysis

Table A3: Processed SCBA (SCBA-600) - EDX analysis

APEX eZAF Smart Quant Results

Project : New Project | New Sample | Area 767 | Live Map 1

QuantMethod : eZAF
KV : 10 Live Time (sec) : 40.96 AmpTime : 3.84 TakeOffAngle : 36.11 Resolution : 130.76

Element	Line	Weight %	Atomic %	Error %	Net Int.	R	A	F
C K	K	33.40	46.17	11.15	101.50	0.9133	0.2798	1.0000
O K	K	40.56	42.09	9.03	363.60	0.9252	0.3671	1.0000
Na K	K	0.08	0.05	83.21	1.05	0.9388	0.6043	1.0034
Mg K	K	0.49	0.34	20.45	9.47	0.9430	0.7264	1.0059
Al K	K	1.81	1.11	9.02	34.35	0.9470	0.8088	1.0095
Si K	K	12.12	7.16	4.83	225.99	0.9507	0.8637	1.0051
S K	K	0.11	0.06	72.25	1.40	0.9578	0.9058	1.0114
K K	K	3.02	1.28	13.07	22.29	0.9678	0.9674	1.0250
Ca K	K	1.13	0.47	23.74	6.47	0.9710	0.9731	1.0275
Ti K	K	0.37	0.13	67.33	1.44	0.9776	0.9847	1.0497
Mn K	K	0.62	0.19	74.96	0.93	0.9876	0.9941	1.0663
Fe L	L	0.93	0.28	33.72	3.82	0.9306	0.3430	1.0000
Rb L	L	0.21	0.04	82.15	1.96	0.9507	0.8565	1.0021
Zr L	L	0.46	0.08	60.86	3.23	0.9557	0.8764	1.0028
Sn L	L	0.18	0.02	74.90	0.50	0.9713	0.9724	1.0072
Te L	L	0.67	0.09	65.06	1.44	0.9744	0.9777	1.0089
Nd L	L	3.84	0.44	47.36	3.10	0.9872	0.9927	1.0133

A4: Hardened concrete block surface from SCBA-20 Mix -EDX analysis

Table A4: Hardened concrete block surface from SCBA-20 Mix -EDX analysis

APEX eZAF Smart Quant Results

Project : New Project | New Sample | Area 765 | Live Map 1

QuantMethod : eZAF
KV : 10 Live Time (sec) : 40.96 AmpTime : 3.84 TakeOffAngle : 34.47 Resolution : 130.76

Element	Line	Weight %	Atomic %	Error %	Net Int.	R	A	F	
C K	K	12.11	21.08	12.27	36.54	0.8887	0.3704	1.0000	
O K	K	43.59	56.94	10.58	212.64	0.9027	0.2660	1.0000	
Na K	K	0.05	0.04	99.99	0.43	0.9190	0.5434	1.0031	
Mg K	K	0.06	0.05	86.08	0.74	0.9241	0.6764	1.0053	
Al K	K	1.03	0.80	13.83	14.05	0.9289	0.7738	1.0089	
Si K	K	1.71	1.27	11.07	23.63	0.9335	0.8412	1.0134	
S K	K	0.20	0.13	68.74	1.97	0.9423	0.9210	1.0359	
K K	K	0.36	0.19	69.21	2.23	0.9550	0.9723	1.1457	
Ca K	K	35.26	18.39	4.92	150.78	0.9592	0.9797	1.0138	
Ti K	K	0.22	0.10	84.20	0.61	0.9680	0.9611	1.0247	
Mn K	K	0.74	0.28	84.65	0.81	0.9819	0.9845	1.0417	
Fe L	L	0.03	0.01	99.99	0.07	0.9091	0.2795	1.0000	
Rb L	L	0.05	0.01	99.99	0.34	0.9335	0.8332	1.0056	
Zr L	L	0.15	0.03	88.14	0.78	0.9397	0.8929	1.0104	
Sn L	L	0.54	0.09	63.51	1.17	0.9596	0.9758	1.0108	
Te L	L	1.29	0.21	73.75	2.07	0.9637	0.9746	1.0043	
Nd L	L	2.63	0.38	66.46	1.58	0.9814	0.9807	1.0078	

APPENDIX B- XRF Analysis

B1: Bamburi Powerplus CEM I/42.5N Portland cement XRF analysis

Table B1: Bamburi Powerplus CEM I/42.5N Portland cement XRF analysis

01181-GeoChem.pdz	AssayTime: 05/02/2024 15:17:46	ElapsedTime: 50
Alloy 1:	Match No:	

Field Info			
Operator	SUPERVISOR	Sender name	KIBET
Sample type	CEMENT	Sender ref	CEM 1
LAB NO		REF	BAMBURI 42.5

Element Name	Min	%	Max	+/- [*3]
MgO	0	0.000	0	2.783
Al2O3	0	3.695	0	0.437
SiO2	0	17.068	0	0.499
P2O5	0	0.888	0	0.127
S	0	2.644	0	0.069
Cl	0	0.037	0	0.019
K2O	0	0.371	0	0.030
CaO	0	71.592	0	0.196
Ti	0	0.225	0	0.016
V	0	0.007	0	0.009
Cr	0	0.000	0	0.006
Mn	0	0.054	0	0.012
Fe	0	3.079	0	0.061
Co	0	0.000	0	0.007
Ni	0	0.000	0	0.005
Cu	0	0.069	0	0.007
Zn	0	0.069	0	0.004
As	0	0.002	0	0.002
Se	0	0.000	0	0.001
Rb	0	0.003	0	0.002
Sr	0	0.115	0	0.004
Y	0	0.000	0	0.002
Zr	0	0.033	0	0.002
Nb	0	0.005	0	0.002

01181-GeoChem.pdz	AssayTime: 05/02/2024 15:17:46	ElapsedTime: 50

Alloy 1:	Match No:

Element Name	Min	%	Max	+/- [*3]
Mo	0	0.013	0	0.003
Ag	0	0.000	0	0.004
Cd	0	0.000	0	0.006
Sn	0	0.021	0	0.027
Sb	0	0.000	0	0.012
Ba	0	0.000	0	0.039
La	0	0.000	0	0.089
Ce	0	0.000	0	0.036
Hf	0	0.000	0	0.005
Ta	0	0.001	0	0.003
W	0	0.000	0	0.002
Pt	0	0.002	0	0.003
Au	0	0.000	0	0.004
Hg	0	0.000	0	0.002
Tl	0	0.000	0	0.002
Pb	0	0.009	0	0.003
Bi	0	0.000	0	0.005
Th	0	0.000	0	0.008
U	0	0.000	0	0.011

B2: Processed SCBA (SCBA-600) XRF analysis

Table B2: Processed SCBA (SCBA-600) XRF analysis

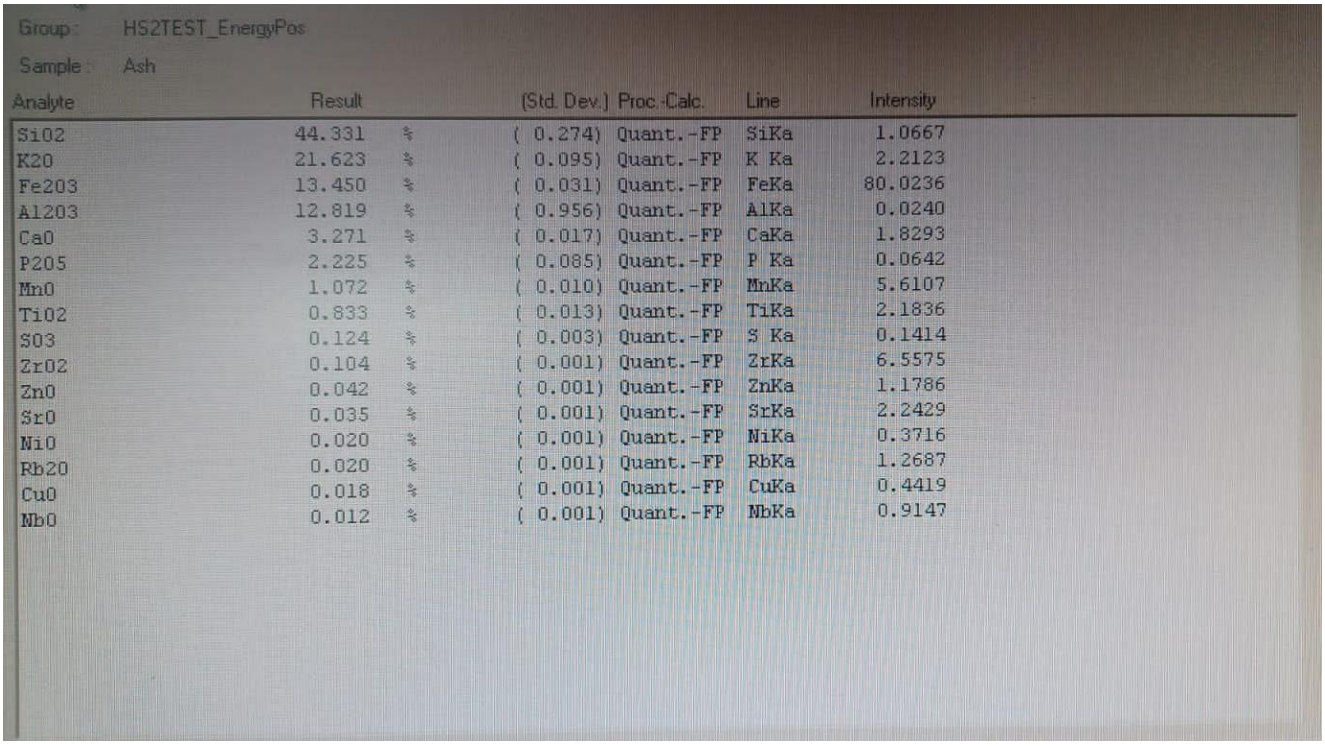

Group : HS2TEST_EnergyPos

Sample : Ash

Analyte	Result		(Std. Dev.)	Proc.-Calc.	Line	Intensity
SiO2	44.331	%	(0.274)	Quant.-FP	SiKa	1.0667
K2O	21.623	%	(0.095)	Quant.-FP	K Ka	2.2123
Fe2O3	13.450	%	(0.031)	Quant.-FP	FeKa	80.0236
Al2O3	12.819	%	(0.956)	Quant.-FP	AlKa	0.0240
CaO	3.271	%	(0.017)	Quant.-FP	CaKa	1.8293
P2O5	2.225	%	(0.085)	Quant.-FP	P Ka	0.0642
MnO	1.072	%	(0.010)	Quant.-FP	MnKa	5.6107
TiO2	0.833	%	(0.013)	Quant.-FP	TiKa	2.1836
SO3	0.124	%	(0.003)	Quant.-FP	S Ka	0.1414
ZrO2	0.104	%	(0.001)	Quant.-FP	ZrKa	6.5575
ZnO	0.042	%	(0.001)	Quant.-FP	ZnKa	1.1786
SrO	0.035	%	(0.001)	Quant.-FP	SrKa	2.2429
NiO	0.020	%	(0.001)	Quant.-FP	NiKa	0.3716
Rb2O	0.020	%	(0.001)	Quant.-FP	RbKa	1.2687
CuO	0.018	%	(0.001)	Quant.-FP	CuKa	0.4419
NbO	0.012	%	(0.001)	Quant.-FP	NbKa	0.9147

APPENDIX C- Scanning Electron Micrographs (SEM)

C1: Bamburi Powerplus CEM I/42.5N Portland cement SEM images at different magnifications

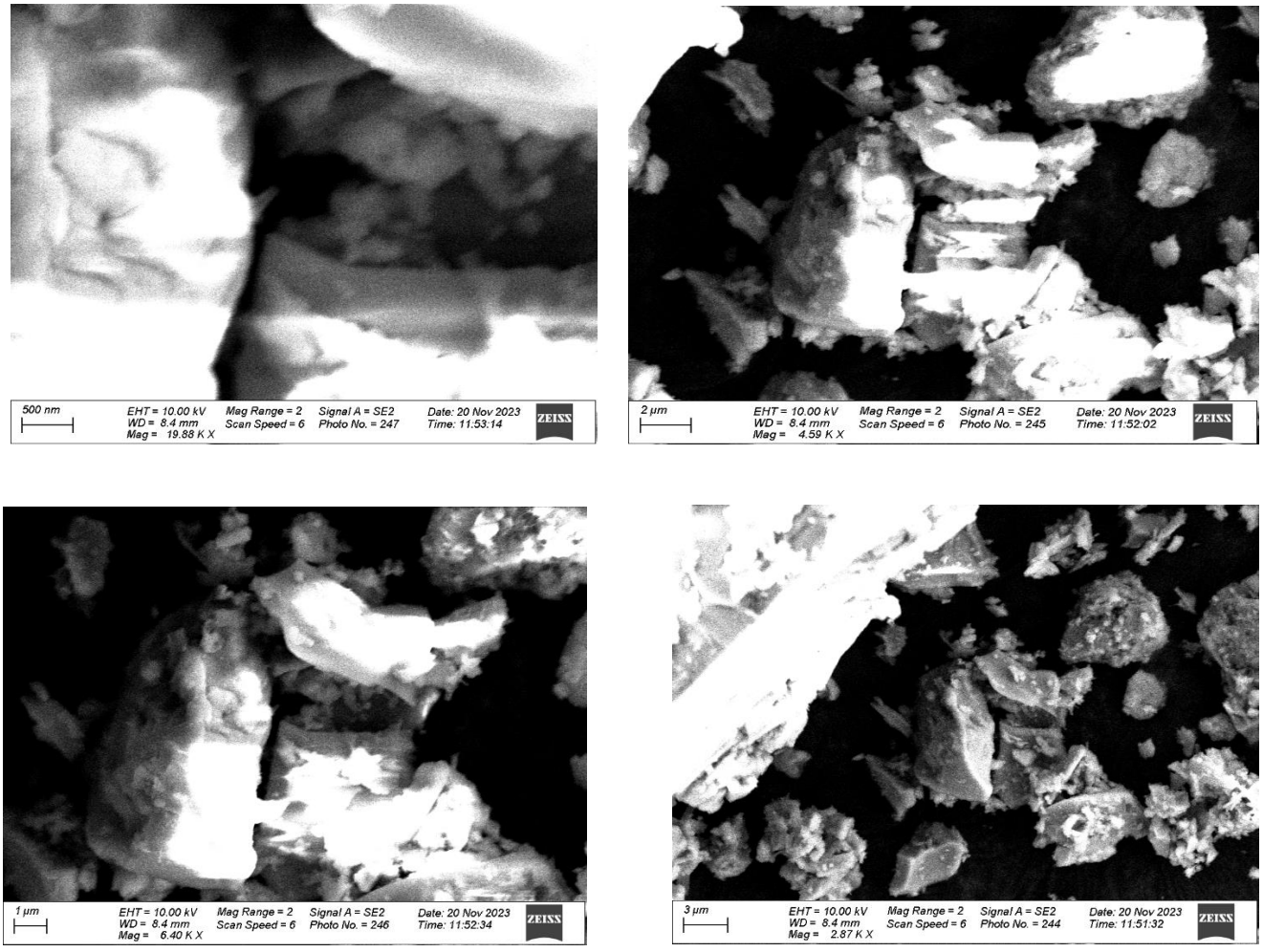

Figure C1: Bamburi Powerplus CEM I/42.5N Portland cement SEM images at different magnifications

C2: Raw SCBA SEM images at different magnifications

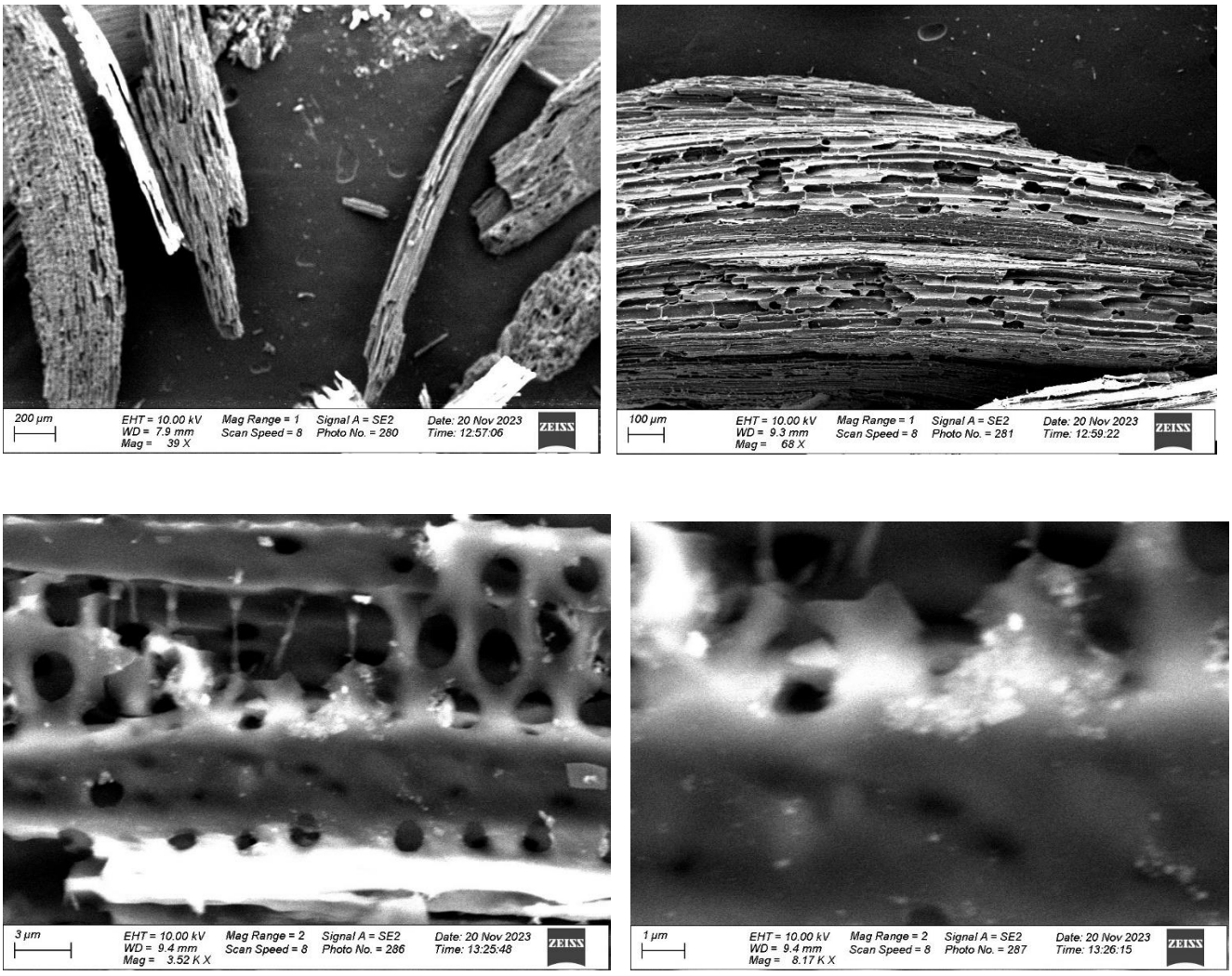

Figure C2: Raw SCBA SEM images at different magnifications

C3: Processed SCBA (SCBA-600) SEM images at different magnifications

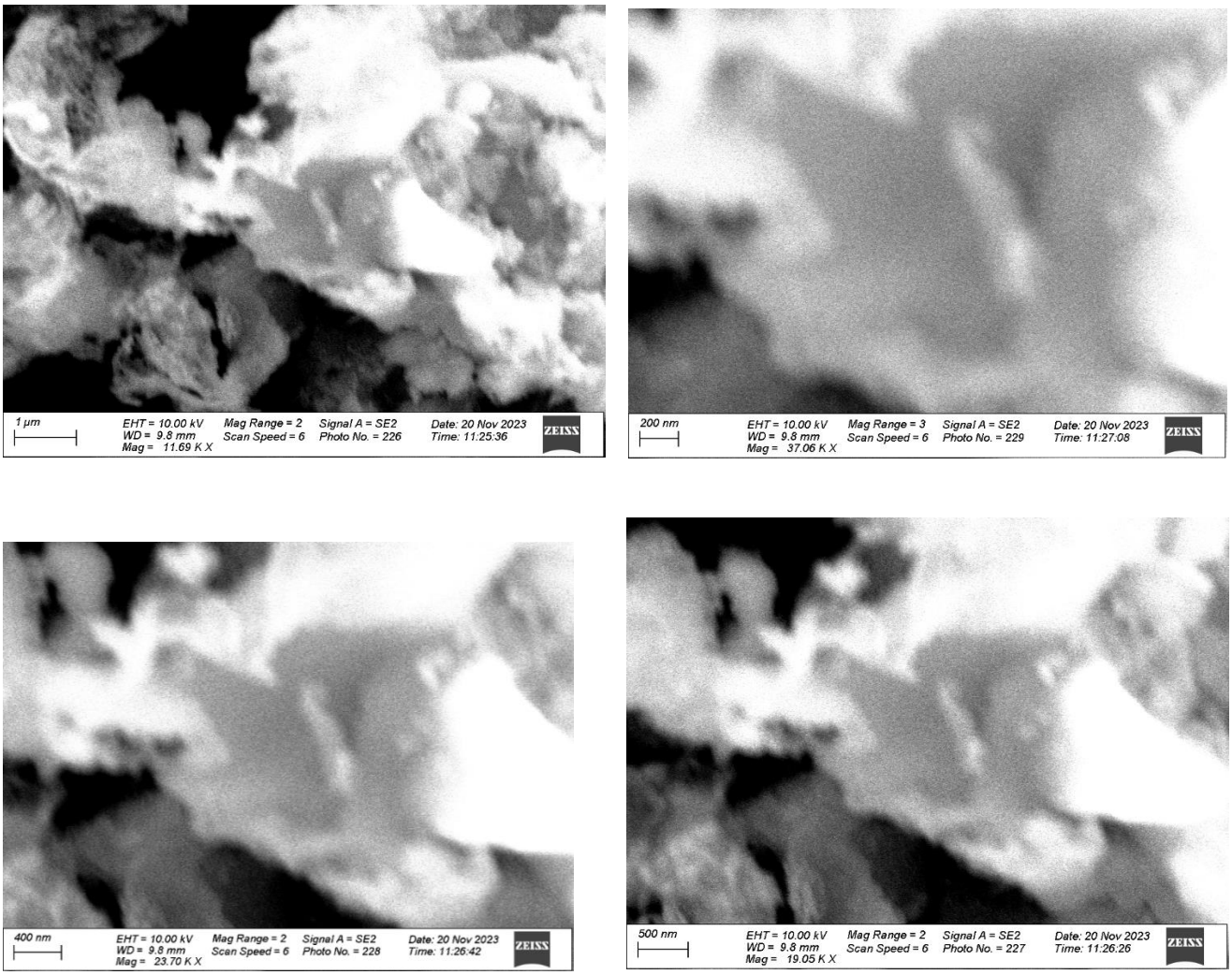

Figure C3: Processed SCBA (SCBA-600) SEM images at different magnifications

C4: Hardened concrete surface from SCBA-20 Mix SEM images

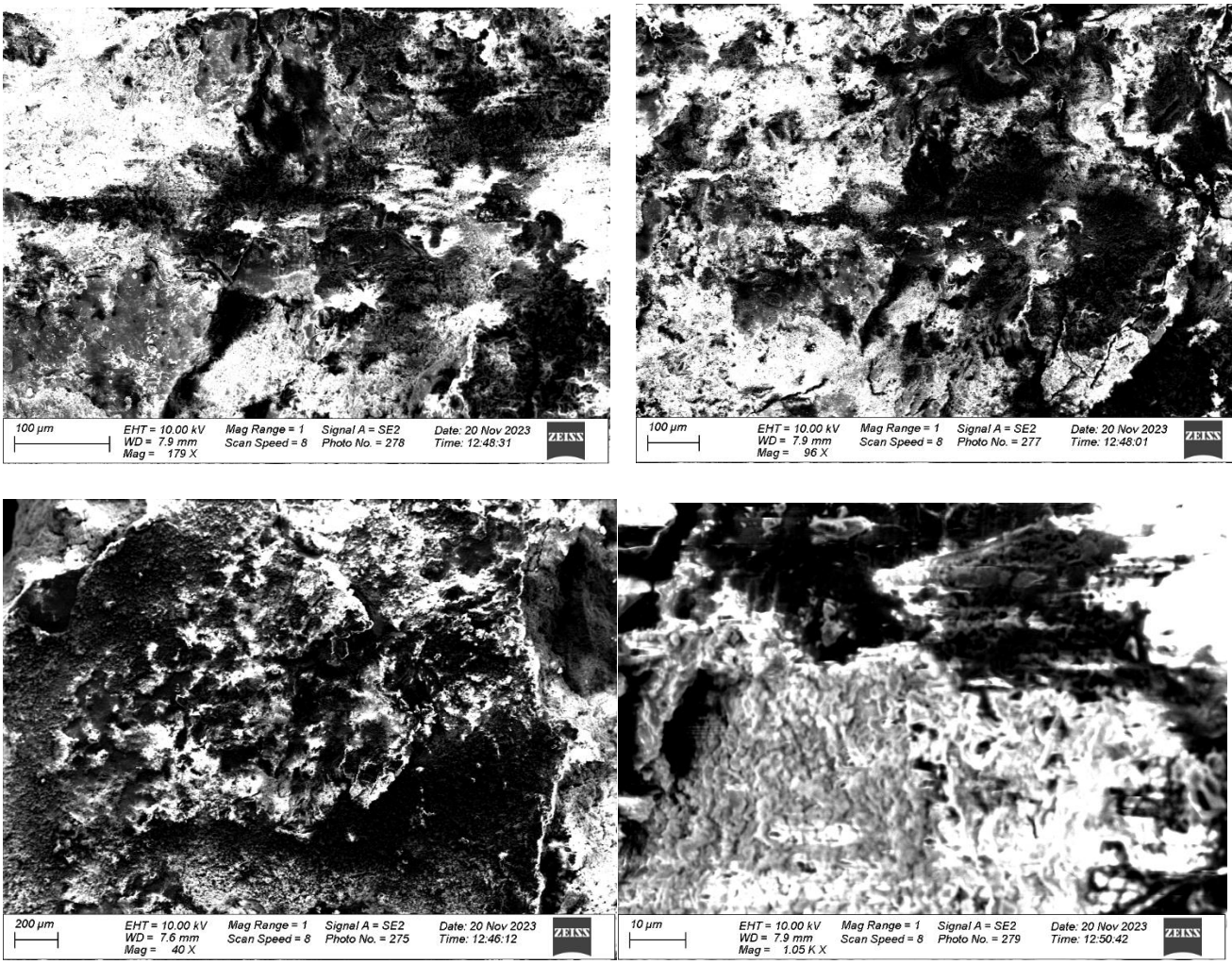

Figure C4: Hardened concrete surface from SCBA-20 Mix SEM images

APPENDIX D- Hardened Concrete Mechanical Properties Statistical Analysis

D1: Flexural strength statistical analysis.

Table D1: Flexural strength statistical analysis

% SCBA Dose	N total	Average Flexural Strength	Standard Deviation	SE of mean	Lower 95%CI of Mean	Upper 95% CI of Mean	Variance	Sum
		Nmm^{-2}	Nmm^{-2}	Nmm^{-2}	Nmm^{-2}	Nmm^{-2}	Nmm^{-2}^2	Nmm^{-2}
% SCBA Dose	Descriptive Statistics	Average Flexural	Standard Deviation	SE of mean	Descriptive Statistics	Descriptive Statistics	Variance	Descriptive Statistics
[Book1]"Fle								
SCBA 0	4	7.675	0.45735	0.22867	6.94726	8.40274	0.20917	30.7
SCBA 10	4	7.075	0.93229	0.46615	5.59152	8.55848	0.86917	28.3
SCBA 20	4	8.175	0.37749	0.18875	7.57433	8.77567	0.1425	32.7
SCBA 30	4	6.775	0.74106	0.37053	5.59581	7.95419	0.54917	27.1

% SCBA Dose	Skewness	Kurtosis	Uncorrected Sum of Squares	Corrected Sum of Squares	Coefficient of Variation	Mean absolute Deviation	Geometric Mean	Mode	Sum of Weights
			Nmm^{-2}^2	Nmm^{-2}^2		Nmm^{-2}	Nmm^{-2}	Nmm^{-2}	
% SCBA Dose	Skewness	Kurtosis	Descriptive Statistics	Descriptive Statistics	Coefficient of Variation	Mean Absolute Deviation	Descriptive Statistics	Descriptive Statistics	Descriptive Statistics
[Book1]"Fle									
SCBA 0	0.94865	2.00892	236.25	0.6275	0.05959	0.3125	7.66495	7.6	4
SCBA 10	0.88577	-1.04482	202.83	2.6075	0.13177	0.725	7.03041	--	4
SCBA 20	1.27806	0.84826	267.75	0.4275	0.04618	0.275	8.16858	7.9	4
SCBA 30	0.23036	-4.51651	185.25	1.6475	0.10938	0.625	6.74477	--	4

% SCBA Dose	HarmonicMean	Minimum	Median	Maximum
	Nmm^{-2}	Nmm^{-2}	Nmm^{-2}	Nmm^{-2}
% SCBA Dose	DescriptiveStatistics	DescriptiveStatistics	Median	DescriptiveStatistics
[Book1]"Fle				
SCBA 0	7.65508	7.2	7.6	8.3
SCBA 10	6.98753	6.3	6.85	8.3
SCBA 20	8.16229	7.9	8.05	8.7
SCBA 30	6.71487	6.1	6.7	7.6

D2: Compressive strength statistical analysis

Table D2: Compressive strength statistical analysis

% SCBA Dose	N total	Average Compressive Strength	Standard Deviation	SE of mean	Lower 95% CI of Mean	Upper 95% CI of Mean	Variance	Sum
		Nmm^{-2}	Nmm^{-2}	Nmm^{-2}	Nmm^{-2}	Nmm^{-2}	$Nmm^{-2}\wedge 2$	Nmm^{-2}
% SCBA Dose	Descriptive Statistics	Average Compressive	Standard Deviation	Descriptive Statistics	Descriptive Statistics	Descriptive Statistics	Variance	Descriptive Statistics
[Book1]"Co								
SCBA 0	4	36.25	3.06866	1.53433	31.36707	41.13293	9.41667	145
SCBA 10	4	33.95	2.59551	1.29775	29.81996	38.08004	6.73667	135.8
SCBA 20	4	39.75	1.30767	0.65383	37.6692	41.8308	1.71	159
SCBA 30	4	30.575	1.02429	0.51214	28.94513	32.20487	1.04917	122.3

% SCBA Dose	Skewness	Kurtosis	Uncorrectedd Sum of Squares	Corrected Sum of Squares	Coefficient of Variation	Mean absolute Deviation	Geometric Mean	Mode	Sum of Weights
			$Nmm^{-2}\wedge 2$	$Nmm^{-2}\wedge 2$		Nmm^{-2}	Nmm^{-2}	Nmm^{-2}	
% SCBA Dose	Skewness	Kurtosis	Descriptive Statistics	Descriptive Statistics	Descriptive Statistics	Mean absolute	Descriptive Statistics	Descriptive Statistics	Descriptive Statistics
[Book1]"Co						Deviation			
SCBA 0	-0.35298	-2.90662	5284.5	28.25	0.08465	2.5	36.15137	--	4
SCBA 10	-0.98004	1.81094	4630.62	20.21	0.07645	1.775	33.87347	--	4
SCBA 20	-1.00174	-0.48993	6325.38	5.13	0.0329	1	39.73368	--	4
SCBA 30	-0.14447	1.32264	3742.47	3.1475	0.0335	0.675	30.5621	--	4

% SCBA Dose	HarmonicMean	Minimum	Median	Maximum
	Nmm^{-2}	Nmm^{-2}	Nmm^{-2}	Nmm^{-2}
% SCBA Dose	DescriptiveStatistics	DescriptiveStatistics	DescriptiveStatistics	DescriptiveStatistics
[Book1]"Co				
SCBA 0	36.05181	32.6	36.55	39.3
SCBA 10	33.79489	30.4	34.4	36.6
SCBA 20	39.71718	38	40.1	40.8
SCBA 30	30.54918	29.3	30.6	31.8

APPENDIX E- Copy Rights Permissions

Gmail

Image Copyrights
3 messages

mike evans <nzuguam22@gmail.com>
To: salehan.pub@mailfence.com, kavianpour@civilejournal.org, office@civilejournal.org

Hello,
I am Michael Evans Nzugua from Kenya writing my dissertation and would like to be granted permission to use one of the SEM images(Figure 4 a and b) for comparison purposes. This image is in one of your published articles as described below;

Title: Mechanical Properties of Eco-friendly Concrete Made with Sugarcane Bagasse Ash
Issue: Vol. 8, No. 06, June, 2022
Authors: Tareg Abdalla Abdalla , David O. Koteng , Stanley M. Shitote , M. Matallah

Your assistance will be highly appreciated

Nzugua M.E
+254712356895
+256756384531

office@civilejournal.org <office@civilejournal.org>
To: mike evans <nzuguam22@gmail.com>

Dear Nzugua M.E,

Thank you for the email.
There is no problem with mentioning the source.

Regards,
Office C.E.J
Civil Engineering Journal
[Quoted text hidden]

APPENDIX F- Research Introductory Letter

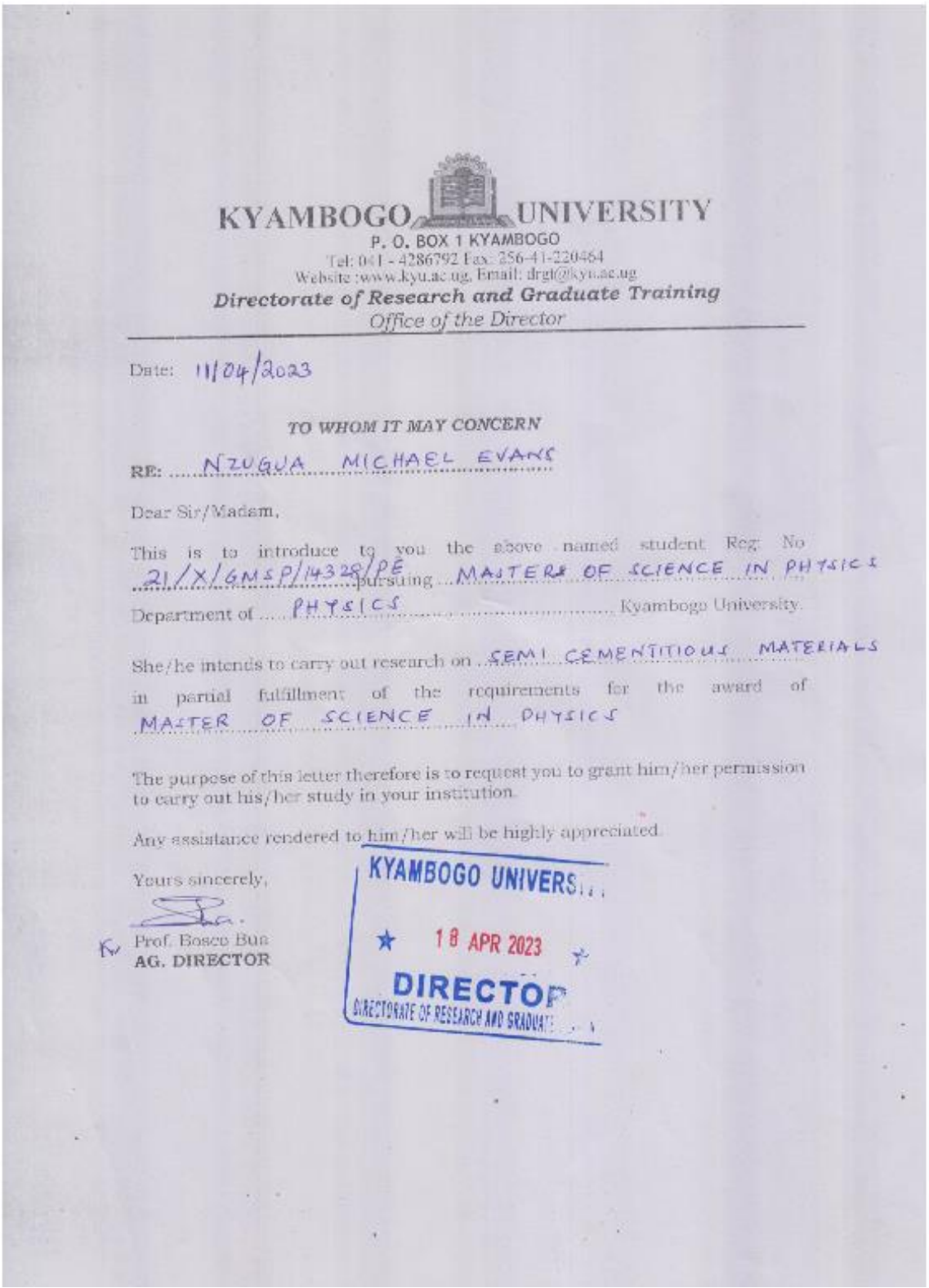

KYAMBOGO UNIVERSITY
P. O. BOX 1 KYAMBOGO
Tel: 041 - 4286792 Fax: 256-41-220464
Website :www.kyu.ac.ug, Email: drgt@kyu.ac.ug
Directorate of Research and Graduate Training
Office of the Director

Date: 11/04/2023

TO WHOM IT MAY CONCERN

RE: NZUGUA MICHAEL EVANS

Dear Sir/Madam,

This is to introduce to you the above named student Reg: No 21/X/6MSP/14328/PE pursuing MASTERS OF SCIENCE IN PHYSICS Department of PHYSICS Kyambogo University.

She/he intends to carry out research on SEMI CEMENTITIOUS MATERIALS in partial fulfillment of the requirements for the award of MASTER OF SCIENCE IN PHYSICS

The purpose of this letter therefore is to request you to grant him/her permission to carry out his/her study in your institution.

Any assistance rendered to him/her will be highly appreciated.

Yours sincerely,

Prof. Bosco Bua
AG. DIRECTOR

KYAMBOGO UNIVERSITY
18 APR 2023
DIRECTOR
DIRECTORATE OF RESEARCH AND GRADUATE